A Conservative Mechanism of Polarization Drives Hyphal Growth in the Opportunistic Yeast Pathogen *Candida albicans*

A DISSERTATION
SUBMITTED TO THE FACULTY OF THE GRADUATE SCHOOL
OF THE UNIVERSITY OF MINNESOTA BY

REBECCA E. PULVER

IN PARTIAL FULFILLMENT OF THE REQUIREMENTS
FOR THE DEGREE OF
DOCTOR OF PHILOSOPHY

DR. CHERYL GALE, CO-ADVISOR
DR. JUDITH BERMAN, CO-ADVISOR

August 2014

ACKNOWLEDGEMENTS

I'd like to thank my graduate adviser Cheryl Gale for the opportunity to work in her lab and for her patience with me and all of my crazy numbers. I'd also like to thank the members of the Gale Lab both past and present, in particular Tim Heisel and Sara Gonia, for all of their hard work. I hope that all of you come to love and appreciate the usefulness of profile plotting.

Thank you to Judy Berman, Mark McClellan, Maryum Gerami-Nejad, and the rest of the Berman Lab. You've all been a wonderful resource for this work.

To my fellow graduate students Katie Furniss-Smith and Jess Curtis, thank you for all of the moral support; I couldn't have hoped for better Itasca bunk-mates.

DEDICATION

Completion of this degree marks the end of what has been an 18 year journey. Thankfully, I have been fortunate enough to have to have a small but ever present group of family, friends, and teachers, whose love and support have kept me moving past every hurdle life has place in my path. When I've leaped gracefully, you've cheered. When I've had to take more time and go around, you've reminded me that it's not a race, it's about finishing. When I've seemingly slammed into the hurdle and fallen flat on my face in a manner that rivals what one would see on a blooper reel, you've helped me to bandage the situation up, to get over myself, and to keep moving forward. This work is dedicated to all of you. In particular, to my parents and my son Brennan; I know this hasn't been easy, but your belief in me has kept me going through those times when all of this seemed like a hopeless endeavor. I would not have been able to achieve this without you. Thank you.

ABSTRACT

In eukaryotes, different cell morphologies are generated by fine-tuning the spatiotemporal regulation of the polarized growth machinery. Studying hyphal growth in the multimorphic opportunistic yeast pathogen *Candida albicans* provides a unique opportunity to understand how highly polarized cell structures are generated and maintained, and has the potential to provide insight into mechanisms of pathogenesis. Hyphal cell morphology requires that polarized growth machinery be held at hyphal tips over extreme distances and through multiple cell cycles. Deletion of the bud-site selection GTPase Rsr1 in *C. albicans* results in defects in cell size and shape not observed in studies of its ortholog in the related yeast *Saccharomyces cerevisiae*. This suggests that, in addition to its role in bud site selection, Rsr1 has expanded function in *C. albicans*, which impacts polarized growth and the generation of the hyphal morphology. Here, I show that loss of Rsr1 results in changes to a hyphal-specific tip structure, the Spitzenkörper, a downstream developmental indicator of Cdc42 signaling, and key regulator of polarized growth. Also, my results show that Rsr1's function impacts the spatiotemporal distribution of Bem1 a marker of the active form of Cdc42. Interestingly, the changes in the distribution of Cdc42 activity are also correlated with reduced expression of the hyphal transcriptional program. In addition, I also show the differential effects of the guanine nucleotide binding states of Rsr1, through the manipulation of the Rsr1 GAP, Bud2, and GEF, Bud5. Through the action of Bud2, Rsr1-GDP acts as a global inhibitor that limits competitive, stochastically-activated clusters of Cdc42, and also as a lateral inhibitor of growth at hyphal tips that strongly influences the overall width of the hypha. In contrast, Rsr1-GTP, through Bud5 activity, is needed to efficiently nucleate single clusters of Cdc42 activity during hyphal emergence, and also contributes to the extremely narrow morphology of the hypha. Altogether, the data presented here suggest that Rsr1 cycling supports a conservative mechanism of polarization that optimizes the efficiency with which polarization occurs, which is required for the maintenance of polarized growth.

TABLE OF CONTENTS

LIST OF TABLES

LIST OF FIGURES

LIST OF ABBREVIATIONS

Analysis of variance	ANOVA
Bud site selection	BSS
Confidence interval	CI
Differential interference contrast	DIC
GTPase activating protein	GAP
Guanine nucleotide exchange factor	GEF
Germ tube	GT
Hyphal specific gene	HSG
New end take off	N.E.T.O.
Region of interest	ROI
Standard error of the mean	SEM
Spitzenkörper	Spk
Yellow fluorescent protein	YFP
Wild-type	WT

Chapter 1

Polarized Growth and Hyphal Development of *C. albicans*

I. The Cell Morphology of *C. albicans* is Linked to Virulence

Candida albicans is an important opportunistic fungal pathogen of humans. *Candida* is the 4th leading cause of hospital acquired infection with *C. albicans* being the most frequently isolated species (76, 77). While it is commonly associated with mild to moderate mucosal infections of the oral and vaginal tract, in immunocompromised individuals, it is associated with far more serious infections of the bloodstream and vital organs. In these high-risk populations, approximately 49% of patients who acquire a disseminated *Candida* infection will die as a result of the infection, whereas only an estimated 12% will die as a result of the underlying disease (77).

C. albicans can reversibly switch between three major cell morphologies (Fig.1.1): round to ellipsoid cells that separate completely are considered yeast, elongated cells that often form chains are classified as pseudohyphae, and highly elongated, parallel sided cells are categorized as hyphae. For the process of infection, both yeast and hyphal growth forms are thought to be important and, in particular, the ability to change between growth forms is thought to give *C. albicans* "morphogenetic plasticity" that enhances its virulence potential by allowing it to adapt to different environmental situation (64, 79, 86). During infection, the yeast form is thought to be well-suited for dissemination in the blood stream, as this yeast cell shape is thought to move through blood vessels with minimal resistance; the hyphal form, in contrast, is associated with invasion and causing damage to host tissues. Indeed, one study's findings show that strains held in the yeast growth form, using a regulatable promoter system, regains its ability to invade tissue once allowed to transition into the hyphal form post-infection (86). Further, in the same study, only mice in which hyphal growth was permitted succumbed to the infection, despite having an equivalent fungal burden as those in treatment groups where hyphal growth was not permitted. Interestingly, *C. albicans* was shown to invade more frequently and cause more epithelial cell damage than non-hyphal forming *Candida spp*, or *C. dubliniensis* (37), a *Candida* species, which can form hyphae albeit less efficiently than *C. albicans*(92). Together these data implicate that the hyphal growth form is important for *C. albicans* virulence and provide the rationale for the continued study of

mechanisms of *C. albicans* hyphal development, its regulation, and its link to the pathogenesis process during human infection.

II. *C. albicans* Hyphal Morphogenesis is a Model for Extremes in Polarized Growth

C. albicans hyphal formation, in addition to being of interest to human health, can also serve as a more general experimental model for fungal hyphal development. Other fungal pathogens of humans (*Malasseia spp*, dermatophytes, *Aspergillus fumigatus*) and plants (*Fusarium graminearum*, *Pucciniales spp*. *Ashbya gossypii*) also form hyphae as part of the infective process and /or as part of their life cycle (reviewed in(19, 95). As compared to most other hyphal forming fungi, *C. albicans* is easily cultured and has a well-developed set of genetic tools available for its manipulation, making greater advances in knowledge possible on a shorter timescale. Studies using model yeasts like *Saccharomyces cerevisiae* and *Neurospora crassa* have provided a base of information for the understanding of these and other eukaryotic systems. However, *S. cerevisiae* does not undergo continuous polarized growth (i.e. no true hyphal from) and neither organism is inherently pathogenic. With this in mind, studies of *C. albicans* hyphal growth can act as a platform for understanding fungal pathogenicity and polarized growth in other fungi.

As a general biological model for polarized growth, two interesting aspects of hyphal elongation are the efficiency with which it proceeds (up to 1um /sec, (60)) and the ability to maintain continuous polarization. Hyphal elongation in *C. albicans* is somewhat unique in that it is linear (0.3 μm/min(45)); yet, even in filamentous fungi that display pulsed growth patterns, polarization remains consistently directed toward hyphal tips (66). Understanding the mechanisms of how such extremes in polarization are achieved may give insight into how highly polarized structures are formed in other non-fungal eukaryotic systems; and while all aspects of polarized growth may not be conserved, knowledge gained in studying fungal morphogenesis may improve our understanding of other extreme examples of polarized growth such as pollen tubes in plants and neurons in animals.

III. Polarized Growth and GTPase Function in Fungal Hyphae and Yeasts

Cdc42 activity is the driving force behind polarized growth throughout the Fungal Kingdom and much of eukaryotic life. Cdc42 orchestrates the assembly of polarized growth machinery, and the associated cytoskeletal elements, at hyphal tips, which ultimately results in polarized growth (44, 91). In the model yeast *S. cerevisiae*, the site of polarization in budding yeast cells is determined by a group of proteins collectively known as bud site selection (BSS) proteins, which act as landmarks to place Cdc42 activity. Cdc42 is part of the Ras-superfamily of monomeric GTPases that cycle between GDP and GTP bound forms, assisted by guanine nucleotide exchange factors (GEF) and GTPase activating proteins (GAP) (Fig.1.2). The GEF is thought to facilitate the formation of a GDP/GTP bound intermediate that ultimately results in loading of GTP to the active site of the GTPase (104). Juxtaposed to this is the function of the GAP, which facilitates the hydrolysis of GTP to GDP and completes the cycle. In *C. albicans*, Cdc42 has one GEF, Cdc24, and two GAPs, Bem3 and Rga2. During hyphal growth, both Cdc24 and Bem3 localize to hyphal tips, (8, 32) whereas Rga2 is sequestered away from hyphal tips, as a result of its hyperphosphorylation by the Cdc28/Hgc1 complex (105). Down-regulation of Rga2 activity during hyphal induction is thought to prolong the state of Cdc42 activation, and help to drive the constitutive state of polarized secretion associated with hyphal growth (32, 105).

IV. Models of Initiation and Maintenance of Polarized Growth

Polarized growth is initiated when a cluster of Cdc42 activity is formed within a localized region, such that only a discrete portion of the membrane protrudes. It is likely that the mechanisms which control the earliest stages of hyphal emergence are similar to those of bud initiation during yeast growth. As such, I will briefly review and highlight the relevant aspects of four current models of polarized growth initiation that are primarily based on work done in *S. cerevisiae* and *Schizosaccharomyces pombe*.

Two models proposed for bud emergence focus primarily on how Cdc42 is directed to, and accumulates within, the membrane during budding. The first model utilizes a Turing-type, activator-inhibitor mechanism to explain the process of "symmetry breaking" (i.e. polarization in the absence of bud site selection landmarks). This model demonstrates that Cdc42 activity forms a positive feedback loop that involves interactions between its GEF, Cdc24, a scaffold protein (Bem1), and the p21 activated kinase (Cla4) (17, 49, 50, 52, 53, 62). Data from these studies also show that this mechanism is sufficient to drive polarization independent of actin, as cells were still able to polarize in the presence of Latrunculin A, a drug which disrupts actin cables by binding to the free monomers (17, 50, 62). Two important assumptions are inferred in this empirical model: 1) spatial regulation of the cluster is assumed to be self-limiting and 2) membrane diffusion is negligible. That is, Cdc42-GTP does not persist long enough at the membrane (likely because of hydrolysis) for it to diffuse outward and result in a uniform membrane distribution. The second, similar model used to understand polarized growth initiation uses a different approach to follow spontaneous cell polarization events. It takes advantage of a GTP-locked version of Cdc42 to generate spontaneous clusters of Cdc42 activity even in the presence of landmarks (68, 90, 99). In this model, changes in the amount and spatial distribution of Cdc42 activity within a defined window on the membrane are critical for initiating polarized growth and generating cell shape. This model supports the hypothesis that Cdc42 activity at the membrane is limited by a combination of a slow acting, actin-based recycling mechanism, and the fast acting, Cdc42 guanine nucleotide dissociation inhibitor, Gdi1 (68, 90). However, this model neglects the important role of the Cdc42 GAPs in limiting Cdc42 activity, as Cdc42-GTP is unable to be hydrolyzed in this model. In addition, the two separate modes of action, Gdi1-and actin-based recycling, are viewed as redundant, since neither deletion by itself affects the ability to form a bud.

Closely related to these empirically based models for polarized growth is a computational model of particle clustering. The particle clustering model is used as an abstraction to understand how proteins and/or any group of macromolecules accumulate

in a localized manner (reviewed in (72)). The model, focused on polarization as an outcome of particle clustering, showed that the most feasible way for a cell to polarize involved relatively low numbers of total particles, and a low ratio of random particle membrane associations to the amount of directed feedback to the site of interaction (3). This predictive computational model is consistent with results from a biochemically "re-wired" version of the symmetry breaking system, where cells were "re-wired" to increase the strength of feedback into the system and resulted in the production of two, short-lived, but simultaneously growing buds (49, 50).

The final model of polarized growth initiation that I will discuss as part of this review comes from work in the fission yeast, *S. pombe.* *S. pombe* grows in a bipolar fashion and so, results using this model system are pertinent to the understanding of how polarized growth can be supported simultaneously at two spatially separate sites of growth. In *C. albicans*, this phenomenon occurs transiently at the close of the cell cycle when polarized growth is being directed to both the hyphal tip and the septum. In *S. pombe*, this phenomenon occurs during the transition from unipolar growth at the "old end", to bipolar growth when growth begins at the site of "New End Take Off" (NETO). Transition from unipolar to bipolar growth occurs in cells > 9μm in length (71) and was ultimately shown to be dependent on substrate availability (34). As the transition begins, there is a dynamic competition between growth sites and Cdc42 activity oscillates between the two ends. This competition is resolved when there is a sufficient increase in the physical distance between the two sites, so that the two sites no longer compete for the same pool of limiting substrates, and by the increased availability of limiting substrates through general protein synthesis (i.e. there is no time specific up-regulation).

V. Hyphal Development in *C. albicans*

Hyphal induction itself is complex, and a large number of environmental factors have been shown to influence hyphal growth (reviewed (16, 35, 87)). Single and varying combinations of growth temperature, presence of serum, pH, and nitrogen depletion are

able to activate one or more signaling pathways that result in the induction of hyphal-form growth (reviewed (43)).

Once activated, *C. albicans* hyphae undergo a two-step successive cell biological process of hyphal development, starting with germ tube (GT) formation in the first cell cycle, and then moving to mature hyphal growth in subsequent cell cycles. The transition from GT to mature hyphal growth involves induction of the hyphal transcriptional program as well as the activation of polarized growth machinery. In turn, these two processes feedback into one another to perpetuate the transition to mature hyphal growth (4, 25, 67). During GT development, there is a reduction of hyphal-repressing transcription factors, such as Nrg1, Rfg1, and Tup1, that is coordinated with the up-regulation of hyphal-promoting transcription factors (21, 57, 67) (Fig.1.3). Occurring concomitantly with these changes in gene expression is the recruitment of Cdc42 to a single site and the initiation of polarized growth (8). These processes are thought to be related to one another by the up-regulation of Ume6, a positive regulator of hyphal growth, whose expression is de-repressed upon the down regulation of Nrg1 (4, 25). Up-regulation of Ume6 is associated with more hyphal-like morphologies, even when cells are growing in conditions that do not favor hyphal morphogenesis, and increased virulence in animal models of infection (4, 25). Ume6's influence on hyphal growth is likely through its control over the level and duration of Hgc1expression (106), the sole hyphal-specific cyclin. Hgc1 complexes with the master cyclin Cdc28 to phosphorylate Rga2, a GAP of Cdc42 (Fig.1.2), and causes Rga2 to be sequestered away from hyphal tips, thereby promoting Cdc42 activity within that region. Increased activity of Cdc42 is thought to feedback through a cAMP-based signaling mechanism that promotes maintenance of hyphal specific (HSG) gene expression (8). In addition, changes in Cdc42 activity itself may also influence the strength and duration of cAMP signaling during GT formation. Activation of Cdc42 results in actin remodeling, and free actin has been shown to bind to and take part in the activation of the adenylate cyclase, Cry1(85). In addition, increased Cdc42 activity also results in increased expression of the Cdc42 GEF, Cdc24, via the transcription factor Tec1, reinforcing its own activity (8).

The interplay between hyphal gene expression and Cdc42 activity during GT development may influence the transition to mature hyphal form growth. If the level and period of cAMP signaling during GT development is sufficient, there is a secondary chromatin remodeling step, involving the histone deacetylase Hda1that blocks any further expression of Nrg1, which would result in shift back toward yeast-form growth (67). This chromatin remodeling occurs within the average time frame of the first cell cycle, and sets the hypha into its maintenance phase for successive cell cycles.

Finally, it should be noted that, despite the observation that each of the growth forms have what are considered to be defining features (as detailed in the next section), the three morphologies exist on a continuum with one another. This idea is important because the degree of feedback between the hyphal gene expression program and Cdc42 activity are thought to contribute to the overall strength of hyphal induction. For example, when the expression of Ume6 is upregulated in a stepwise fashion, cell shapes transition from yeast to pseudohyphal to hyphal (4,19). Likewise, if cAMP signaling during GT initiation doesn't reach sufficient levels to result in chromatin remodeling, Nrg1 levels will begin to increase. This results in an inability to maintain hyphal growth and a cell morphology that appears more pseudohyphal. Thus, varying degrees of induction are thought to result in the intermediate morphologies observed in culture (21, 25, 57, 58, 67).

VI. Defining Morphogenesis in *C. albicans*

Yeast, pseudohyphae, and hyphae have distinct morphological features that are thought to arise from changes in the way polarized growth is associated with cell cycle events. The most distinctive of these morphological features are commonly used to assess and categorize the growth form (reviewed in (93)). Both yeast and pseudohyphal growth are coupled to the cell cycle, such that there is an initial period of polarized growth in G1 that is soon followed by a period of isotropic growth. Then, at the close of the cell cycle, polarized secretion is redirected toward mother-bud junctions. Qualitatively, yeast cell morphology is round to oblong, and cells separate completely

from one another (Fig.1.1). Pseudohyphae have an extended period of polarized growth, but do eventually transition to isotropic growth. Thus, pseudohyphal cells appear more elongated than yeast, and although cytokinesis occurs, mother and daughter cells remain connected by constricted cell junctions. In contrast, during hyphal cell development, growth remains constitutively directed toward hyphal tips, even at the close of each cell cycle. This growth pattern yields hyphae that are highly elongated, have parallel-sided walls, and are extremely narrow (~2μm). Hyphal compartments are delineated by specialized non-constricted cell-cell junctions called septa. Although these qualitative aspects of morphology seem to be quite distinctive, the morphologies that are exhibited by cells in culture exist on more of a continuum. To better assess and categorize *C. albicans* cellular morphology, morphometric features can be measured and combined into a single unit, called the morphological index, which provides a quantitative means of comparing morphologies between cellular populations (Fig.1.4) (70). This index is often used to assess the robustness of hyphal induction by a particular strain, and in the assessment of mutant strains in which morphology is defective.

The pattern of nuclear division is another distinguishing feature exhibited by *C. albicans* growth forms. In yeast and pseudohyphae, nuclear division occurs across the mother-bud junction. In hyphae, the site of cellular division (i.e. the site of septum formation) is called the presumptum, marked by localization of septin proteins (38). During nuclear division, the nucleus migrates into the elongating hypha and divides across the presumptum. The nucleus destined for the mother cell migrates back into the basal cell, whereas the daughter nucleus remains in the apical hyphal compartment. Interestingly, presumptum formation and nuclear division show a greater dependency on hyphal length than on the time of entrance into the cell cycle (38).

One final unique feature observed in *C. albicans* hyphae is the Spitzenkörper (Spk). The Spk is a hyphal specific organelle that, with few exceptions, is found ubiquitously in hyphal-forming fungi, and its presence is often used as a hallmark of the hyphal growth form. First described in two species of *Coprinus* (22), it was later found that the Spk is an apically localized, spherical, cloud-like accumulation of vesicles (42,

48, 85) and proteins (33, 56, 88), with no defined boundaries. The most widely accepted model of Spk function postulates that it is a vesicle supply center, which provides the hyphal tip with components for growth (5, 6). Computational models of hyphal growth demonstrate that the shape and size of the Spk are mathematically related to hyphal width and give rise to the acicular shape of the hyphal tip (5, 6, 83). Further, the position of the Spk within hyphal tips has been shown to affect the directionality of growth (18). At least a portion of the vesicles that comprise the Spk are derived directly from endocytosis, because the lipophilic dye FM4-64 stains the Spk prior to any other part of the endomembrane system (39), and because assembly and maintenance of the Spk require a polarized cytoskeleton (14, 15, 33). Treatment of hyphae with drugs that disrupt F-actin causes the Spk to disperse and tip growth to become isotropic (15, 33). The presence of polarized actin cables at hyphal tips is a downstream consequence of Cdc42 activity (36). It is then logical to think that the integrity of the Spk is dependent upon Cdc42 activity at hyphal tips.

VII. Rsr1 is a Bud-Site Selection Protein That Also Impacts Morphogenesis in *C. albicans*

Bud-site selection (BSS) is a process that occurs prior to polarized growth initiation. BSS establishes a landmark for the placement of Cdc42 activity at the incipient site of bud growth, but does not influence the process of polarized growth itself. This distinction is based on work done in *S. cerevisiae* where, in the absence of proteins involved in BSS, cells are able to polarize and form buds, albeit in a disrupted pattern on the mother cell cortex (59). There are three main classes of BSS proteins: those that control axial budding (e.g. new growth adjacent to previous growth site), those that control bipolar budding (new growth either adjacent to, or directly opposite to that of the previous growth site), and those that are needed for both budding patterns (reviewed (26)). Deletion of genes encoding for this final class of BSS proteins results in cells with randomly-placed buds. Deletion of BSS proteins in *S. cerevisiae* results in disrupted budding pattern, but show no other obvious effects on the morphology of the cell or in

the efficacy of budding (11, 28). In *C. albicans* this does not appear to be the case for one such BSS protein, Rsr1.

Deletion of Rsr1, as well as its GAP Bud2, in *C. albicans* results in an enlarged cell phenotype in all growth forms (45). *C. albicans rsr1*Δ/Δ and *bud2*Δ/Δ strains appeared more pseudohyphal, and were curvier than wild-type (WT) strains when grown in hyphal-inducing conditions. In addition, deletion of Bud2 results in an increased branching frequency, as compared to WT. Changes in the organization of the actin cytoskeleton were also detected in *rsr1*Δ/Δ and *bud2*Δ/Δ strains when grown under yeast- and hyphal-inducing conditions. The asymmetric distribution of actin patches was disrupted in both yeast and hyphae of *rsr1*Δ/Δ and *bud2*Δ/Δ cells, and hyphae of both strains showed fewer polarized actin cables extending from hyphal tips, than were observed in WT cells (45). These disruptions in the cellular morphology suggest that Rsr1 has an expanded role in cell growth in *C. albicans*.

In *S. cerevisiae,* Rsr1 was first described as a multi-copy suppressor of temperature-sensitive (Ts^-) mutations in Cdc24 (11) and Ras2 (80). The regulators of Rsr1, Bud5 (GEF) and Bud2 (GAP) (Fig.1.5), were identified in a similar manner (10). Rsr1 was also shown to have direct physical interactions with Cdc42 and Cdc24 in *S. cerevisiae* (61) (Fig.1.3B). These interactions are likely to be conserved at some level in *C. albicans*. The enlarged cell morphologies observed in *rsr1*Δ/Δ strains are similar to those observed in Cdc24 and Cdc42 mutant strains (1, 45). This observation not only supports that the interactions between Rsr1 and Cdc42 are conserved in *C. albicans*, but also suggest that loss of Rsr1 in *C. albicans* may disrupt the activity of Cdc42. In *S. cerevisiae* and *C. albicans* Rsr1 localizes throughout the entire yeast cell membrane, and also becomes enriched at the incipient bud site during initial bud formation (60). As the cell progresses through the cell cycle, the localization of Rsr1 becomes more evenly distributed throughout the plasma membrane. At cytokinesis, the localization of Rsr1 is enriched at the site of the cytokinetic ring. In *S. cerevisiae* the observed changes in Rsr1 localization are thought to be related to the ability of Rsr1 to dimerize with itself. Using bimolecular fluorescence complementation, dimerization of Rsr1 was shown to occur at

bud tips and to be dependent on its activation(59). In *S. cerevisiae*, the localization of the Rsr1 regulators, Bud5 and Bud2, are thought to control the localization of Rsr1 activity during the cell cycle. In G1, both Bud5 and Bud2 localize to the presumptive bud site (75). During budding, Bud2 moves to the mother-bud neck and then becomes delocalized in M-phase. Bud5 remains at the site of bud growth during bud emergence and then, during M-phase, localizes to a double ring at the mother-bud neck

VIII. Current Objectives

Previous work (20, 45) demonstrates that the proposed role for Rsr1 in *S. cerevisiae* in BSS does not explain the morphological phenotypes of *C. albicans rsr1*Δ/Δ strains. The overall increase in cell size and more pseudohyphal appearance of *rsr1*Δ/Δ hyphae suggests that, in *C. albicans*, Rsr1 is involved in the initiation and maintenance of growth, in addition to its functionality as a landmark. Based on these ideas, the central hypothesis of this work is that Rsr1 impacts morphogenesis through the regulation of polarized growth machinery.

The work herein aims to test this hypothesis by analyzing the effects of loss, as well as changes in the efficiency, of Rsr1 cycling on downstream effectors of Cdc42, a keystone in the process of polarized growth. Chapter 2 of this thesis addresses how the loss of Rsr1 impacts Cdc42 activity at hyphal tips. In Chapter 3, I assess the contributions of the GTP and GDP bound forms of Rsr1 to the process of GT emergence and hyphal maintenance, and how changes in Rsr1 cycling impact the downstream outcomes of Cdc42 activity.

IX. Chapter 1 Figures

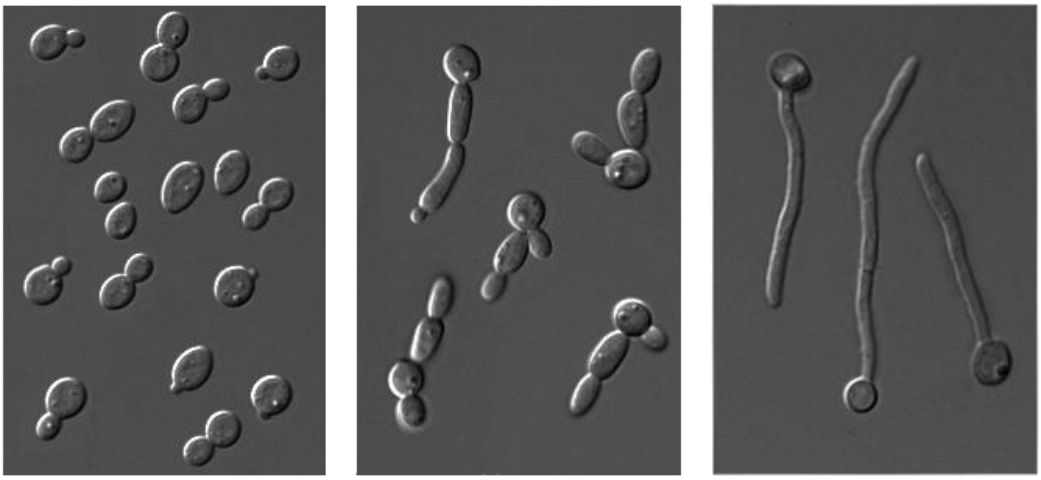

Fig.1.1. *Candida albicans* Morphologies. Differental interference contrast (DIC) images depicting three morphologies of *C. albicans.* From left to right: yeast, pseudohyphae, and hyphae. Image modified from *Candida and Candidiasis* 2nd edtion(23).

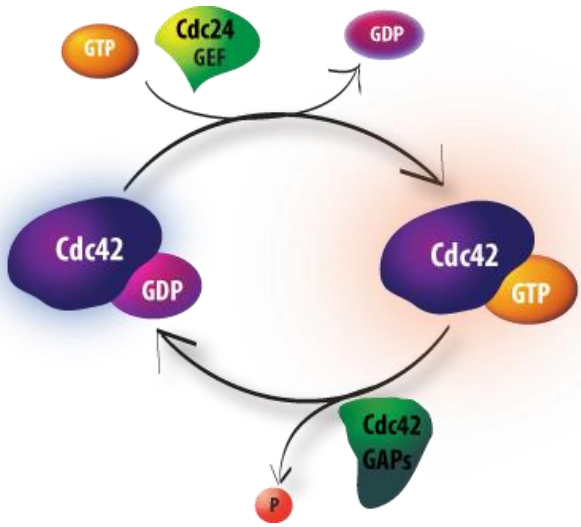

Fig.1.2. Cdc42 Cycling. A diagram of Cdc42 cycling between GTP and GDP bound forms. The Cdc42 GEF is Cdc24, and there are two known GAPs for Cdc42 in *C. albicans*, Rga2 and Bem3.

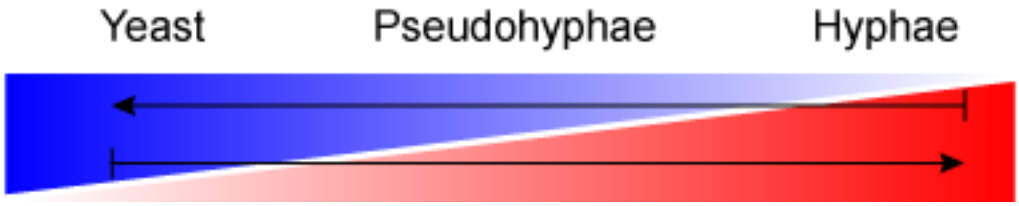

Fig.1.3. Induction of the Hyphal Program. This diagram depicts the down regulation of hyphal repressing transcription factors (blue), and the up regulation of hyphal promoting transcription factors (red) that are needed for transcriptional and cell biological expression of the hyphal morphogenesis program. The converse relationship is thought to be true for yeast morphogenesis.

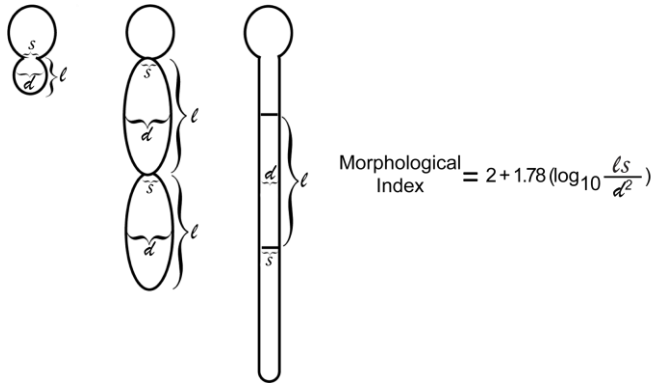

Fig.1.4. Morphological Index (MI) in *C. albicans*. A diagrammatic depiction of the components of the MI in three *C. albicans* morphologies, where d = diameter at the widest point of the cell, s = the width of the junction (constriction and/or septum) between cells, and ℓ = the length of the cellular compartment. Because the yeast, pseudohyphal and hyphal morphologies of *C. albicans* exist on a continuum, the calculated MIs are categorized into ranges. Cells that have an MI of <2 are considered yeast or elongated yeast, MIs between 2.5-3.4 are considered pseudohyphal, and MIs >3.4 are categorized as true hyphae (70).

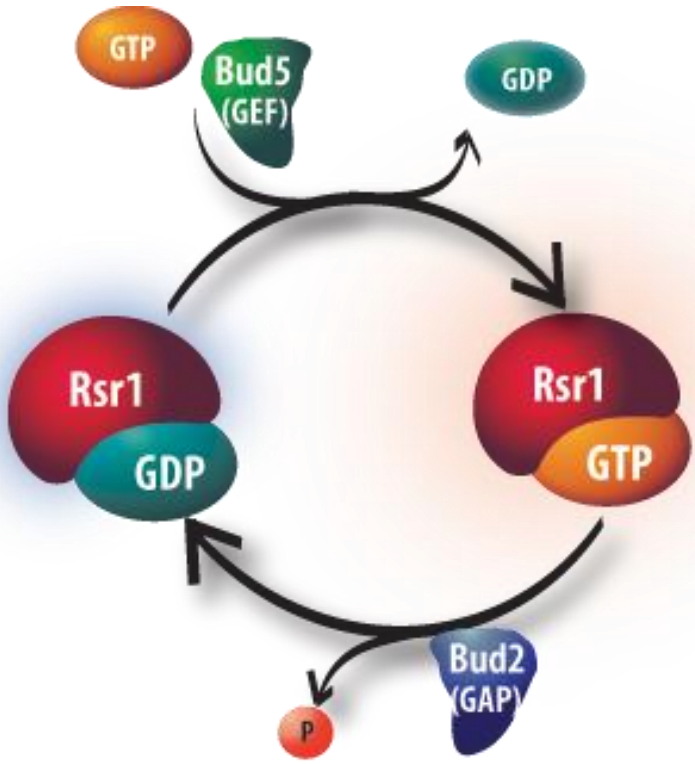

Fig.1.5. Rsr1 Cycling A diagram depicting Rsr1cycling between GDP and GTP bound forms. Its GEF, Bud5, removes GDP and aids in the loading of GTP. The GAP, Bud2, facilitates the hydrolysis of GTP.

Chapter 2

Rsr1 Focuses Cdc42 Activity at Hyphal Tips and Promotes Maintenance of Hyphal Development in *Candida albicans*

Rebecca Pulver[2], Timothy Heisel [1], Sara Gonia[1], Robert Robins[1], Jennifer Norton[1*], Paula Haynes[1†], Cheryl A. Gale[1,2]

This chapter is an original research manuscript, previously published. Reproduced with permission from *Eukaryotic Cell April 2013 vol. 12 no. 4 482-495*

I. Introduction

Fungal hyphae are able to elongate over large distances and must allocate their cellular resources in order to maintain extremely polarized growth for extended periods of time. The multimorphic opportunistic fungal pathogen *Candida albicans* provides a useful model system in which to investigate the basic cell biological and genetic mechanisms that generate highly polarized cell shapes and the requirements for hyphal development. *C. albicans* has a true hyphal growth form, as well as pseudohyphal and yeast forms, and reversibly switches between these morphologies depending on environmental conditions (reviewed in (93)). Yeast cells are ellipsoid in shape, propagate by budding, and undergo cytokinesis and cell separation. Pseudohyphae are more elongated than yeast and do not undergo cell separation, resulting in the formation of chains of elongated daughter cells. Hyphae, in contrast, are extremely elongated narrow cells, and their development can be thought of as two continuous stages, early growth and development of germ tubes (GTs) followed by the development and maintenance of mature hyphae. GTs enter the maintenance phase of polarized growth, transitioning to mature hyphae, after the formation of the first septum, a specialized structure that delimits cellular compartments. Whereas morphogenesis mechanisms in *C. albicans* yeast and pseudohyphae appear to follow those of the similar morphologies in *S. cerevisiae*, it is unclear if, or how, these mechanisms are modified to enable the development of the highly elongated hyphal form.

Localized activation of Rho GTPases underlies actin-based cell polarization and morphogenesis in eukaryotic cell systems (reviewed in (55)). In *C. albicans*, the role of the essential Rho GTPase, Cdc42, is thought to impact hyphal development in *C. albicans* in at least two ways. First, the amount of Cdc42 affects the morphogenesis program at the transcriptional level. Strains expressing reduced levels of Cdc42 have decreased expression of hyphal-specific genes, some of which are important for production of hyphal morphogenesis characteristics and hyphal-associated virulence factors (8). Second, Cdc42 activates and localizes proteins needed for polarized growth.

Decreasing cellular levels of Cdc42 results in both yeast and hyphae that have larger and rounder cell shapes indicative of a defect in polarized growth (7, 96, 97). Clusters of Cdc42 localize at incipient growth sites periodically during bud initiation in yeast while during *C. albicans* hyphal morphogenesis, Cdc42 clusters localize constitutively to hyphal tips in an F-actin dependent manner (46). In yeast cells, growth sites are dictated by internal landmarks such as the Ras-like GTPase Rsr1 (45). In hyphae, although germ tube emergence sites can be directed by external electrical cues(20), it is unclear if an internal landmark mechanism directs germ tube emergence sites in non-cued conditions (27, 47). In the end, effectors of Cdc42 are recruited to these growth initiation sites and direct the polarization of the actin cytoskeleton to ultimately target secretion to the daughter cell apex.

C. albicans hyphae contain a tip-localized polarity structure, not found in yeast and pseudohyphae, called a Spitzenkörper (Spk). The Spk is a developmental hallmark of hyphal growth that is observed in the majority of cultured filamentous fungi, and is required for hyphal cell shape (reviewed in (44)). Formation and maintenance of the Spk require that polarized actin cables, a downstream result of localized Cdc42 activity, be directed toward hyphal tips (33). Spks are composed of accumulations of vesicles and proteins and, as a unit, act as reservoirs to supply extending tips with the components needed to maintain continuous hyphal growth (5, 84). Although it is clear that polarity factors such as the Spk need to be maintained constitutively at cell apices for hyphal growth to continue, the mechanism by which this occurs is not understood.

Proposed mechanisms for polarity establishment and maintenance have been derived from results of studies using *S. cerevisiae*. These studies focused on how cortical Cdc42 clusters of an optimized distribution are formed and stabilized to promote bud initiation and early bud growth. These mechanisms require that activated Cdc42 be continually supplied to sites of growth while its lateral diffusion at the membrane is simultaneously restricted in order to generate the discrete focus of Cdc42 activity needed for growth initiation (reviewed in (72)). In addition, the size of the Cdc42 cluster has been shown to influence the shape of the growing daughter cell (90). This optimal Cdc42

cluster, or "window", is proposed to be achieved by a combination of processes including positive feedback mechanisms that increase Cdc42 activity at the growth site, membrane diffusion, local limitation of substrates (e.g. Cdc42, its regulators and/or effectors), and active removal of Cdc42 from the membrane adjacent to the site of growth (34, 53, 90). It remains unknown how, and if, similar Cdc42 regulatory mechanisms are employed to regulate cell shape and maintain continuous polarization during *C. albicans* hyphal morphogenesis.

We previously reported that *C. albicans* strains lacking the landmark GTPase Rsr1 have defects in yeast and hyphal morphogenesis; *rsr1*Δ/Δ yeast cells are larger and rounder, and hyphae are wider, than wild-type (WT) control strains (45). These phenotypes are similar to those observed in *C. albicans* strains with reduced expression of Cdc42 (20) and were unexpected because the ortholog of Rsr1 in *S. cerevisiae*, although interacting physically with Cdc42, is important for bud site selection but not for polarized growth(11). Thus, we hypothesized that *C. albicans* Rsr1 has a role in polarized growth and morphogenesis, beyond that of simply determining the location of Cdc42 activity.

In the current study, we aimed to understand how Rsr1 is involved in the assembly and/or maintenance of tip localized polarity factors and how the localization features of these factors correlate with hyphal morphogenesis. Overall, our results are consistent with the idea that, in *C. albicans*, Rsr1 is needed for the efficient assembly of a focused Cdc42 cluster in GTs that, in turn, is important for the continued maintenance of hyphal development.

II. Materials & Methods

Media and Growth Conditions

Strains were grown on synthetic dextrose complete (SDC) (89) agar medium at 30°C, followed by transfer of a colony into SDC liquid media at 30°C, and grown overnight to obtain stationary phase yeast-form cultures, unless otherwise noted. For all

imaging experiments, hyphae were induced by growth of 25 µL of overnight yeast cultures in 1 mL of pre-warmed (37°C) SDC medium + 10% bovine serum. Uridine (80 µg/ml) was added to all media, except when selecting for uridine prototrophs during strain constructions. Regulatable expression of genes from the *MET3* promoter was achieved by growth of strains in media lacking (expression) or containing (repression) methionine and cysteine, respectively, as previously described (24).

For quantitative fluorescence indexing and fluorescent fusion protein localization experiments in hyphae, 150 µL of diluted cells were placed onto poly-L-lysine (PLL) coated slides and grown in humidified chambers at 37°C. For time-lapse microscopy, hyphae were grown on agarose pads with cover slips applied (except in FM4-64 staining experiments). Growth times were established relative to the completion of the first cell cycle, with 30 and 90 min (depending on the experiment) representing GTs (no septa had formed) and 3hr and 4hr representing mature hyphae (septa were present).

Strains and Strain Constructions

Yeast strains used in this study are listed in Table 1. Fluorescent protein fusions were constructed by PCR-mediated gene modification as previously described (40, 41), using the primers listed in Supplemental Table 1. Constructions were verified by PCR using primers targeting sequences outside of the sites of integration. In addition, expression of fluorescent proteins was evaluated by fluorescence microscopy and western blotting as described below.

Due to the lack of an available auxotrophy in the original *RSR1*-reintegrant control strain, it was necessary to reconstruct *rsr1* null and re-integrant strains in order to introduce *MLC1-YFP* and *BEM1-YFP* fusions into them. To do this, the two *RSR1* alleles were sequentially disrupted in *C. albicans* strain BWP17 by PCR-mediated gene modification using the *dpl200* sequence as previously described (100) using primers 1460 and 1265 (Supplemental Table 1) and plasmid p1653 (100) as the DNA template. Disruption of both *RSR1* alleles in the resulting strain, CA12363, was verified by PCR using primer sequences located outside of the sites of integration and by RT-PCR using

primers targeting *RSR1* mRNA (data not shown). To construct *RSR1*-reintegrant control strains, disrupted and wild-type *RSR1* sequences were integrated into an *rsr1::dpl200* locus using linearized pMG2157 and pMG2128 to construct the control strains CA12431 (*rsr1::rsr1*/*rsr1*) and CA12430 (*RSR1::rsr1/rsr1*), respectively, as previously described (20, 45). Strain constructions were verified by PCR using primer sets that distinguished integration of the disrupted *rsr1* and full-length *RSR1* sequences into the promoter region of the deleted *rsr1* locus and confirmed by RT-PCR of *RSR1* mRNA (data not shown).

Western Blotting

500 µL of yeast cell culture were harvested from overnight cultures, washed in water, inoculated into 10 ml of hyphal-inducing medium, and grown at 37°C to obtain GTs and mature hyphae. The entire 10 ml of each hyphal culture was harvested, washed and resuspended in 150 µL of 4% ULSB (20 mM Tris, pH 6.8, 10% glycerol, 0.005% bromophenol blue, 6 M Urea, 4% SDS and 20 mM dithiothreitol). Cell lysis and denaturation of proteins was achieved in one step by heating the resuspended cells in ULSB for 5 min at 100°C. Protein concentrations of the resulting lysates were determined spectrophotometrically (A280) and diluted to equalize the concentrations of the samples. Protein samples were separated on SDS–polyacrylamide gels (12%) and then transferred to a PVDF membrane, blocked for 30 min with 2% milk buffer (skim milk in TBST [20 mM Tris, pH 7.6, 137 mM NaCl, 0.1% Tween-20]), and incubated with the appropriate primary antibody (mouse-α-GFP: Roche, Indianapolis, IN, 1:2000; rat-anti-Cdc42: Santa Cruz Biotechnology, Santa Cruz, CA, 1:5000; or rat-anti-α-tubulin: Ab-Cam, Cambridge, MA, 1:5000) diluted in 0.2% milk buffer for 1 h. Blots were washed in TBST and incubated with the appropriate horseradish peroxidase-conjugated secondary antibody (goat-α-mouse IgG: Santa Cruz Biotechnology, Santa Cruz, CA, 1:10,000; goat-α-rat IgG: Santa Cruz Biotechnology, Santa Cruz, CA, 1:10,000; or goat-α-rabbit IgG: Southern Biotech, Birmingham, AL, 1:10,000) diluted in 0.2% milk buffer for 1 h. The blots were washed again in TBST and developed using the Supersignal Fempto Chemiluminescent reagent (Pierce, Rockford, IL). The amount of protein

detected (signal intensity) was quantified using an Alpha-Innotech Chemi-Imager (San Leandro, CA) and Image-Quant image analysis software (GE Healthcare Biosciences, Pittsburgh, PA). The background-subtracted intensity was obtained using Image J (82), and the ratio of the amount of the protein of interest to that of tubulin was calculated.

Image Acquisition and Processing

All images (except for those obtained during fluorescence recovery after photobleaching (FRAP)) were collected on a Nikon E600 microscope equipped with 60X/1.4 NA and 100X/1.4 NA objectives, FCS2 objective heaters (Bioptechs, Butler, PA), and epifluorescence. MetaMorph version 6.3r7 (Molecular Devices LLC, Sunnyvale, CA) was used for acquisition and processing of all images. Differential interference contrast (DIC) images were collected in conjunction with fluorescent images in all cases using 50 ms exposures. Final representative images for publication were adjusted for brightness and contrast, cropped and resized as a group, for each set of experiments using Photoshop CS3 (Adobe Systems Inc, San Jose, CA).

Imaging YFP-Rsr1, YFP-Bud5, and YFP-Bud2 localization

Images of YFP-tagged versions of Rsr1 (exposure 800ms, range 10, step size 2, 5 steps), Bud5 (exposure 800ms, range 10, step size 5, 3 steps), and Bud2 (exposure 600ms, range 10, step size 5, 3 steps) were collected using a 60X objective. Resultant stacked images were merged using summation and the intensities were adjusted in MetaMorph before being exported to, and scaled together, in Photoshop.

Imaging FM4-64-stained hyphae

To obtain images used in determining fluorescence indices, hyphae were stained with 165 mM FM4-64 for 10 min (39). Excess medium and stain were aspirated and cells were imaged as soon as technically feasible using the 60X objective. Approximately 10 images were captured for each strain using identical acquisition settings (10 ms exposure, shutter open between steps, 2x2 binning, range 10, step size 5, 3 steps), and replicate experiments were carried out on three separate days. To assess for differences in FM4-64 uptake between mutant and control strains, a mixed subculture of WT cells expressing

Nop1-GFP and *rsr1*Δ/Δ cells was placed on PLL-coated slides, and grown in hyphal-inducing media to obtain either GTs or mature hyphae. Cells were stained as before with FM4-64, cover slips were sealed to slides with stopcock grease, and the cells were imaged using a 60X objective heated to 37°C. A GFP image (50ms exposure time) was captured after completion of the time-lapse acquisition to identify WT (GFP-expressing) hyphae during quantification. FM4-64 localization was imaged over 1 hr at 10 min intervals using identical acquisition settings to those stated above.

Imaging Mlc1-YFP and Bem1-YFP localization in hyphae

All images were acquired using a 60X objective heated to 37°C using the following acquisition settings: for Mlc1-YFP, 500 ms exposure, shutter closed between steps, 2x2 binning, step size 5, 3 steps; for Bem1-YFP, acquisition settings were the same except that 300 ms exposure times were used. The acquisition settings used in the time series were identical to those used in measuring fluorescence intensity indices, with images being obtained every 2 min for the length of the movie. The resultant time-lapse stacks were assembled into a time series as Z-projections using the "Review Multi Dimensional Data" tool of MetaMorph.

Quantification of Fluorescent Signals

Determination of fluorescence intensity index (FM4-64, Mlc1-YFP, and Bem1-YFP)

Stacked images were merged using summation, background correction was performed by batch processing, and then each image was thresholded for quantification manually. Thresholds were established by visually highlighting the region of tip-localized signal for the majority of hyphae in each image. A circular region of interest (ROI) was created around each hyphal tip in order to collect the mean integrated intensity (fluorescence intensity) and the area of the region. The width of the tip-localized signal was obtained using the line tool of MetaMorph and drawing across what was visibly the widest part of the thresholded tip signal. Fluorescence intensity, signal area, and signal width were collected using the "Region Measurements" tool in MetaMorph and exported to

Microsoft Excel (2003). The intensity index was calculated for each individually analyzed cell by dividing the integrated fluorescence intensity per unit area by the width of the signal, which, for tip-localized proteins, approximates the hyphal tip width.

$$Intensity\ Index = \frac{Integrated\ fluorescence\ intensity\ per\ unit\ area}{Width\ of\ tip\ signal}$$

Analysis of FM4-64 uptake dynamics

Timing of dye uptake was determined by visually assessing vacuolar staining in the mixed WT and *rsr1*Δ/Δ hyphal culture at each time frame of the series. The reported times of vacuolar staining represent the 10 min staining period plus the time from the first frame of the movie until the appearance of vacuolar staining in both strains (this occurred simultaneously). For the quantification of final fluorescence intensity, the final frame of the time-lapse series (red channel) and the final still image of Nop1-GFP expressing (WT) cells (green channel) were processed using "no neighbors" 2-D deconvolution in MetaMorph. WT and *rsr1*Δ/Δ hyphae were identified, and measurements were taken using the mean integrated fluorescence intensity of a fixed rectangular region. The region was placed on an in-focus portion of the hyphal cell membrane and spanned into a portion of the intracellular space for both strains in the same field. Background fluorescence intensities were subtracted, and measurements were taken from at least one hypha, per strain, per movie (the final frame of the time-lapse series), for each of three experiments performed on different days.

Determination of percent of hyphae with tip-localized fluorescent signals

Images that were used to determine fluorescence intensity indices were also used to determine the overall percentage of hyphae displaying tip localization of polarity proteins (Mlc1 or Bem1). Hyphal tips that were in focus in DIC images were marked with the "Circular ROI" tool of MetaMorph and counted to determine the total number of hyphae in the analysis. The ROI's were transferred from the DIC image to the corresponding fluorescent image and visible tip-localized signals were manually counted and reported as a percentage of total hyphae.

Fluorescence Recovery after Photobleaching (FRAP)

WT and *rsr1*Δ/Δ strains were grown on cover slips in hyphal-inducing conditions, stained with 5 µL of 165 mM FM4-64 for 2 min and washed prior to imaging on an inverted Olympus Fluoroveiw 2000 microscope (60x/1.42 UPlanApoN objective using 3x digital zoom). A fixed size circular ROI was placed over the FM4-64-stained Spk of each hypha. Three images were collected for baseline fluorescence measurements before bleaching for 2.5 sec using a 408 nm laser. Recovery images were collected at ~1 frame/sec, using the streaming function, until recovery reached a plateau (30-40 sec). Recovery intensities were normalized (78), and resulting recovery curves were fitted using the non-linear regression tool (f=a*(1-exp(-b*x))) of SigmaPlot (version 10.0, Systat Software, San Jose, CA). Time to half-max recovery ($\tau_{1/2}$) values for GTs and mature hyphae of each strain were collected and analyzed for differences (see statistical methods below).

Quantitative Real-Time PCR (qPCR)

Strains were inoculated into yeast peptone adenine dextrose (YPAD; (89)) media and grown overnight at 30°C. Hyphal growth was induced by inoculating overnight cultures as a 1:20 dilution into YPAD + 10% serum (pre-warmed to 37°C) and cells were grown to obtain GTs and mature hyphae. Pseudohyphae were induced by inoculating overnight cultures into YAPD at pH 6.0 and growing at 36°C (74), to time-match the induction times of GT's and mature hyphae. 1.5 ml of cell culture were harvested for RNA extraction using the MasterPure Yeast RNA Purification kit (Epicentre Biotechnologies, Madison, WI), per the manufacturer's instructions. Isolated nucleic acids were then treated with DNAse, RNA quantities were determined using a NanoDrop ND-1000 spectrophotometer (NanoDrop, Wilmington, DE) and RNA (1 µg) was then converted to cDNA using the High-Capacity RNA-to-cDNA Kit (Applied Biosystems, Carlsbad, CA) according to the manufacturer's instructions. qPCR was performed using a Roche LightCycler 480 instrument (Roche Diagnostics, Indianapolis, IN) equipped with LightCycler 480 Software (release 1.5.0 SP3). Primer sequences for hyphal-specific

genes (HSGs) and actin (*ACT1*) were as previously published (8) and are reproduced in Supplemental Table 2. The LightCycler 480 SYBR Green I Master kit (Roche) was used to perform all qPCR experiments, and reactions were set up following the manufacturer's instructions. A total quantity of 0.025 µg of cDNA was loaded into each 20 µl reaction along with 0.25 µM of each primer and 10 µl of 2x Master Mix. Samples were subjected to the following PCR program: a pre-incubation step of 95°C for 5 minutes; an amplification step of 95°C for 10 seconds, 60°C for 10 seconds, and 72°C for 10 seconds, repeated for 45 total cycles, with fluorescence readings taken once during the 72°C stage; and finally a melting curve step of 95°C for 5 seconds, 60°C for 1 minute, and a final temperature of 97°C that is achieved slowly (0.11°C/second), with fluorescence readings being taken continuously. All *ACT1*-specific reactions were done in triplicate on each plate, and all HSG-specific reactions were done in duplicate on each plate. Each experiment was repeated on three separate days using newly obtained RNA from newly grown cells. Each experimental day analyzed two identical plates that were set up together and each plate was run consecutively, with as little time between runs as possible. To determine the relative expression of a given HSG for a given day, the daily mean Cp for that gene was divided by the daily mean Cp for *ACT1*.

Statistical methods

Choice of data set for intensity index determinations

For experiments where the intensity index was calculated, all cells with localizable signals were counted in an effort to obtain the "truest" possible mean for each strain. However, the disparity in the number of cells displaying tip-localized signals left the data sets unbalanced. Thus, a random sample was selected from the original data sets using SPSS 16 (IBM, Armonk, NY). The resultant randomized sample was used in the comparative analysis if it met the following three conditions: 1) data set contained approximately equal numbers of cells for each strain used in the experiment, 2) approximately equal proportions of GTs and mature hyphae were represented in the data

set for each strain, 3) a minimum of 15% of the total cells analyzed were represented by each date of replication, across all days of the experiments.

Statistical analyses

All data analyzed statistically were repeated on at least three different days. Differences were assessed with either univariate or, when appropriate, multivariate analyses using a general linear model in SPSS 16. As part of the analysis, if the main statistical effect of day was significant in the experimental analysis, "date" was blocked in all subsequent analyses. In cases where a blocked ANOVA was used, graphs display error bars using standard error of the mean (SEM), and where unblocked analyses were used, error bars represent 95% confidence intervals (CI). Full factorial analysis of dependent variable(s) against all fixed factors was performed initially (when appropriate), and then separate subsequent assessments for within-strain (file split by strain, fixed factor = growth stage) and between-strain (file split by growth stage, fixed factor = strain) differences were performed. When the number of comparable strains in the analysis was greater than two, post-hoc separation of means procedures were performed using Tukey's honestly significant differences, or when a blocked analysis was performed, least significant differences was used.

III. Results

Rsr1 regulators are localized to the tips of hyphae. We previously reported that Rsr1-YFP localizes to the entire cell membrane of hyphae ((45) and Fig.2.1A). This diffuse membrane localization, while similar to that observed in *S. cerevisiae* and in *Ashbya gossypii* (9, 74), was unexpected because strains lacking Rsr1 have defects specifically at hyphal tips. To ask if Rsr1 cycling is localized to hyphal tips, we analyzed the localization of tagged versions of the Rsr1 GAP, Bud2, and its GEF, Bud5. We looked at the localization of these proteins at the two stages of hyphal development, using the presence of the first DIC-refractive septa (when chitin is visible at septa using DIC optics) as a marker of developmental time. Cells grown in hyphal-inducing conditions

for short periods of time, without septa, were deemed GTs, whereas cells grown for longer times, such that septa were present, were considered mature hyphae. YFP-Bud5 localized to the apices of GT and mature hyphal tips in a discrete crescent (Fig.2.1B) reminiscent of the polarisome proteins, Bud6 and Spa2 (33). When expressed from its native promoter, Bud2-YFP was very dim and fairly long exposure times were needed to resolve a discrete signal. In these images, Bud2 was enriched just behind the apex of hyphal tips appearing as a faint ring at the membrane with a relatively reduced intensity at the extreme tip (data not shown). The localization pattern was also visualized when YFP-Bud2 was expressed from the regulatable *MET3* promoter (Fig.2.1C, asterisks). In addition, YFP-Bud2 was enriched in the concave angle of some curved hyphae (Fig.2.1C, arrowhead) and showed a discrete localization to septa (Fig.2.1C, arrows), based on co-localization with Cdc12 (data not shown). The dual localization of YFP-Bud2 and YFP-Bud5 at both hyphal tips and septa suggests that their localizations during *C. albicans* hyphal morphogenesis do not vary with the cell cycle as they do during yeast-form growth (69). Thus, the localizations of the Rsr1 GAP and GEF suggest that Rsr1 activity is continuously poised to act at the tips of hyphae where polarized growth occurs constitutively. Further, the differential localizations of Bud2 and Bud5 imply that Rsr1-GTP is enriched at the hyphal apex, whereas Rsr1-GDP is favored subapically.

The vesicular Spk is stably maintained during WT hyphal development. The presence of a Spk is associated with hyphal morphogenesis in *C. albicans* and other filamentous fungi. The vesicle component of the Spk can be visualized using FM4-64, a fluorescent lipophilic dye that is internalized by endocytosis and thereby stains the endomembrane system, which is contiguous with the Spk (33, 39). Because of its intimate association with hyphal growth, Spk integrity can be thought of as a down-stream developmental characteristic of hyphal morphogenesis signaling pathways. However, because the overall appearance of the Spk varies considerably, even during wild-type (WT) hyphal development (Fig.2.2A), we developed an intensity index (Materials & Methods) to quantitatively describe and compare, with more accuracy and precision, Spks in WT and mutant strains with defects in polarized growth. The intensity

index is a unidimensional metric akin to the morphological index described by Merson-Davies and Odds (70). It takes into account the integrated fluorescence intensity, per unit area of a localized signal (hereafter referred to simply as the fluorescence intensity), and the distribution (width) of that fluorescent signal, which approximates the hyphal tip width. This yields a single unit that describes tip signals as a proportion of the hyphal width, and facilitates the comparison of fluorescent signals in cells of different sizes. Furthermore, differences between intensity indices of two strains can be further analyzed to determine which individual index parameter (e.g. fluorescence intensity, area, or width) contributes most to changes in the intensity index.

Between-stage analysis of FM4-64 signal characteristics at hyphal tips revealed that the intensity indices of WT Spks were the same in GTs and mature hyphae. Analysis of individual index parameters showed that Spks of mature hyphae had significantly increased fluorescence intensities, as compared to WT GTs ($p < 0.05$). However, the increase in intensity did not result in an increased index for mature hyphae because of a relatively small increase in the size (i.e. area and width) of the signal. Overall, the FM4-64 intensity index results indicate that despite changes in individual localization characteristics, WT Spk integrity is not different between germ tubes and mature hyphae.

Rsr1 function impacts the amount and spatial distribution of vesicles in the Spk. The morphological phenotypes of *rsr1*Δ/Δ strains indicate a defect in polarized growth (20, 45). Because the Spk is an essential organelle for polarized secretion (33), we asked if Spk characteristics differed between GTs and mature hyphae of *rsr1*Δ/Δ and WT strains. In GTs, the mean intensity index of *rsr1*Δ/Δ Spks was similar to that of WT Spks (Fig.2.2B). When the individual components used to calculate the index were compared, *rsr1*Δ/Δ GTs had significantly higher vesicle intensities, areas, and widths. This indicates that although the Spks of *rsr1*Δ/Δ GTs are not identical to those of WT, they are proportionally equal (Fig.2.2B, C). In contrast, in mature hyphae, the intensity index of *rsr1*Δ/Δ Spks was significantly less than that of WT Spks. In addition, the Spk intensity index of mature *rsr1*Δ/Δ hyphae was significantly less than that of *rsr1*Δ/Δ GTs, indicating that Spk integrity is reduced over time in strains lacking Rsr1 ($p < 0.001$,

Fig.2.2C). The reduced Spk intensity index of mature *rsr1*Δ/Δ hyphae was due to a decrease in intensity without a corresponding decrease in width or area of the signal. Importantly, loss of Spk integrity was also observed when we compared *RSR1*-expressing and non-expressing control strains (Supplemental Fig.2.1), indicating that Spk phenotypes in the *rsr1*Δ/Δ strain were due to deletion of *RSR1* and not to non-specific mutations introduced during strain construction.

The observation that overall Spk intensities and intensity indices were lower in mature *rsr1*Δ/Δ hyphae raised the possibility that vesicle delivery to hyphal tips diminishes over time in the *rsr1*Δ/Δ strain. To assess differences in vesicle delivery between GTs and mature stages of hyphal growth within each strain, FM4-64-stained membranes at the tips of WT and *rsr1*Δ/Δ hyphae were studied using Fluorescence Recovery After Photobleaching (FRAP) (Supplemental Table 2). A significant decrease in recovery rates was observed between *rsr1*Δ/Δ GTs and mature hyphae (p=0.032). In contrast, no differences were observed when we compared the recovery rates of WT GTs and mature hyphae. The change in rate observed between *rsr1*Δ/Δ GTs and mature hyphae was specific to hyphal tips since no change in recovery rate was detected between the developmental stages when regions 10 μm behind the hyphal tip were assessed (Supplemental Table 2). The change in recovery rates seen between *rsr1*Δ/Δ GTs and mature hyphae is consistent with the data from the FM4-64 index experiments that showed a significant decrease in vesicle intensity in mature *rsr1*Δ/Δ hyphae as compared to *rsr1*Δ/Δ GTs ($P < 0.001$). Taken together, the results from the FM4-64 index analysis and FRAP experiments infer that Rsr1 is involved in regulating the amount, spatial distribution, and recruitment of vesicles to hyphal tips. Further, the changes observed between stages of growth in *rsr1*Δ/Δ strains indicate that the requirements for Rsr1 may differ between early (GT) and mature hyphae.

FM4-64 staining of the Spk and other cellular structures requires uptake of the dye by endocytosis. To control for potential differences in dye uptake between *rsr1*Δ/Δ and WT strains, we compared them with respect to rate of vacuolar staining and the final fluorescence intensity of FM4-64 in both GTs and mature hyphae. To eliminate

differences in the timing of dye uptake due to preparation of the strains for imaging, we mixed the control WT strain marked with a nuclear GFP reporter with a non-fluorescent *rsr1*Δ/Δ strain, and imaged FM4-64 uptake simultaneously in the two strains. Both strains internalized FM4-64 at similar rates, for both GTs and mature hyphae, with vacuolar staining being visible by 40-50 minutes in all cases, which is within the range of time observed by other investigators (101). In addition, the final mean fluorescence intensity of cell membranes was not different between WT and *rsr1*Δ/Δ strains or within either strain between developmental stages (Supplemental Fig.2.2). Thus, the differences in vesicle intensity seen in *rsr1*Δ/Δ hyphae are not due to differences in the ability of WT and *rsr1*Δ/Δ strains to internalize FM4-64. Further, the data supports the conclusion that Rsr1 is not important for endocytosis, but rather for polarized vesicle trafficking to hyphal tips.

Rsr1 is important for Mlc1 localization within the Spk. The disruption of Spk vesicle integrity in mature *rsr1*Δ/Δ hyphae raised the possibility that Rsr1 is important for the focused localization of other Spk components. Co-localization of FM4-64 stained Spk vesicles with motor-associated proteins like myosin light-chain 1 (Mlc1) (33) indicate that vesicle delivery occurs, at least partly, via actin and myosin. We used Mlc1, fused to YFP, as a representative protein component of the Spk, and compared its signal characteristics in GTs and mature hyphae of *rsr1*Δ/Δ and WT strains (Fig.2.3A). In GTs, there was no difference between the strains with respect to the number of hyphal tips exhibiting discrete, Spk-localized Mlc1signals (Fig.2.3B). The Mlc1 intensity index of *rsr1*Δ/Δ GTs was higher than that of WT GTs (Fig.2.3C). In contrast to the results in GTs, mature *rsr1*Δ/Δ hyphae had significantly fewer tips containing localized Mlc1-YFP as compared to the WT strain (Fig.2.3B), despite both strains expressing the same amount of Mlc1-YFP (Fig.2.3D). In mature *rsr1*Δ/Δ hyphae with localizable signal, the Mlc1-YFP intensity index was the same as that of mature WT hyphae (Fig.2.3C). Comparing Mlc1-YFP localization characteristics of each strain between the two hyphal stages, WT strains maintained Mlc1-YFP intensity index ($P=0.106$) whereas *rsr1*Δ/Δ strains have reductions in this feature over time ($P<0.001$). The Mlc1 results parallel those seen for

FM4-64 stained vesicles; WT strains maintain similar vesicle amounts and distributions over time whereas *rsr1*Δ/Δ strains showed decreased amounts and broader distributions of vesicles over time. To better understand the timing of Mlc1 signal "loss" from the hyphal tips of mature *rsr1*Δ/Δ hyphae, we analyzed Mlc1-YFP localization by time-lapse fluorescence microscopy. During WT hyphal development, Mlc1 localizes to two regions in the cell, constitutively to the Spk (in GTs and mature hyphae), and transiently to septa at the close of the cell cycle ((33), Fig.2.3E, Supplemental Movie 2.1). In contrast, the Spk-localized Mlc1 signal in *rsr1*Δ/Δ GTs became dimmer as growth approached the mitotic phase of the cell cycle, when Mlc1-YFP also localizes to the septum (Fig.2.3E and Supplemental Movie 2.2). In cases where Mlc1-YFP was visibly absent for a brief time (< 10 min) from tips of *rsr1*Δ/Δ hyphae, the hypha would continue to elongate (Fig.2.3E and Supplemental Movie 2.2). When the Mlc1 Spk signal was not visible for longer periods of time, hyphal elongation paused either until Mlc1-YFP re-localized to the original site of growth or the time-lapse image acquisitions stopped. In addition, extended loss of Mlc1-Spk localization and pauses in elongation were also associated with an increased likelihood of re-localization of Mlc1 to new, ectopic growth sites (Supplemental Movies 2.3 and 2.4). Results showing that Rsr1 is important for maintaining the localization of Mlc1to hyphal tips were also obtained using *RSR1*-expressing and non-expressing control strains (Supplemental Fig.2.3A and Supplemental Movies 2.5 and 2.6). Of note, Mlc1-YFP intensity index values of the *RSR1*-expressing reintegrant control strain did not reach the levels seen in the WT strain (P=0.023), suggesting that one copy of *RSR1* is not sufficient for complete restoration of WT Mlc1 localization characteristics in early hyphae (compare re-integrant results in Supplemental Fig.2.3B to WT results in Fig.2.3C). Nevertheless, the Mlc1 localization results for both the experimental and *RSR1*-reintegrant control strains support the idea that Rsr1 is important for the maintenance of Mlc1 localization characteristics during hyphal morphogenesis.

Together, the results of the FM4-64 and Mlc1-YFP analyses have two important implications. First, loss of Rsr1 affects the size of the fixed region to which polarity

components are delivered since, independent of the stage of hyphal growth, the distribution of Spk markers is always broader in *rsr1*Δ/Δ hyphae relative to WT hyphae (Figs.2.2, 2. 3). Second, Rsr1 appears to be involved in both limiting the delivery of polarity components at early stages of growth (GTs) and reinforcing the delivery of those components at later stages of hyphal growth. This statement is supported by data from *rsr1*Δ/Δ strains that consistently show elevated fluorescence intensities of Spk markers in GTs, an inability to maintain those elevated intensities over time, and also by FRAP data showing a tip-specific reduction in the speed of vesicle recovery in mature *rsr1*Δ/Δ hyphae as compared to GTs.

Rsr1 contributes to the maintenance of hyphal-specific gene (HSG) expression. Cells lacking Rsr1, when grown in hyphal induction conditions, have morphologies characteristic of both pseudohyphae and hyphae. Elongation rates of *rsr1*Δ/Δ and WT hyphae are similar, but *rsr1*Δ/Δ cells exhibit pseudohyphal-like growth with wider cells and slight constrictions at septa (Fig.2.4A and (45)). Consistent with this "dual" morphology, nuclear division often takes place within elongating *rsr1*Δ/Δ cells, similar to WT hyphae, but sometimes occurs across the mother-daughter neck, similar to the nuclear division pattern of pseudohyphae (T. Heisel and C. A. Gale, unpublished data). The ability of *rsr1*Δ/Δ cells to form Spks, albeit with altered localization characteristics, is also consistent with a more hyphal than pseudohyphal developmental program. To further characterize the developmental state of *rsr1*Δ/Δ cells grown in hyphal-inducing conditions, we used qPCR to compare the expression of four hyphal-specific genes (HSGs), *ECE1*, *HGC1*, *HYR1*, and *HWP1*, in *rsr1*Δ/Δ and WT strains. HSG expression was analyzed after growth in hyphal-induction conditions for 30 min (GTs) and 4 hours (mature hyphae) (Fig.2.4A). We observed decreased expression of HSGs in the *rsr1*Δ/Δ strain regardless of the developmental stage of hyphal growth (both pooled HSG results, Fig.2.4B and individual HSG results, Supplemental Fig.2.4). Indeed, HSG expression in *rsr1*Δ/Δ strains at both stages of hyphal growth was more similar to that of WT pseudohyphae, than to that of either WT GTs or mature hyphae (Fig.2.4B). In addition, *RSR1*-expressing reintegrant control strains showed significantly

increased expression of HSGs as compared to the *rsr1* null controls, demonstrating that HSG expression defects are specific to disruption of *RSR1* (Supplemental Fig.2.5). Altogether, the HSG expression results indicate that Rsr1, a landmark protein, influences the induction and maintenance of HSG expression during hyphal morphogenesis.

***RSR1* genetically interacts with regulators of *CDC42* to influence hyphal morphogenesis and HSG expression.** Similar to deletion of Rsr1, decreased expression and mutation of the essential Rho GTPase Cdc42 in *C. albicans* hyphae, results in larger, rounder cells and reduced HSG expression (8, 96, 97). In *S. cerevisiae*, Rsr1 facilitates activation of Cdc42 by physically interacting with, and positioning, Cdc42 and its GEF, Cdc24 (61). To investigate the relationship between Rsr1 and Cdc42 with respect to the *C. albicans* hyphal transcriptional program, we analyzed morphology and HSG expression in an *rsr1*Δ/Δ strain that also contained deletions of the Cdc42 GAPs, Bem3 and Rga2. Deletion of Cdc42 GAPs is predicted to slow the rate of GTP hydrolysis and result in an enrichment of membrane-associated Cdc42-GTP at hyphal tips (33). We reasoned that if the morphology and HSG expression defects of the *rsr1*Δ/Δ strain are due to reduced Cdc42 activation, then enrichment of Cdc42-GTP levels by deletion of the Cdc42 GAPs may rescue *rsr1*Δ/Δ phenotypes. Deletion of *RSR1* in combination with *RGA2* and *BEM3* (triple deletion strain, hereafter referred to as *3X* strain) resulted in narrow hyphal morphologies similar to the WT and *rga2*Δ/Δ *bem3*Δ/Δ (double deletion, hereafter referred to as *2X*) strains (Fig.2.4A). HSG expression in the *2X* strain was reduced, however, relative to that of the WT strain, for both GTs and mature hyphae (Fig.2.4B). This result suggests that while disrupting normal GTP/GDP cycling and increasing Cdc42-GTP levels affects HSG expression to a small extent, it does not dramatically affect the ability to form a WT hyphal morphology. In contrast, HSG expression in GTs of the *3X* strain did not differ from that of WT GTs and was significantly increased as compared to *rsr1*Δ/Δ and *2X* GTs (Fig.2.4B). HSG expression in mature *3X* hyphae was reduced to levels equal to that of the *2X* strain, but still significantly higher than that of the strain containing deletion of *RSR1* alone (Fig.2.4B). These HSG expression results correlate with our morphology observations (Fig.2.4A). A

more hyphal-like morphology is seen in strains with increased HSG expression (e.g. WT, *2X*, and *3X* strains) as compared to strains with lower HSG expression (e.g. *rsr1*Δ/Δ strain). In addition, the results imply that genetic interactions between *RSR1* and regulators of *CDC42* impact HSG expression differently in GTs and mature hyphae. In GTs, loss of the Cdc42 GAPs in conjunction with deletion of *RSR1*, suppresses the defects of the individual deletions. In contrast, in mature hyphae the effect of slowing Cdc42 hydrolysis by deletion of the Cdc42 GAPs is epistatic to that of *RSR1* deletion.

Rsr1 affects the amount and distribution of Cdc42 activity at hyphal tips. To ask if the reduced HSG expression exhibited by some of the mutant strains was associated with changes in Cdc42 expression, *CDC42* mRNA and Cdc42 protein levels were determined by qPCR and western blot, respectively. No differences in *CDC42* expression were found in comparing WT, *rsr1*Δ/Δ, *2X*, or *3X* deletion strains in either GTs or mature hyphae (P=0.211 and P=0.061, respectively, by ANOVA). *CDC42* levels also did not differ between *RSR1*-expressing and non-expressing reintegrant control strains (data not shown). In addition, no differences were observed in Cdc42 protein levels among the strains at either time point (Fig.2.5A). Thus, deletion of *RSR1* does not affect total cellular *CDC42* or Cdc42 protein levels in GTs or mature hyphae.

Although the total cellular amounts of *CDC42* and Cdc42 are not affected in hyphae lacking Rsr1, the possibility remained that Rsr1 could be affecting the amount and/or activity of Cdc42 specifically at hyphal tips. To compare the amount and distribution of active Cdc42 (Cdc42-GTP) in WT, *rsr1*Δ/Δ, *2X* and *3X* deletion strains, the expression and localization characteristics of a reporter protein, Bem1, fused to YFP were analyzed (Fig.2.5A, B). Bem1 is a polarity establishment scaffolding protein that binds the GTP-bound form of Cdc42 and is used as a marker of Cdc42-GTP localization (61). No differences were observed in the amounts of Bem1-YFP expressed in GTs or mature hyphae for any of the mutant strains as compared to the WT strain (Fig.2.5A). In comparing the localization of Bem1-YFP, the majority of GTs of all strains had a visible tip-localized fluorescent signal (~75-80% of cells) (Fig.2.5C); however, when the Bem1-YFP signal characteristics in GTs were compared, significant differences were observed

between the strains. The fluorescence intensities of Bem1-YFP were significantly increased in *2X*, *3X*, and *rsr1*Δ/Δ GTs as compared to the WT strain (Fig.2.5D).

The results from *2X* and *3X* strains, along with those of Court and Sudbery (32), support the idea that loss of the Cdc42 GAPs result in an enrichment of active GTP-bound Cdc42. In *rsr1*Δ/Δ GTs, the increased fluorescence intensity levels of Bem1-YFP parallel the results of FM4-64-stained vesicles and Mlc1-YFP, implicating a role for Rsr1 in limiting the localization of polarity factors during early hyphal (GT) growth. However, the increased intensity of Bem1-YFP in *rsr1*Δ/Δ GTs was associated with a broader signal distribution, resulting in a lower, less focused Bem1-YFP intensity index as compared to the WT strain. In contrast, the Bem1-YFP distributions of *3X*, and *2X* GTs were smaller, yielding a WT or greater than WT intensity index, respectively. In comparing Bem1-YFP intensity indices with HSG expression in GTs, we observed that WT Bem1-YFP intensity indices (WT and *3X* strain) are associated with WT levels of HSG induction whereas indices that are either higher (*2X* strain) or lower (*rsr1*Δ/Δ strain) than WT are associated with reduced HSG expression.

In mature hyphae, significantly fewer *rsr1*Δ/Δ cells had visible Bem1-YFP signals at their tips as compared to all other strains (Fig.2.5C). These results are similar to those observed in the analysis of Mlc1 localization (Fig.2.3B), and are consistent with *rsr1*Δ/Δ strains being unable to maintain tip-localization of polarity proteins during hyphal morphogenesis. Mature *rsr1*Δ/Δ hyphae that were able to localize Bem1-YFP to their tips exhibited an intensity index that was similar to mature WT hyphae (P=0.835) and showed an increasing trend relative to *rsr1*Δ/Δ GTs (P=0.065). Interestingly, the size (area) of the Bem1-YFP signal was the only parameter of the intensity index that showed a significant change between *rsr1*Δ/Δ GTs and mature hyphae (P = 0.041). This indicates that the decrease in signal area was the primary influence in mature *rsr1*Δ/Δ hyphae being able to attain a WT intensity index. The finding that some mature *rsr1*Δ/Δ hyphae do not have visible Bem1-YFP at their tips indicates that there were two, potentially distinct, populations of cells analyzed in the HSG expression experiments. It is possible that the population that lacked Bem1-YFP tip localization had low HSG

expression levels and the population with WT Bem1-YFP localization and intensity indices had near WT levels of HSG expression, such that, together, an overall reduction in HSG expression was observed. Mature hyphae of the *2X* and *3X* strain, which were able to localize Bem1-YFP to a similar extent as the WT strain (Fig.2.5C), exhibited more WT levels of HSG expression than mature *rsr1*Δ/Δ hyphae. In analyzing the *RSR1*-reintegrant control strain, we observed that GTs did not exhibit a WT Bem1 intensity index (Supplemental Fig.2.6A), however, mature hyphae did achieve WT levels for Bem1-YFP tip localization and intensity indices (Supplemental Figs.2.6B and 2.6A, respectively). These data suggest that one copy of *RSR1* is not sufficient to focus Cdc42 in GTs, but that one copy is sufficient to focus Cdc42 and maintain Cdc42 tip-localization in mature hyphae. Altogether, the Bem1 localization results show a positive correlation between HSG expression and the focused localization of Cdc42-GTP at hyphal tips. In addition, the requirements for Rsr1 are different depending upon the stage of hyphal growth. In GTs, Rsr1 is needed for focusing Cdc42 activity and, in mature hyphae, it is important for maintaining Cdc42 activity at hyphal tips. Further, the results are consistent with the idea that establishment of a focused distribution of Cdc42 activity in GTs is important for its continued maintenance at cell tips as hyphal development progresses.

IV. Discussion

Establishment and maintenance of polarity are highly regulated biological processes that are required for initiation of cell growth, variations in cell morphology, and generation of specialized cell types in multicellular organisms. In this study, we used a *C. albicans* strain with abnormal hyphal morphology as a tool to understand the requirements for constitutive polarized growth and the highly elongated morphology of hyphae. In *S. cerevisiae*, Rsr1 functions as a landmark, positioning new daughter cell growth with respect to that of the previous cell cycle, and is not essential for bud shape or cell size (11). Herein and in previous work (45) from our lab, we found that deletion of

the GTPase Rsr1 resulted in significant defects in polarized growth and cell shape. Similarly, in the filamentous fungus *A. gossypii*, hyphae lacking Rsr1 have defects maintaining polarized growth and the localization of polarity structures at hyphal tips (9). Thus, in filamentous fungi, Rsr1-like proteins appear to have an expanded role in polarized growth.

The differential localization of Bud2 and Bud5 in *C. albicans* supports a role for Rsr1 activity specifically at hyphal tips. Bud5 localization predicts that the very apex of the hypha is enriched for GTP-bound Rsr1, whereas Bud2 localization predicts that GDP-bound Rsr1 is favored subapically. Given that a number of key polarity proteins (e.g. Cdc42, Cdc24, and Bem1) physically interact with the two guanine nucleotide-bound forms of Rsr1 in *S. cerevisiae* (73), a gradient of Rsr1 activity along hyphal tips could provide a way to regulate the localization and activity of Rsr1 effectors. For example, ScRsr1 has been shown to have a higher affinity for Cdc24 when Rsr1 is in its GTP-bound form, whereas the interaction between Bem1 and Rsr1 is stronger when Rsr1 is GDP-bound. If this paradigm holds true in *C. albicans*, different zones of Rsr1 activity would be expected to limit the diffusion of Rsr1 effectors away from the tip and to hold them in proximity to regions of active growth.

Our results support the idea that focused localization of Cdc42 activity early on in hyphal development (e.g. GTs) is related to the ability of mature hyphae to maintain polarization and the localization of polarity proteins at hyphal tips. During WT hyphal growth, Cdc42-GTP (Bem1) and its downstream targets (e.g. components of the Spk) were constitutively localized to hyphal tips and showed no significant changes in either the maintenance of their localization or focused distribution between GTs and mature hyphae. In GTs lacking Rsr1, localization of Cdc42 activity lacked focus; this was associated with an inability to maintain hyphal growth and tip-localization of Bem1 and Spk components over time. Indeed, in mature *rsr1*Δ/Δ hyphae, the only cells able to maintain tip-localization of Bem1 and polarized growth, were those able to exhibit a WT-like focus of Cdc42 activity. The idea that mature hyphae are dependent upon processes originating in GTs is supported by the report that defects in chromatin remodeling at

HSG promoters during GT growth do not affect GT morphology but yield mature hyphae with a pseudohyphal appearance and an inability to maintain expression of HSGs (67).

In *C. albicans,* we found that Rsr1 contributes to hyphal morphogenesis by regulating the amount and distribution of Cdc42 activity at hyphal tips. In addition, we observed that the ability to localize and focus Cdc42-GTP is associated with the ability to express genes specific to the hyphal transcriptional program. These results are particularly interesting as *rsr1*Δ/Δ strains show defects in their ability to invade and cause damage in both *in vitro* and *in vivo* models of invasive candidiasis (20, 37), implicating a role for tip distribution of Cdc42 in the pathogenesis process. Our results extend those of Bassilana and coworkers (8) who found that reducing total cellular amounts of Cdc42, as well as its GEF, Cdc24, attenuated the expression of HSGs that are regulated by the transcription factor Tec1. Tec1 was also found to regulate a transient increase in Cdc24 expression at hyphal induction, suggesting that Tec1 and the Cdc42 GEF, which localizes at the hyphal tip, form a positive feedback loop. Our data provides additional support for the idea that tip-localization and focus of Cdc42 are associated with expression of the hyphal transcriptional program. We propose that Rsr1, a landmark protein, supports this morphogenesis feedback mechanism by fine-tuning the localized distribution of Cdc42 and/or downstream targets of Cdc42 activity. It still remains to be shown how tip-localization characteristics of the Cdc42 module are directing gene expression. One possibility is that Cdc42 localization sets up a physical platform for actin-dependent regulation of hyphal signaling pathways. Indeed, it has been shown that *ECE1*, *HGC1*, *HWP1* and *HYR1* are induced via the cAMP-dependent protein kinase A signaling pathway and that their expression is reduced in the face of genetic and chemical disruptions of the actin cytoskeleton (55, 102). The recent discovery that actin and adenylate cyclase physically interact with each other in a complex, and that this complex is required for the efficient production of cAMP (107), provides strong support for the idea that the cellular status of polarized actin modulates gene transcription during hyphal morphogenesis.

Overall, these results lead us to propose a model where Rsr1 is needed to create a focused, dynamic cluster of Cdc42 activity that is associated with optimized Cdc42-dependent feedback to the hyphal transcriptional program (Fig.2.6). In WT GTs, Rsr1 acts to generate a focused cluster of Cdc42 activity at hyphal tips with a limited amount of Cdc42-GTP (supported by lower Bem1 fluorescence intensities in WT as compared to *rsr1*Δ/Δ GTs and hyphae). In the absence of Rsr1, the clusters of Cdc42 activity that are generated contain higher amounts of Cdc42 and the localization is more broadly distributed. This results in an inability to generate the extremely narrow shape of GTs and a reduced ability to provide positive feedback to the hyphal transcriptional program. As hyphal growth progresses, if the Rsr1-independent mechanism of cluster formation is able to generate a sufficient focus of Cdc42 activity, which happens with a greatly reduced efficiency, polarized growth continues (Fig.2.6, pathway 2); if not, tip-localization of polarity proteins is lost and the progression of polarized growth is disrupted (Fig.2.6, pathway 1). Thus, elongation of GTs does not absolutely require an optimized focus of Cdc42 activity. However, if an optimal Cdc42-GTP distribution is not present by the end of the cell cycle, polarized growth will not continue. Our model is supported by results from *2X* and *3X* GTs that showed a positive relationship between increased intensity indices for Bem1-YFP and HSG expression. In GTs, the *3X* strain was the only mutant that had a WT Bem1-YFP intensity index and this correlated with a WT HSG expression profile. This suggests that in GTs, altering Cdc42 cycling in favor of the GTP-bound form compensates for the absence of Rsr1 by increasing Cdc42 focus, which in turn provides positive feedback to the hyphal program. The increase in the intensity index of the *3X* strain may have been achieved by a cytoskeletal-dependent mechanism. Given the role of active Cdc42 in directing cytoskeletal changes, holding Cdc42 in its GTP-bound state by deletion of its GAPs could have allowed sufficient reorganization of the cytoskeleton to reinforce Cdc42 activity at hyphal tips. Indeed, mathematical models of polarization events support the idea that altering Cdc42 cycling rates influences Cdc42 clustering (3). This idea is further supported by data from the *2X* strain, where altering Cdc42 cycling in the presence of the Rsr1-dependent focusing

mechanism, resulted in a hyper-focused Bem1 signal. Despite the higher than WT focus of *2X* GTs, HSG expression remained reduced as compared to the WT strain. These observations suggest that, while Cdc42 enrichment drives polarized cell shapes in *C. albicans* (32), an optimized distribution of normally cycling Cdc42, mediated in part through Rsr1 activity, is required to reinforce the hyphal transcriptional program and potentially, the expression of morphogenesis-associated virulence functions.

Although mature hyphae of the *3X* strain exhibited a WT Bem1 intensity index, they did not completely reach WT levels of HSG expression. There are two potential explanations for these findings. First, mature *3X* hyphae had a relatively small but significant loss in the number of cells exhibiting tip-localized Bem1 signal (Fig.2.5). This is similar to the situation with the *rsr1*Δ/Δ strain in that the HSG data was from a mixed population of cells and, thus, could potentially contribute to the reduced HSG expression in the total population of mature *3X* hyphae. Alternatively, the reduced HSG expression levels of mature *3X* (and *2X)* hyphae as compared to the WT strain could be attributed to changes in Cdc42-GTP hydrolysis rates. This would mean that there is an epistatic relationship between Cdc42-GTP hydrolysis rate and the distribution of Cdc42 activity for feedback to the hyphal transcriptional program in mature hyphae. In WT strains, we propose that Rsr1 supports Cdc42 cycling such that Cdc42 activity achieves a focused distribution without a change in the rate of hydrolysis.

A "fine-tuned" amount and/or distribution of Cdc42 has been proposed to be required for cells to break symmetry and generate polarized cell shapes in the model yeast *S. cerevisiae* (62, 90). While aspects of these models are still being worked out, our results support the idea that, in *C. albicans*, Rsr1 is part of the mechanism that creates the finite window of Cdc42 activity that is needed for polarized morphogenesis of yeast, pseudohyphae and hyphae as well as for maintenance of continuous hyphal growth. Thus, CaRsr1 has a larger impact on polarized growth than its ortholog in *S. cerevisiae*. It is possible that an additional level of Cdc42 regulation, provided by CaRsr1, is required for the continuum of reversible morphologies exhibited by *C. albicans*. *C. albicans* and *S. cerevisiae* also differ with respect to the number of growth zones that are simultaneously

present within the cell. In budding yeast, symmetry breaking is achieved by a "winning" Cdc42 cluster that initiates growth of a single bud (49, 50). In contrast, *C. albicans* hyphal development requires that Cdc42 be strongly maintained at hyphal tips, even as it transiently acts at a second site (the incipient septum) at septation (46). The observation that polarization defects took place coincident with septa formation in *rsr1*Δ/Δ hyphae implicates Rsr1 in limiting the competition for Cdc42 between the incipient septum and the hyphal tip. Similarly, recent studies in the fission yeast, *Schizosaccharomyces pombe*, suggest that there is a relationship between the competition for Cdc42 at multiple (bipolar) sites and polarized morphogenesis (34). Thus, we propose that the role of Rsr1 in limiting Cdc42 activity might serve as a mechanism that both initiates highly polarized cell shapes and also reserves a pool of Cdc42 to maintain continuous polarized growth throughout *C. albicans* hyphal development.

ACKNOWLEDGEMENTS

We thank Russ Johnson, Kendra Van Beusekom, and Abigail DiPasquale for technical assistance, Maryam Gerami-Nejad and Stephen Bentivenga for technical advice, and Peter Sudbery for providing strains. We are very grateful to Judith Berman, Melissa Gardner and the faculty of the Mount Desert Island Biological Laboratory (MDIBL) course on Quantitative Fluorescence Microscopy for helpful discussions during preparation of the manuscript. Software support for analysis of microscopic images was provided by the Minnesota Supercomputing Institute at the University of Minnesota.

This work was supported by NIH AI057440 and University of Minnesota Pediatrics Foundation awards to C.G. and by an Agilent scholarship to R.P. to attend the MDIBL microscopy course

V. Chapter 2 Tables & Figures

Table 2.1. Strains Used in This Study

Strain	Relevant Genotype	Source
BWP17	*ura3::imm434/ura3::imm434 his1::hisG/his1::hisG arg4::hisG/arg4::hisG*	(100)
CA1243	(BWP17) *rsr1::dpl200/rsr1::dpl200 MLC1/MLC1-YFP:HIS1 rsr1::dpl200::rsr1:URA3*	(This study)
CA8880	(BWP17) *rsr1::ARG4/rsr1::HIS1 arg4::hisG/ARG4-URA3::arg4::hisG*	(45)
CA8832	(BWP17) *rsr1::ARG4/rsr1::HIS1*	(45)
CA9151	(BWP17) *rsr1::ARG4/rsr1::HIS1 MLC1/MLC1-YFP:URA3*	(This study)
CA9215	(BWP17) *rsr1::ARG4/pURA3-RSR1::rsr1::HIS1*	(45)
CA9339	(BWP17) *rsr1::ARG4/pURA3-rsr1::rsr1::HIS1*	(20)
CA10055	(BWP17) *URA3:P_{MET3}:YFP::BUD2/BUD2*	(This study)
CA10271	(BWP17) *rga2::HIS1/rga2::ARG4 bem3::ura3(5'Δ)/bem3::ura3(5'Δ)*	(32)
CA10755	(BWP17) *rga2::HIS1/rga2::ARG4 bem3::ura3(5'Δ)/bem3::ura3(5'Δ) rsr1::dpl200/rsr1::dpl200*	(This study)
CA12168	(JB7783) *BEM1/BEM1-YFP:URA3*	(This study)
CA12172	(BWP17) *rga2::HIS1/rga2::ARG4 bem3::ura3(5'Δ)/bem3::ura3(5'Δ) BEM1/BEM1-YFP:HIS1*	(This study)
CA12173	(BWP17) *rga2::HIS1/rga2::ARG4 bem3::ura3(5'Δ)/bem3::ura3(5'Δ) rsr1::dpl200/rsr1::dpl200 BEM1/BEM1-YFP:HIS1*	(This study)
CA12183	(BWP17) *rsr1::ARG4/rsr1::HIS1 BEM1/BEM1-YFP:URA3*	(This study)
CA12188	(BWP17) *rga2::HIS1/rga2::ARG4 bem3::ura3(5'Δ)/bem3::ura3(5'Δ) arg4::hisG/ARG4-URA3::arg4::hisG*	(This study)
CA12191	(BWP17) *rga2::HIS1/rga2::ARG4 bem3::ura3(5'Δ)/bem3::ura3(5'Δ) rsr1::dpl200/rsr1::dpl200 arg4::hisG/ARG4-URA3::arg4::hisG*	(This study)
CA12343	(BWP17) *URA3:P_{MET3}:YFP::BUD5/BUD5*	(This study)
CA12345	(BWP17) *URA3:P_{MET3}:YFP::RSR1/RSR1*	(This study)
CA12363	(BWP17) *rsr1::dpl200/rsr1::dpl200*	(This study)
CA12388	(BWP17) *rsr1::dpl200/rsr1::dpl200 MLC1/MLC1-YFP:HIS1*	(This study)
CA12430	(BWP17) *rsr1::dpl200/rsr1::dpl200 MLC1/MLC1-YFP:HIS1 pURA3-RSR1::rsr1::dpl200*	(This study)
CA12567	(BWP17) *rsr1::dpl200/rsr1::dpl200 pURA3-RSR1::rsr1::dpl200*	(This study)
CA12570	(BWP17) *rsr1::dpl200/rsr1::dpl200 pURA3-rsr1::rsr1::dpl200*	(This study)
CA12595	(BWP17) *rsr1::dpl200/rsr1::dpl200 pURA3-RSR1::rsr1::dpl200 BEM1/BEM1-YFP:HIS1*	(This study)
CA12598	(BWP17) *rsr1::dpl200/rsr1::dpl200 pURA3-rsr1::rsr1::dpl200 BEM1/BEM1-YFP:HIS1*	(This study)
JB6284	(BWP17) *his1::hisG/hisG::his1::HIS1 arg4::hisG/ARG4-URA3::arg4::hisG*	(13)
JB7783	(BWP17) *his1::hisG/hisG::his1::HIS1 arg4::hisG/ARG4::arg4::hisG*	(12)
MG7139	(BWP17) *MLC1/MLC1-YFP:URA*	(33)

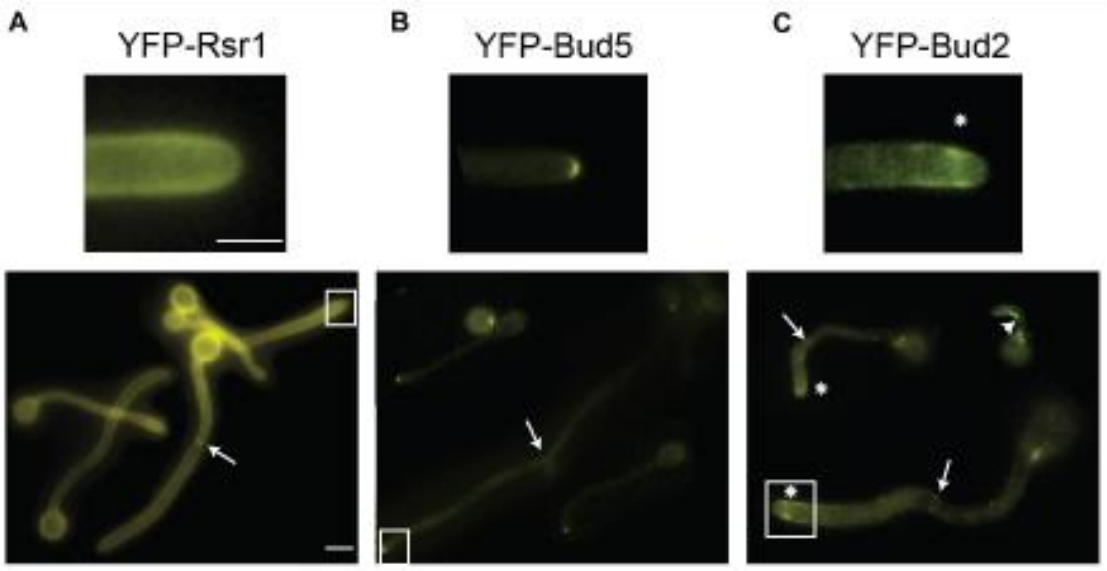

Fig.2.1. Positive and Negative Regulators of Rsr1 Localize at Tips of GTs and Mature Hyphae. Representative images of strains expressing YFP-tagged versions of Rsr1 (A, 12345), Bud5 (B, 12343), and Bud2 (C, 10055). Arrows indicate enrichment of YFP-tagged proteins at septa. Arrowhead (in C) denotes enrichment of YFP-Bud2 at the inner curve of a non-linear GT. Asterisks (in C) indicate subapical enrichment of YFP-Bud2. Scale bars, 5 μm

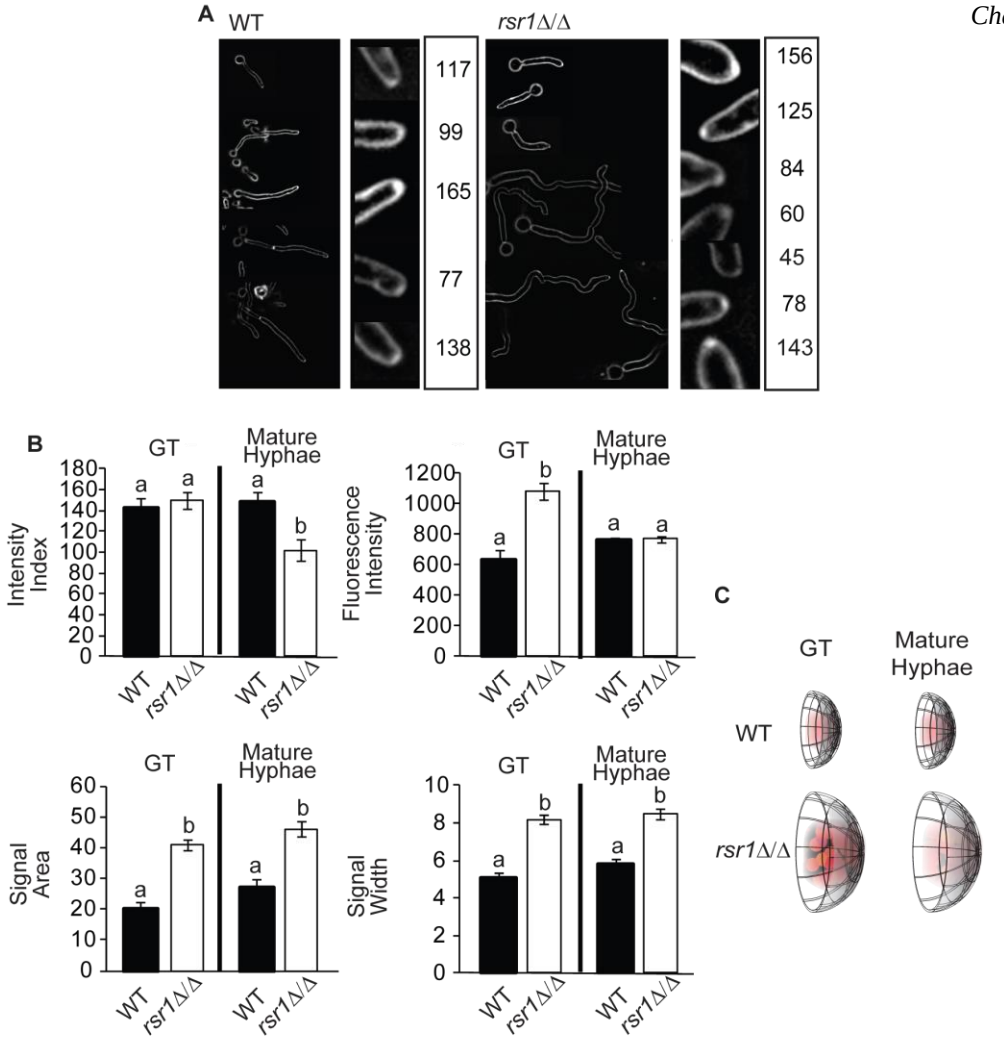

Fig.2.2. Comparison of Vesicular Spks in WT and *rsr1* Δ/Δ Hyphae. A. Representative fluorescence images of WT (9955) and *rsr1*Δ/Δ (8880) hyphae stained with FM4-64. To the right of each set of images is the calculated intensity index for each of the representative FM4-64 stained Spks. Tip signals that appear less intense (lower fluorescence intensity), or have broader distributions (increased area and width), have lower intensity indices than signals that are more intense and/or are more focused at the hyphal tip. Scale bar, 5 µm. B. Bar graphs depicting the mean intensity index, fluorescence intensity, area and width of the FM4-64 signal obtained for GTs and mature hyphae of the strains featured in A. Stage-specific differences between strains (i.e. WT GT vs. *rsr1*Δ/Δ GT, etc.) are shown. Pertinent within strain differences between time points (i.e. WT GT vs. WT mature hyphae, etc.) are stated within the text. Error bars show SEM and data sharing the same letter (a or b) designations are not significantly different from each other. Statistical differences are at the level of $P<0.05$ for both hyphal stages (~100 cells per strain for each of 3 independent experiments). C. Diagrammatic representation of the differences in appearance of FM4-64 stained Spks of WT and *rsr1*Δ/Δ hyphae, based on the data presented in B.

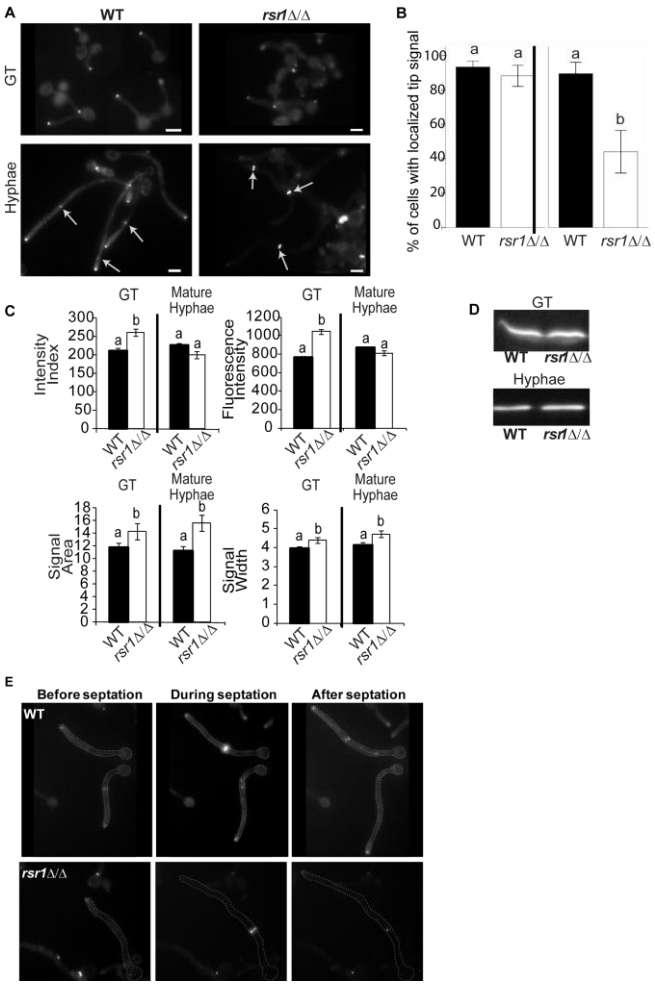

Fig.2.3. Comparison of Mlc1-YFP Localization Characteristics in WT and *rsr1*Δ/Δ Hyphae. A. Fluorescence micrographs of WT (7139) and *rsr1*Δ/Δ (11729) strains expressing Mlc1-YFP in GTs and mature hyphae. Arrows show Mlc1-YFP at septa. Scale bar, 5 µm. B. Bar graph depicting the percent of hyphae with localized Mlc1-YFP signal at the tip for the WT and mutant strains listed in A. Means represent data from an average of ~70 images for each strain, from 3 independent experiments. Error bars show SEM. C. Bar graphs depicting the mean intensity index and index parameters of the strains featured in A. Means represent ~100 cells per strain from each of 3 independent experiments. Stage-specific data sharing the same letter designation are not significantly different from each other. Statistical differences are at the level of $P<0.05$ for both hyphal stages. D. Representative western blot of Mlc1-YFP expression in the strains depicted in A, at both stages of hyphal development. The mean background subtracted ratio of Mlc1-YFP to tubulin in WT to *rsr1*Δ/Δ strains was 1.04 ± 0.18 and 1.16 ± 0.09 for GT and mature hyphae, respectively (n=3). E. Representative still fluorescence images taken from time-lapse movies (Supplemental Movies 1 and 2) of Mlc1-YFP localization in the strains featured in A prior to, during, and after a septation event.

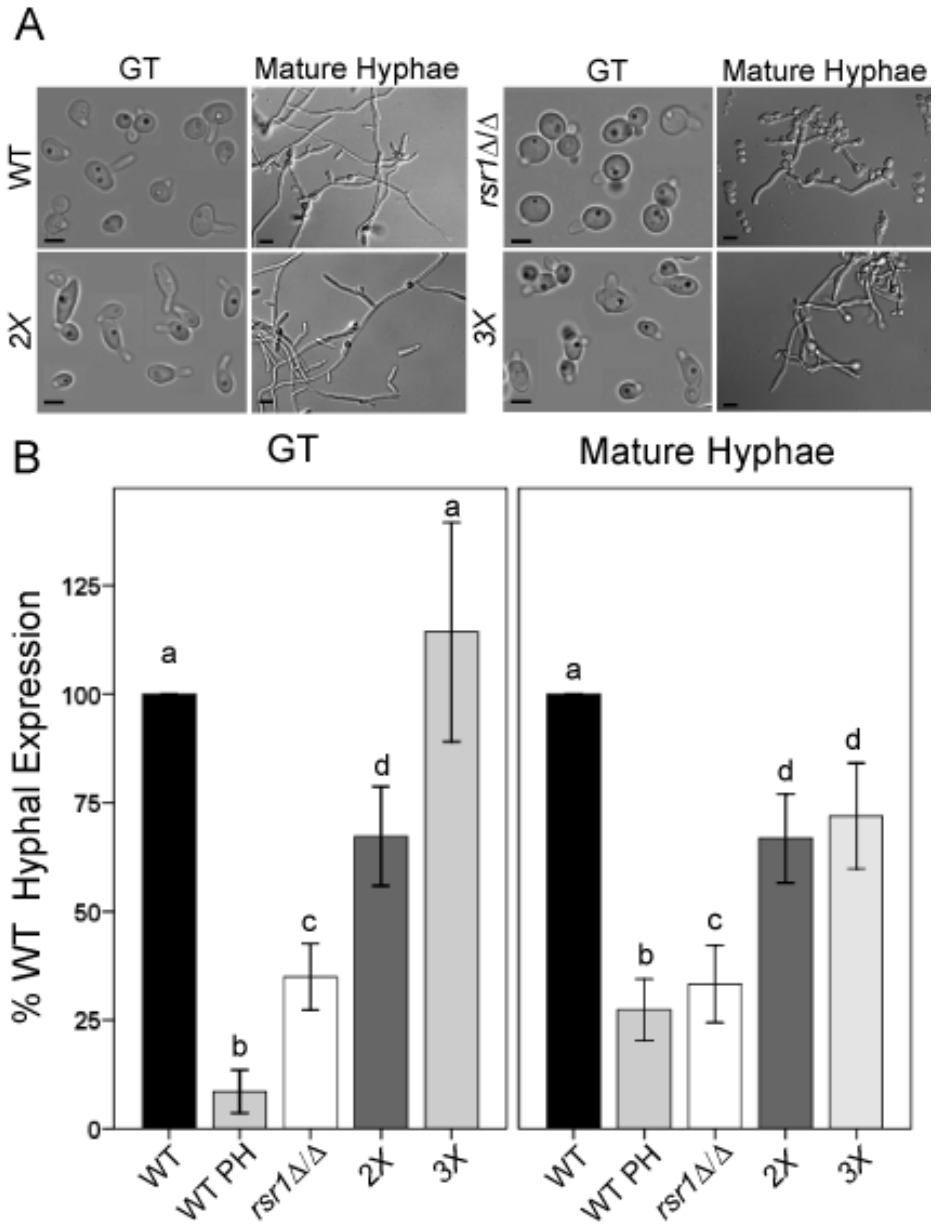

Fig.2.4. *RSR1* Genetically Interacts with *RGA2* and *BEM3*, Genes that Encode Regulators of Cdc42, to Influence the Hyphal Morphogenesis Program. A. Representative images of WT (12168), *rsr1*Δ/Δ (12182), *rga2*Δ/Δ *bem3*Δ/Δ (*2X*, 12172) and *rga2*Δ/Δ *bem3*Δ/Δ *rsr1*Δ/Δ (*3X*, 12173) strains. Scale bars, 5 µm in GTs; 10 µm in mature hyphae). B. Mean, pooled HSG expression levels for each strain were determined by qPCR, normalized to *ACT1* levels, and expressed as a percentage of WT HSG expression for that day (n=3 for each strain). PH, pseudohyphae. Stage-specific data sharing the same letter designation are not significantly different from each other. Error bars show SEM. Statistical differences are at the level of $P \leq 0.002$ for GTs and $P < 0.001$ for mature hyphae.

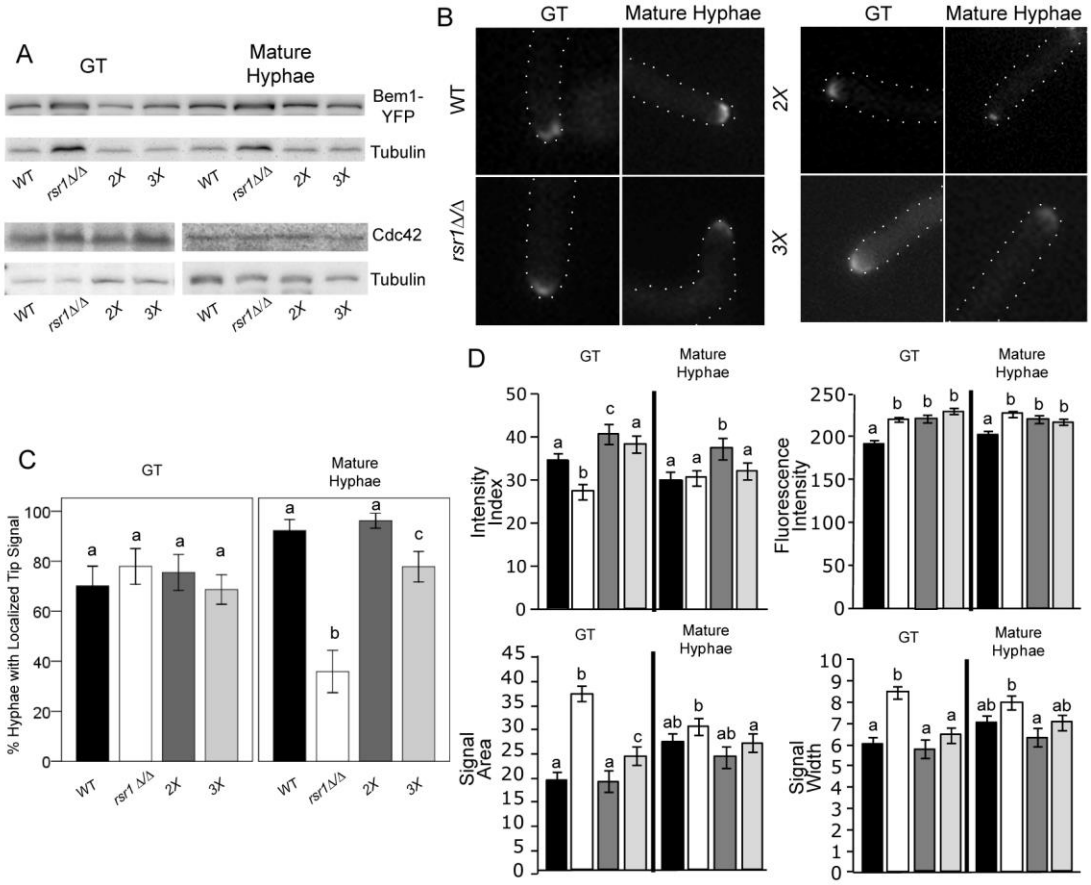

Fig.2.5. Rsr1 Focuses Cdc42 Activity at Tips of GT's and is Required to Maintain Polarized Growth in Mature Hyphae. A. Representative western blot of Bem1-YFP and Cdc42 levels in GTs and mature hyphae of WT (12168) and mutant strains (*rsr1*Δ/Δ, 12183; *2X*, 12172; *3X*,12173). Tubulin levels are shown as a reference for protein loading. B. Representative fluorescent images of Bem1-YFP tip-localization at both stages of hyphal growth, for each of the strains listed in A. C. Bar graph depicting the percent of hyphae with localized Bem1-YFP signal at the tip for the WT and mutant strains listed in A. Means represent data from ~60 images for each strain, from 3 independent experiments. Error bars show 95% CI. D. Bar graphs depicting the mean intensity index and index parameters from cells with visible Bem1-YFP tip signals, in GTs and mature hyphae, for the strains listed in A. Strains are as depicted by bar color in panel C. Means represent ~45 cells per strain from 3 independent experiments. Stage-specific data sharing the same letter designation are not significantly different from each other. Pertinent within strain differences between time points are stated within the text. Statistical differences are at the level of $P<0.05$ for both hyphal stages and error bars show SEM.

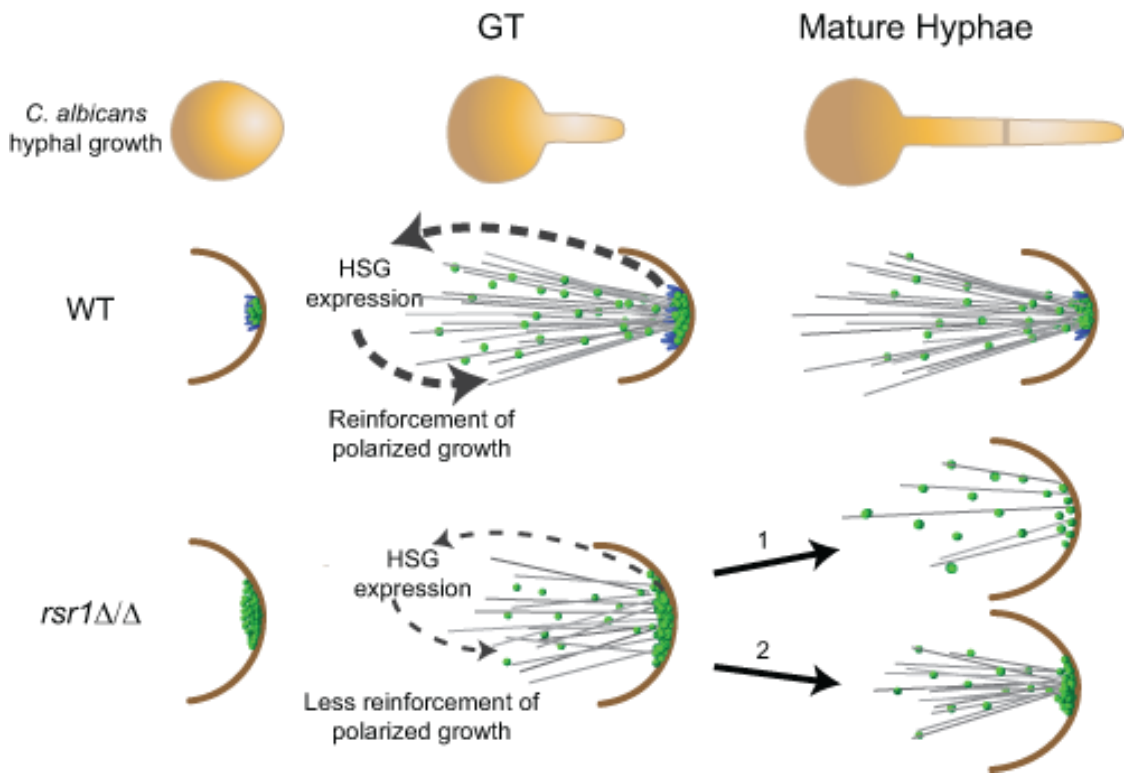

Fig.2.6. Model of How Rsr1 Impacts the Hyphal Morphogenesis Developmental Program. In WT strains, Rsr1 (blue spheres) limits the amount of Cdc42-GTP (green spheres), focuses the distribution of Cdc42 activity during germ tube growth, and maintains the localization of Cdc42 activity during mature hyphal growth. Focused, tip-localized Cdc42 activity contributes to the induction (in GTs) and maintenance (in mature hyphae) of HSG expression, as well as maintenance of Spk integrity (not pictured). In GTs lacking Rsr1, the amount of tip-localized Cdc42-GTP is elevated relative to WT, but is also more broadly distributed at the hyphal tip. The diffuse localization of Cdc42 activity provides weak feedback and results in decreased HSG expression, as well as unregulated (excessive) delivery of Spk-associated components (not pictured) to the hyphal tip. In mature hyphae lacking Rsr1, some cells can no longer localize Cdc42 activity effectively at hyphal tips (pathway 1), whereas others in the population (i.e. those with Cdc42 distributions similar to wild type) are able to maintain localization of Cdc42 activity, Spk integrity (not pictured), and polarized hyphal growth (pathway 2).

Chapter 2 Supplemental Tables & Figures

Supplemental Table 2.1. Oligonucleotide Primer Sequences Used in This Study

Primer Name	Primer Sequence (5'→3')	Source
1076 *MLC1-YFP* F	AAAGGGGTCAATGTAACTTCTGATGGAAATGTG GATTATGTTGAATTTGTCAAATCAATTTTAGACC AAGGTGGTGGTTCTAAAGGTGAAGAATTATT	(93)
1077 *MLC1-YFP-HIS1* R	CCAATTCGAACAAGACTATACAATAACTATAATT TGTAAAACTTGTAGTATATATATTTCAATGGTTA ATTGTCTAGAAGGACCACCTTTGATTG	(93)
1265 *rsr1::dpl200* R	TCACATAATTGTGCAGCACTTGCTTCCTGAGCTA GACTTTGGGTGATCATTAATTGATTGTTTCAATC TGTGTGGAATTGTGAGCGGATA	(This Study)
1276 P_{MET3}-*YFP-BUD2* F	GACTGTGTACGGTTATCCACATTTTTAAATTAAA ACTATCTGTATTATTATTACTTATAAAGATAATC TATCTAGAAGGACCACCTTTGATTG	(This Study)
1327 *MLC1-YFP-HIS1* R	CCAATTCGAACAAGACTATACAATAACTATAATT TGTAAAACTTGTAGTATATATATTTCAATGGTTA ATTGGAATTCCGGAATATTTATGAGAAAC	(93)
1460 *rsr1::dpl200* F	AGGTATGTACATTCAACAAAAGCCCGTTACACTT GTATTTCAATAACCCTATATACTAACTTTTGTTTT GGTTTTCCCAGTCACGACGTT	(This Study)
1530 P_{MET3}:*YFP::BUD5* F	ATTCACTGAATTTCACTTATATATATAAATTCATT TGACATCCCGTTTACAGAAATAGTTCCCGTATAT ATCAAGTTCTAGAAGGACCACCTTTGATTG	(This Study)
1702 P_{MET3}-*YFP-RSR1* F	ACACCAGAAAAAAAATAGTAATTCTGTATACCT TTATACAAATAAGATTTTAAAGCCTATTCACAAA CATCAATCTTCTAGAAGGACCACCTTTGATTG	(This Study)
1717 P_{MET3}:*YFP::BUD5* R	GGCACTGTTCGAGTCAGGATATACGCTAGATGA TGTACTGATATGTTTGCCTGGATCTGAATAGTTT GGTTGTTGAAATTTGTACAATTCATCCATAC	(This Study)
2540 P_{MET3}-*YFP-BUD2* R	TGTGACCTTCAAATACTCCTTTATCACGAGAAAT GATTTTATGAAATGCAGATTGATAAGCTGGAGG CATTTTGTACAATTCATCCATAC	(This Study)

Supplemental Table 2.1 Continued

Primer Name	**Primer Sequence (5'→3')**	**Source**
2602 *BEM1-YFP-HIS1* R	TTTCCTCTCAACTTGAAAATATATATATATATAT ATATAATACAAAAGTAAAACAATTCTTCTCGAAT TCCGGAATATTTATGAGAAAC	(This study)
2601 *BEM1-YFP* F	TGAAGTTAATGATGATGAAAAATTTCAAAGTATT TTATTTGATAAATGTAAATTAATGGTTTTAGTAT ATGGTGGTGGTTCTAAAGGTGAAGAATTATT	(This study)
2739 *BEM1-YFP-URA3* R	TTTCCTCTCAACTTGAAAATATATATATATATAT ATATAATACAAAAGTAAAACAATTCTTCTCTCTA GAAGGACCACCTTTGATTG	(This study)
4429 RSR1F	GAGAGATTATAAAGTCGTAGTA	(This study)
4430 RSR1R	TCACATAATTGTGCAGCACTT	(This study)
4456 ACT1F	ATGTTCCCAGGTATTGCTGA	(55)
4457 ACT1R	ACATTTGTGGTGAACAATGG	(55)
4458 ECE1F	CCAGAAATTGTTGCTCGTGTTG	(55)
4459 ECE1R	CAGGACGCCATCAAAAACG	(55)
4460 HGC1F	AAAGCTGTGATTAAATCGGTTTTGA	(55)
4461 HGC1R	AATTGAGGACCTTTTGAATGGAAA	(55)
4462 HWP1F	CGGAATCTAGTGCTGTCGTCTCT	(55)
4463 HWP1R	TAGGAGCGACACTTGAGTAATTGG	(55)
4464 HYR1F	CTCAACCTCAGTGCTGCATTAGAA	(55)
4465 HYR1R	AGCCCAAGTAGCACCAGAATGA	(55)
5410 CDC42F	TCCCCAATCACCCAGGAA	(55)
5411 CDC42R	TGCAGCTACTATAGCCTCGTCAA	(55)

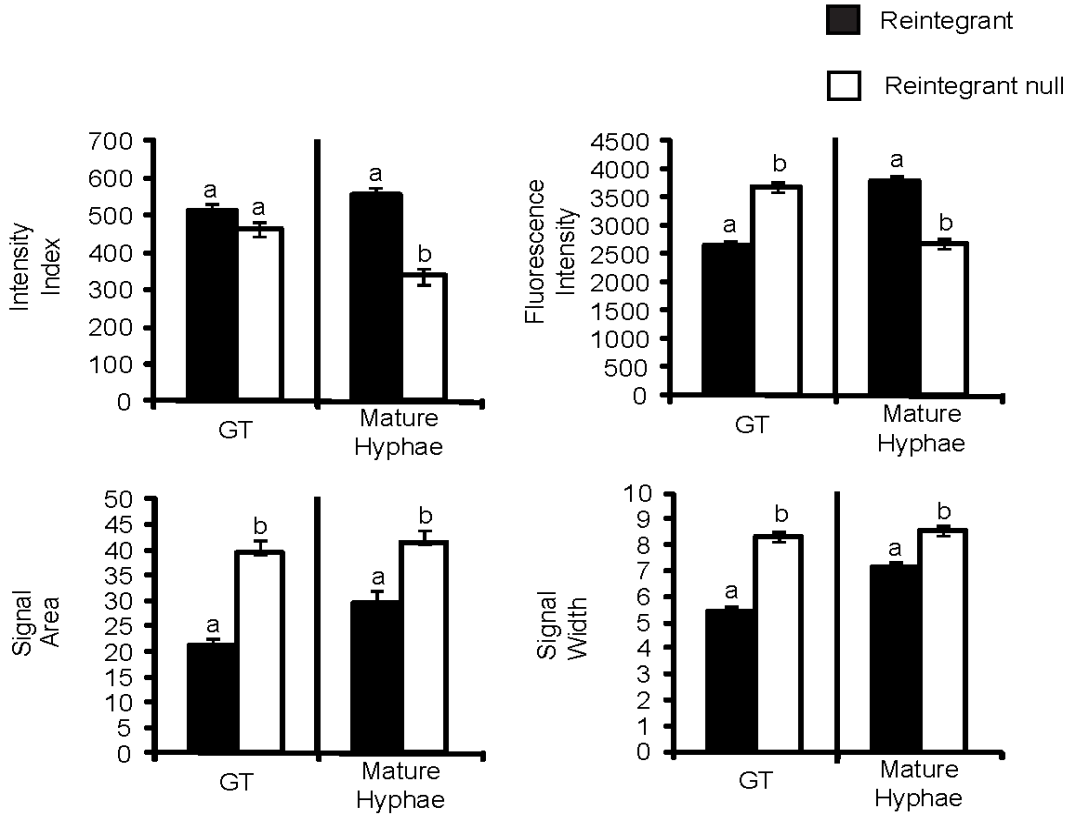

Supplemental Fig.2.1. Spk Vesicle Localization Characteristics in *RSR1*-Reintegrant Control Strains, Visualized by Staining with FM4-64. A. Bar graphs showing the intensity index and index parameters of strains containing either a reintegrated complete (reintegrant, 9215) or disrupted (reintegrant null, 9339) copy of *RSR1*. Error bars show SEM. Stage-specific (GT or mature hyphae) data sharing the same letter designation are not significantly different from each other. Statistical differences were at the level of $P<0.001$ for both hyphal stages. N=140 cells per strain for each of 3 independent experiments.

Supplemental Table 2.2. Vesicle Trafficking Characteristics Determined by FRAP in GTs and Mature Hyphae of WT (9955) and *rsr1* Δ/Δ (8880) Strains*

	Location/Stage of Growth	Mean $\tau_{1/2}$ (in sec)	N
WT	*At hyphal tips*	p=0.925	
	GT	5.10	10
	Mature Hyphae	5.20	8
	10μm behind hyphal tips	p=0.227	
	GT	6.63	10
	Mature Hyphae	5.22	6
***rsr1*Δ/Δ**	*At hyphal tips*	p=0.032	
	GT	3.98	4
	Mature Hyphae	6.73	6
	10μm behind hyphal tips	p=0.566	
	GT	5.93	4
	Mature Hyphae	5.38	7

* Photobleaching experiments were performed on hyphal tips (encompassing the Spk signal) as well as on cytoplasmic regions 10 μm from the hyphal tip, to evaluate hyphal tip-specific changes. Note the significant decrease in recovery times (τ1/2 sec) between GTs and mature hyphae that is specific to *rsr1*Δ/Δ hyphal tips. P values indicate differences within a given strain with respect to developmental stage.

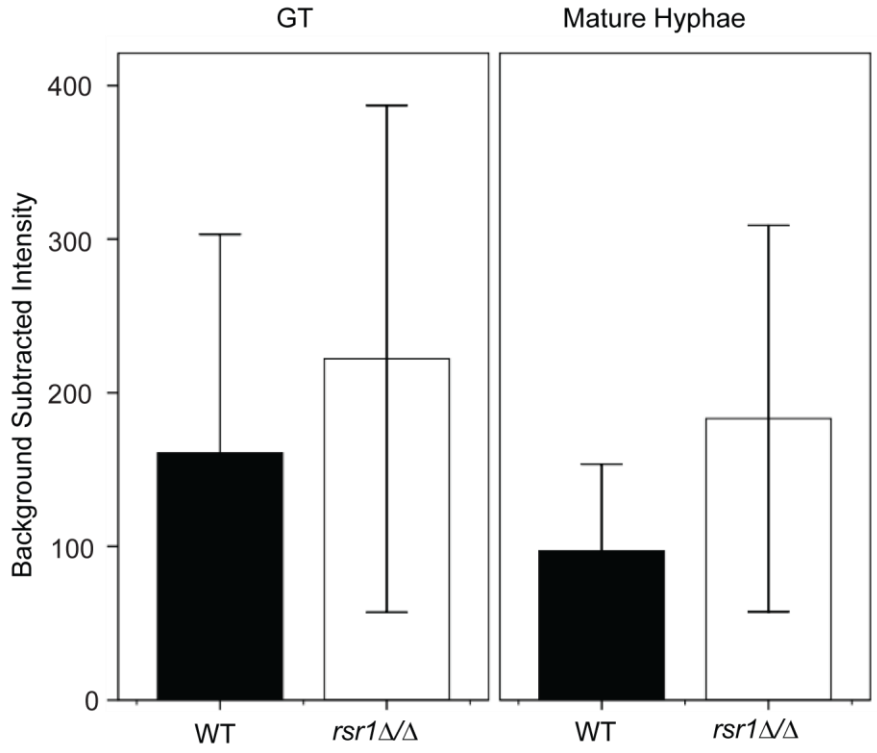

Supplemental Fig.2.2. Internalization of FM4-64 by GTs and Mature Hyphae of WT (9955) and *rsr1*Δ/Δ (8880) Strains. Bar graph depicting the background subtracted fluorescence intensities of cells collected from the final frames of time-lapse movies of mixed cultures of *rsr1*Δ/Δ and WT (expressing a GFP-tagged nuclear marker) cells (GTs and mature hyphae) stained with FM4-64. Error bars show 95% CI. Measurements were taken from one or two in-focus GT(s) and mature hyphae for each strain. Movies of GTs and mature hyphae were taken on the same day from a common subculture, to make comparisons between stages, and movies were obtained on 3 separate days.

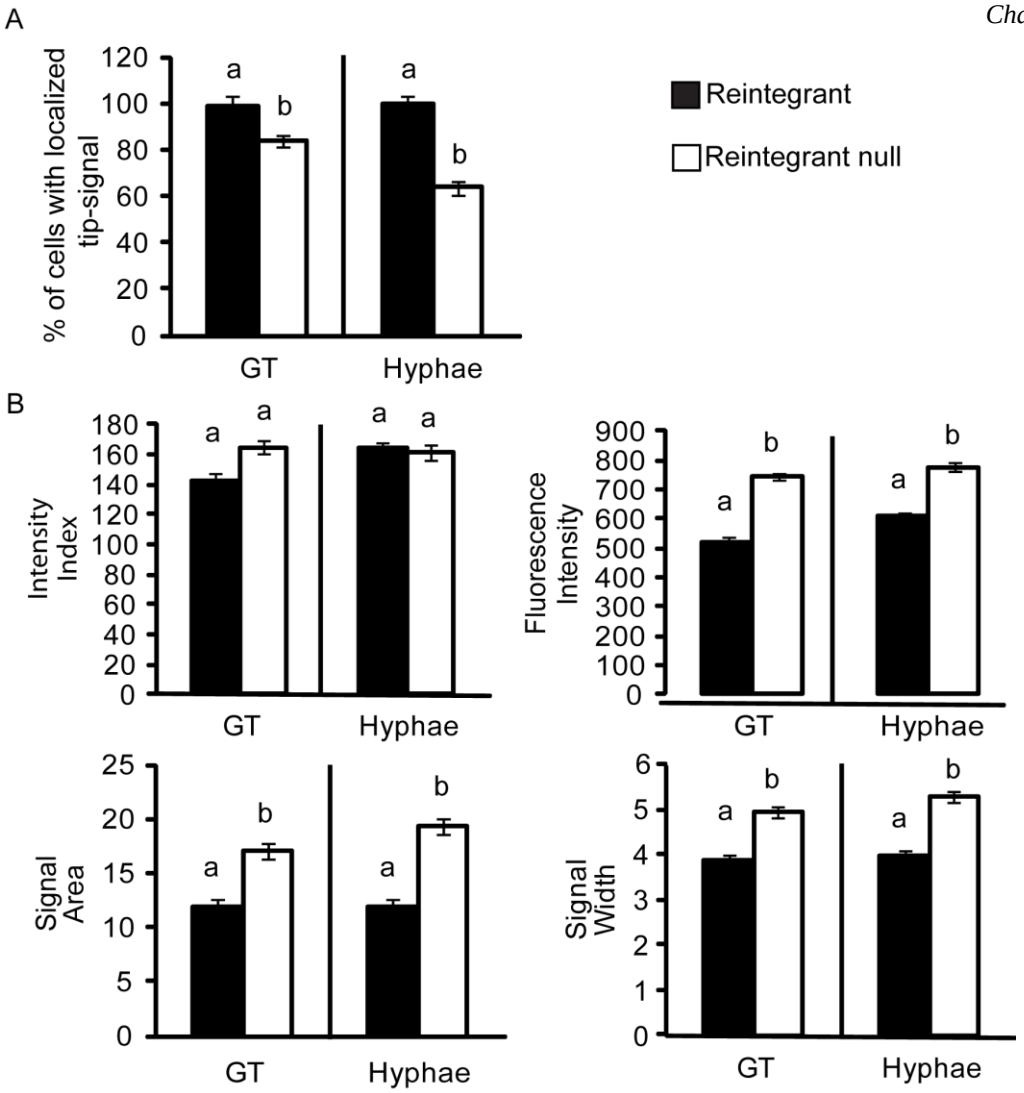

Supplemental Fig.2.3. Mlc1 Localization Characteristics of *RSR1*-Reintegrant Control Strains Expressing Mlc1-YFP. A. Bar graph depicting the percent of cells showing localization of Mlc1-YFP to the Spk in GTs and mature hyphae of *RSR1*-integrant (12430) and *rsr1* null reintegrant (12431) strains. Stage-specific data sharing the same letter designation are not significantly different from each other. Statistical differences were at the level of $P<0.001$ for both hyphal stages. Means represent data from an average of ~85 images for each strain, from 3 independent experiments. Error bars show 95% CI. B. Bar graphs depicting the mean intensity index and index parameters of the strains listed in A. Means represent ~ 325 cells per strain from each of 3 independent experiments. Stage-specific data sharing the same letter designation are not significantly different from each other. Statistical differences were at the level of $P<0.001$ for both hyphal stages. These data, in combination with the localization data in A, show a similar relationship as that seen in experimental WT and *rsr1*Δ/Δ strains, where the ability to maintain Mlc1 localization correlates with the ability to attain a WT Mlc1 intensity index.

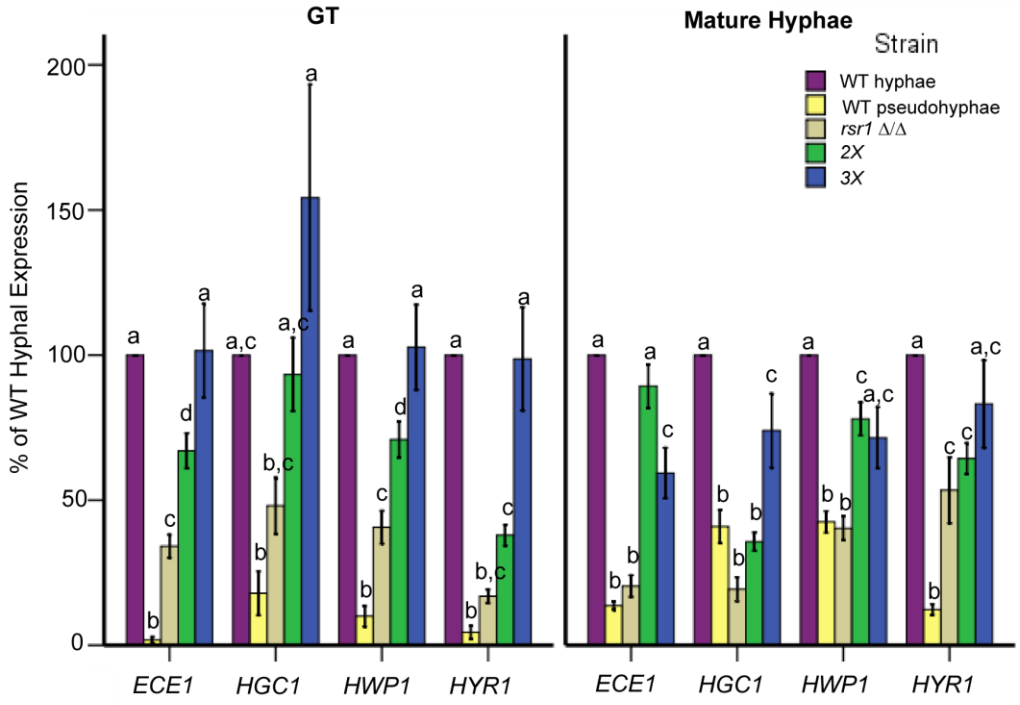

Supplemental Fig.2.4. Expression of HSGs (*ECE1*, *HGC*, *HWP1*, and *HYR1*) by *C. albicans* Strains WT, 9955; *rsr1*Δ/Δ, 8880; *bem3*Δ/Δ *rga2*Δ/Δ (*2X*), 12188; *bem3*Δ/Δ *rga2*Δ/Δ *rsr1*Δ/Δ (*3X*), 12191. Bar graph showing expression levels of individual HSGs, determined by qPCR, as a percentage of the stage-specific WT strain grown in hyphal induction conditions, normalized to 100%. Stage-specific data sharing the same letter designation are not significantly different from each other. Statistical differences were at the level of $P<0.05$ for both hyphal stages. N=3 for each strain and hyphal stage.

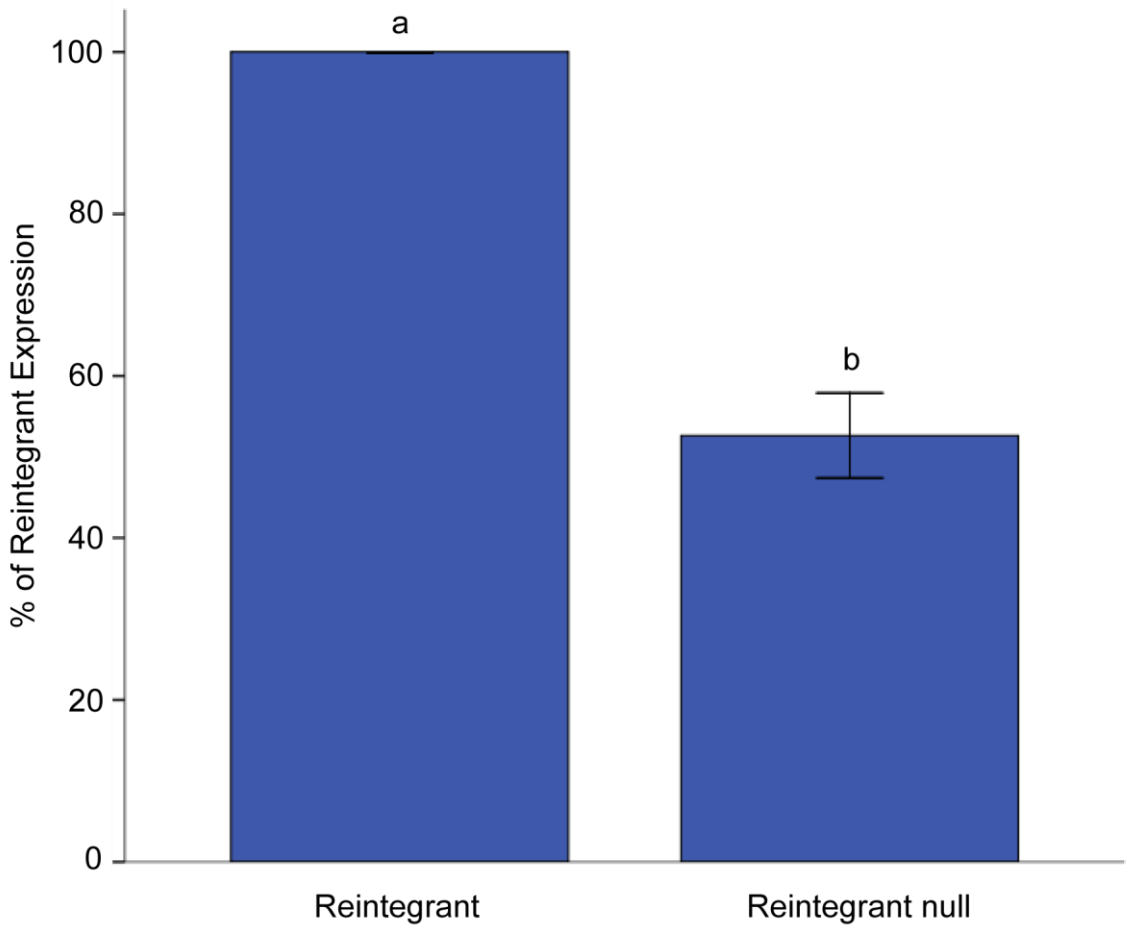

Supplemental Fig.2.5. HSG Expression in *RSR1*-Reintegrant (12567) and *rsr1* Null-Reintegrant (12570) Control Strains in GTs and Mature Hyphae. Bar graph showing pooled HSG (*HGC, ECE1, HWP1, and HYR1*) expression levels (after 120 min of hyphal induction), measured by qPCR, as a percentage of the *RSR1*-reintegrant strain, normalized to 100%. Error bars are SEM. Statistical difference was at the level of $P<0.05$. n=3 for each strain.

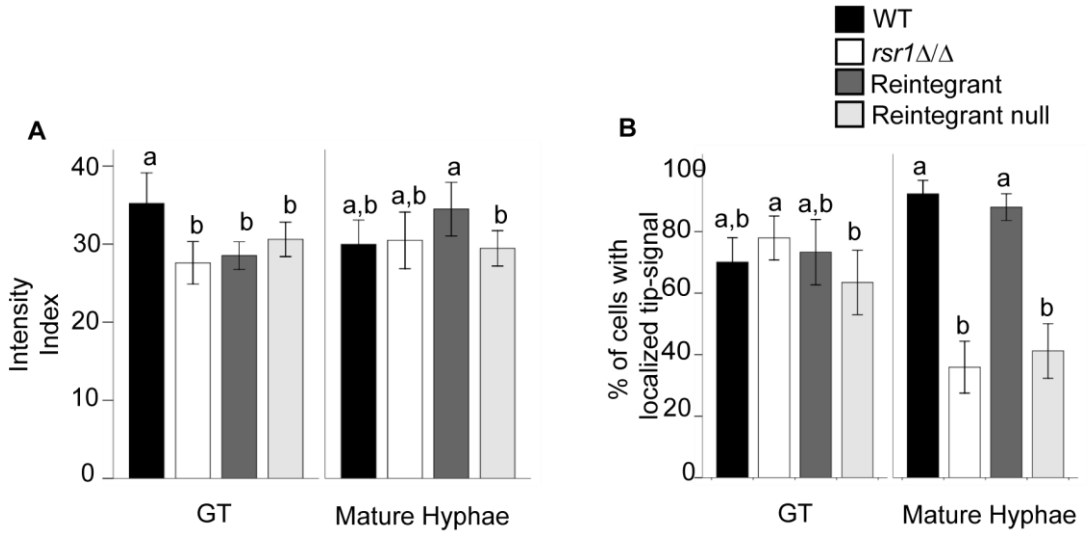

Supplemental Fig.2.6. Bem1-YFP Localization Characteristics in *RSR1*-Reintegrant (12595) and *rsr1* Null-Reintegrant (12598) Strains. A. Bar graph depicting the percent of cells showing localization of Bem1-YFP at the tips of GTs and mature hyphae. Stage-specific data sharing the same letter designation are not significantly different from each other. Statistical differences were at the level of $P<0.05$. Means represent data from an average of ~65 images for each strain, from 3 independent experiments. Error bars show 95% CI. B. Bar graphs depicting the mean intensity index and index parameters of the strains listed in A. Error bars show 95% CI. Means represent an average of ~90 cells per strain from each of 3 independent experiments. Stage-specific data labeled with the same letter are not significantly different from each other. Statistical differences were at the level of $P<0.05$ for both hyphal stages. These results are similar to those observed in Mlc1 experiments, suggesting that one copy of Rsr1 is not sufficient to restore the localization or the index at early time points, but is sufficient for recovery of characteristics in mature hyphae.

Chapter 3

Rsr1-GTPase Cycling Promotes Efficient Clustering Of Cdc42 and Limits Competition For Polarity Factors During *C. albicans* Hyphal Development

All experiments performed and data analyzed completely by REP except:
MI and hyphal branching data collection (Figs.3.1, 3.2) performed with the help of Sara Gonia.
Time-lapse Mlc1 localization experiments and data collection (Figs.3.3, 3.4) performed with help from Jennifer Norton and Kendra Van Beusekom.
RNA expression experiments (Fig.3.5) performed by Tim Heisel; data analyzed by REP.

I. Introduction

GTPases are often described as cellular switches, 'on' in their GTP-bound state and 'off'' in their GDP-bound state. However, it is thought that cycling between these forms, rather than any single guanine nucleotide bound state, is important to the function of GTPases in a number of biological processes, including polarized growth (20, 29, 45, 53, 65, 73).

The process of polarization has been the topic of many investigations using the yeast *S. cerevisiae,* and involves the creation of a stable cluster of activated Cdc42, a Rho-GTPase, to the site of growth followed by emergence of a daughter bud (17, 52). Models of spontaneous polarization in both *in silico* and "feedback re-wired" *S. cerevisiae* strains, support the idea that the ratio between the rate of Cdc42 activation (K_{on}) and the amount of positive feedback (K_{fb}) to the growth site controls polarization frequency, and can influence the number of Cdc42 clusters able to persist in a cell at any one time (3, 65). The computational model predicts that when the K_{on} is relatively large as compared to the K_{fb}, the accumulation of Cdc42 at the membrane quickly becomes uniform and polarization is less likely. In contrast, as the K_{on} decreases with K_{fb} remaining constant, the ability to form a stable cluster increases and polarization events are more likely to occur. Results from feedback re-wired *S. cerevisiae* strains suggest that increasing feedback to the site can generate multiple clusters, but that multiple Cdc42 clusters within the same cell compete for polarity components and usually result in a "winner takes all" situation (50). The inactivation of Cdc42 is also critical to the process of polarized growth (53, 65, 90). Inactivation of Cdc42-GTP by either hydrolysis, via the Cdc42 GAPs, or its removal from the membrane, via the guanine nucleotide dissociation inhibitor, Gdi1, limits the region of Cdc42 activity on the membrane and impacts bud shape (65, 90). However, one caveat to these models is that unlike the situation in *S. cerevisiae,* or even during *C. albicans*' yeast form growth, clustering of Cdc42 during *C. albicans* GT emergence is F-actin dependent (46). During GT emergence, the stability or maintenance of Cdc42 clusters is thought to be dependent on the activation of

downstream effectors of Cdc42 at the growth site. As a result, actin cables are directed to the site of growth and growth is reinforced to the region through directed transport (46, 52-54, 62). Polarization during *C. albicans* hyphal growth requires that this process must also be continually maintained at hyphal tips throughout development. After the initial polarization event at emergence, Cdc42 activity must be restricted to a small region at the hyphal tips to generate the narrow morphological characteristics of GTs and mature hyphae (33). As the cell transitions to the mature stage of hyphal growth, two simultaneous regions of Cdc42 activity are present within the cell; one narrow region of Cdc42 activity is maintained at the hyphal tip and a second, transient, region of Cdc42 activity forms at what will become the septum. After septation is completed, Cdc42 activity is again localized exclusively to hyphal tips for the remainder of the cell cycle.

Data from the previous chapter show that Rsr1 is involved in focusing Cdc42 activity at hyphal tips, and is important for the maintenance of polarized growth. Only cells with WT or higher Bem1-YFP intensity indices were able to maintain Bem1-YFP localization in mature hyphae. In addition, time-lapse movies of the Spk, marked by Mlc1-YFP, suggested that the failure to transition to the mature stage of hyphal growth often coincided with septum formation, indicating that hyphal growth maintenance is particularly sensitive to disruption when two sites of growth are simultaneously supported. A potential mechanism to address how *two sites* of polarized growth are initiated and maintained has been proposed in *S. pombe* (34). Results from that study suggest that in order to initiate and maintain two sites of growth, there must be sufficient spatial separation to limit competition, and/or sufficient polarized growth components must be produced to support the second growth site. In both single and dual site growth models, polarization is dependent on the cell's ability to recruit Cdc42 to specific sites, while restricting its activity in other areas (3, 17, 49, 50, 52-54, 62, 90, 103). The common requirement in all of the models proposed is that creation and maintenance of a growth zone(s) is, at least to some degree, dependent on the availability of Cdc42.

In *C. albicans*, Cdc42 is uniformly localized throughout the yeast cell membrane and as GT growth is initiated, Cdc42 is re-localized to the site of growth (31). The region

of activity is thought to be enhanced through positive feedback mechanisms until there is a sufficient amount of components and activity to drive polarized secretion (8, 46). Data presented in Chapter 2 suggest that Rsr1 helps to focus Cdc42 activity at hyphal tips (Fig.2.5), and that focusing Cdc42 is needed to facilitate the feedback that maintains the expression of the hyphal transcriptional program (Fig.2.4). Localized Rsr1 activity at hyphal tips, along with the predicted interactions of the Rsr1 GTP-and GDP-bound forms with the polarity proteins Cdc42, Cdc24, and Bem1 (11, 73, 81), provides a possible mechanism for how Rsr1-cycling activity could spatially restrict the activity of Cdc42 and support continuous polarized hyphal growth. I hypothesize that Rsr1 activity, by cycling between its GTP and GDP bound forms, has the capability to control both positive feedback to regions of Cdc42 activity, as well as the negative feedback that delimits the region of Cdc42 activity.

In this chapter, I use the deletion of the Rsr1-GAP (Bud2) and-GEF (Bud5) to examine the effects of Rsr1-GTP and GDP on growth initiation and maintenance, hyphal morphogenesis, and the expression of the hyphal transcriptional program. My data show that Bud2 activity strongly affects hyphal widths by limiting the window of Cdc42 activity, and supports polarized growth initiation. In comparison, Bud5 activity does not have as strong of an effect on hyphal widths, but does support growth maintenance in mature hyphae. Together, these data support my previous hypothesis that Rsr1 helps focus Cdc42 activity at hyphal tips, and extends those results to show how spatial restrictions may be imposed by Rsr1 cycling to affect growth initiation, morphology, hyphal gene expression, and maintenance of hyphal growth. Using these results and those from the previous Chapter, I propose a mechanism of conservative polarization in which Rsr1-cycling limits the amount of Cdc42 needed to achieve polarization at GT initiation, and enhances the maintenance of polarized growth by slowing Cdc42 activation rates and spatially restricting the region of Cdc42 activity at hyphal tips.

II. Materials & Methods

Strains, Culture Conditions, and General Procedures

Strains were grown as previously described (81), unless otherwise noted. *C. albicans* strains used in this study are listed in Table 3.1. Strains were constructed as previously described using PCR-mediated gene modification (26, 27). Primers used in the construction of strains are listed in Supplemental Table 3.1. Constructions were verified by PCR using at least one primer that targeted a sequence outside of the site of integration. In addition, expression of fluorescent proteins was evaluated by fluorescence microscopy and western blotting as described in Chapter 2(81). DAPI (4',6-Diamidino-2-Phenylindole, Dihydrochloride, Roche, #10236276001) was used in determining the number of nuclei in each cell during yeast form growth. Briefly, exponentially growing cells from each strain were harvested from a 4 hr subculture, resuspended in DAPI (5mg/ml) in phosphate buffered saline (PBS) solution for 5 min, and rinsed with PBS before imaging.

Image Acquisition and Processing

Still and time-lapse images were collected as previously described in Chapter 2 (81) using a Nikon E600 microscope equipped with 60X/1.4 NA and 100X/1.4 NA objectives, FCS2 objective heaters (Bioptechs, Butler, PA), and epifluorescence. MetaMorph version 6.3r7 (Molecular Devices LLC, Sunnyvale, CA) was used for acquisition and processing of all images, with the exception of FRAP experiments. Image acquisition settings and processing for time-lapse images of Mlc1-YFP localization, as well as still images of Bem1-YFP localization were identical to those listed in Chapter 2(81). For MI and hyphal branch analysis, strains were grown for 4 hr under identical time-matched conditions, and DIC images were collected on each of three separate days. A maximum of 20 fields were collected for each strain on each day using 60X objective and acquisition setting of: 50 ms exposure, 6 steps, with a step size of 3. Stacked DIC images were merged using the “Best Focus” algorithm in MetaMorph.

Images of DAPI staining were collected using the Nikon E600 listed above (acquisition settings, 60X objective, 50 ms exposure, 86004v2 JP5 filter cube). Final images were adjusted for brightness and contrast, and were cropped and resized as a group for each set of experiments using Adobe Photoshop CS3 (Adobe Systems Inc, San Jose, CA).

Image Quantifications

To assess MI, the hyphal length, width, and septal/cell junction distance were collected using the measurements tool in MetaMorph version 6.3r7, logged to Microsoft Excel. The MI was calculated for each cell (70). For hyphal branch analysis the number of branches, per hypha were counted. Branches were considered aberrant if the branch placement was <10µm from the septa and/or if the branch occurred in the apical compartment. The number of hyphae with apical branches was also logged separately, for each strain, for use in apical branching analysis. Fluorescence Recovery after Photobleaching (FRAP) experiments were performed, and images were collected and analyzed as previously described in Chapter 2. Briefly, recovery intensities were normalized (78, 81) prior to fitting using the non-linear regression tool (f=a*(1-exp(-b*x))) of SigmaPlot (version 10.0, Systat Software, San Jose, CA). The values of coefficient of determination (i.e. R^2 values) for GTs and mature hyphae of each strain were analyzed for differences (see statistical methods below). Bem1-YFP tip localization and intensity indices were determined as described in the previous chapter.

Mlc1-YFP localization analysis

Results from Chapter 2 noted that the times at which the Mlc1-YFP Spk-associated signal was no longer visible coincided with septum formation in *rsr1*Δ/Δ strains. Thus, to focus the analysis on changes in Mlc1-YFP tip localization *during septum formation*, only the 10th frame prior to the first visible septum up until the 10th frame after the septum was no longer visible where quantified from and included in the analysis of the time lapse movies. The percent of Mlc1-YFP localized to hyphal tips during time-lapse imaging, was calculated for each frame of the time-lapse movie using the following equation: $(I_{Spk}\text{-Bkgr}/I_{WC}\text{-Bkgr})*100$. Where I_{Spk} is equal to the mean

integrated intensity of the Spk, Bkgr is equal to the background fluorescence levels from a region outside the cell, and I_{WC} is equal to the whole cell fluorescence intensity.

Quantitative Real-Time PCR (qPCR)

Quantitative real-time PCR assays, used to determine the expression levels of HSGs, were performed as previously described in Chapter 2(81) using the primers listed in Supplemental Table 2.2.

Statistical methods

Bem1-YFP localization and intensity index data were analyzed as previously described in Chapter 2 (81). Morphological assessments (i.e. MI and branch analysis) were performed using multivariate analyses using the general linearized model (GLM) option in SPSS 16 (IBM, Armonk, NY). MI data was assessed using a Main Effects Model in the GLM, and excluding the intercept to blocking for day-to-day variation in hyphal induction. A repeated measures analysis of variance, was performed on time lapse data obtained from Mlc1-YFP localization movies (P=0.052), but the analysis was abandoned for two reasons. First, I was not confident in the resultant trend based on the sample size, which was limited because data collection for this analysis was extremely labor intensive. Second, the means obtained by pooling the percent of localized florescence for all time points in the time-lapse movie (the Spk and septa) appeared to be an accurate representation of our observations that also had a clear biological rational for the changes in Mlc1 localization at the tips of *rsr1*Δ/Δ hyphae. Comparison of percent localization and whole cell intensity values of Mlc1-YFP were also done using the multivariate analysis in the GLM. Percent localization for Spk and septa, and whole cell Mlc1-YFP intensity values were assessed using a Main Effects Model with the intercept included. Post-hoc separation of means procedures were performed in all cases using Tukey's Honestly Significant Differences.

III. Results

Hyphal morphology defects of *bud2*Δ/Δ strains are more severe than those of *bud5*Δ/Δ strains. Changes in morphogenetic characteristics from those of wild-type *C. albicans* cells in response to a mutation or environmental perturbation can give us insight into the regulation of polarized growth. By carefully quantifying aspects of these morphological changes, I am better able to understand the specific requirements for morphogenesis. Previously, both *rsr1*Δ/Δ and *bud2*Δ/Δ strains, unlike *S. cerevisiae* strains with the orthologous deletions, were reported to have enlarged cell sizes and have more rounded cell shapes (45). In addition, hyphae of *rsr1*Δ/Δ and *bud2*Δ/Δ strains had a more pseudohyphal appearance, and *bud2*Δ/Δ hyphae branched more frequently than hyphae of WT *C. albicans* strains (45). To further quantify morphological observations in *rsr1*Δ/Δ and *bud2*Δ/Δ hyphae, and to make initial observations of *bud5*Δ/Δ hyphae, the MI for WT and each of the null mutant strains was quantified and compared after growth in hyphal induction medium for 4 hrs. Consistent with previous qualitative observations that both *rsr1*Δ/Δ and *bud2*Δ/Δ appeared more pseudohyphal (Fig.3.1A), the MIs of both *rsr1*Δ/Δ and *bud2*Δ/Δ hyphae were significantly lower than WT hyphae grown on the same days (Fig.3.1B). In comparison, *bud5*Δ/Δ hyphae appeared more hyphal-like and had a significantly higher mean MI than *rsr1*Δ/Δ and *bud2*Δ/Δ hyphae; however, the MI of *bud5*Δ/Δ hyphae was reduced compared to that of WT hyphae. In addition, I compared the individually measured components of the MI to address how morphology was specifically altered in the null mutant hyphae (Supplemental Fig.3.1). Hyphal lengths and widths of *bud2*Δ/Δ and *rsr1*Δ/Δ hyphae did not differ from one another, and while septa of *rsr1*Δ/Δ hyphae were less constricted than those of *bud2*Δ/Δ hyphae, the difference did not impact the MI overall. In comparison, the lengths of *bud5*Δ/Δ hyphae were equal to those of WT, whereas the lengths of *bud2*Δ/Δ and *rsr1*Δ/Δ hyphae were significantly shorter than both *bud5*Δ/Δ and WT hyphae. The hyphal widths of the *bud5*Δ/Δ strain were intermediate, significantly narrower than either *bud2*Δ/Δ or *rsr1*Δ/Δ,

but still not equal to those of WT strains. These data suggest that both Rsr1-GDP and Rsr1-GTP play roles in maintaining hyphal widths and lengths. Hyphae from *bud2*Δ/Δ strains, thought to be enriched in Rsr1-GTP, had a more pseudohyphal appearance. In comparison, hyphae of the *bud5*Δ/Δ strains, which logically are enriched in Rsr1-GDP, are statistically wider than the WT strain. Together, these results support the idea that efficient Rsr1 cycling (a specific balance between Rsr1-GTP and GDP) is needed to achieve the WT hyphal morphology.

In addition, I quantified and compared the branching frequency in mature hyphae of the Rsr1 cycling mutants with those of the WT strain (Fig.3.2A) to investigate the role of Rsr1 cycling in polarity establishment during hyphal morphogenesis. Branching represents the ability to form new clusters of Cdc42, and the frequency with which new clusters are formed in the growing hypha. The average number of branches per hypha in the *bud2*Δ/Δ strain was greater than in WT, and *rsr1*Δ/Δ hyphae had an intermediate branching frequency. In contrast, the branching frequency of *bud5*Δ/Δ hyphae was equal to that of WT and significantly less that of the *bud2*Δ/Δ strain. Branch positioning was also assessed. WT *C. albicans* hyphae form branches adjacent to septa, proximal to the mother cell. In *rsr1*Δ/Δ and *bud2*Δ/Δ hyphae, branch positioning is defective (45). Upon closer observation, in these mutant strains, branches formed at a distance greater than 10 μm from the septum and/or were located in the apical compartment more frequently than in WT hyphae. The aberrant branching frequencies of *bud2*Δ/Δ hyphae were the highest among all of the strains; *rsr1*Δ/Δ and *bud*5Δ/Δ strains both had an intermediate aberrant branching frequency as compared to that of WT and *bud2*Δ/Δ hyphae (Supplemental Fig.3.2). Even more striking in this analysis was the increased frequency of apical branching (branching in the most apical compartment) in *bud2*Δ/Δ hyphae that resulted in bifurcated hyphal compartments (Fig.3.2B, C). A potential explanation for this phenotype in *bud2*Δ/Δ hyphae can be derived from the localization of Bud2-YFP as observed during hyphal development (Fig.2.1). Diffusely localized Bud2-YFP in the apical, actively elongating, compartment suggests the possibility that Bud2 acts in inhibiting the stochastic activation of Rsr1, thereby preventing branch formation in the apical

compartment. Together, the results from the hyphal branching analyses suggest that regulating the amount and spatial distribution of Rsr1-GTP is important in preventing ectopic Cdc42 clustering and in maintaining a singular focus of polarized secretion during WT hyphal elongation.

In addition, *rsr1*Δ/Δ and *bud2*Δ/Δ strains often contain multiple nuclei, whereas WT cells are mononuclear (Fig.3.3). The multinuclear phenotype of the mutant strains is likely a consequence of defects in cytoskeleton polarization ((45) and unpublished data). Interestingly, *bud5*Δ/Δ strains that exhibited hyphal morphologies more like those of the WT strain, also had a reduced frequency of multi-nucleate cells as compared to *rsr1*Δ/Δ and *bud2*Δ/Δ strains (Fig.3.3). These data support the idea that Rsr1 function is important for cytoskeletal organization, and promotes the faithful segregation of nuclei during polarized growth. Altogether, these data and results from the morphological analysis support the idea that negative regulation of Rsr1 (i.e. GDP-bound) plays an active role in polarization events and that a balanced proportion of the GTP/GDP-bound forms of Rsr1 are needed to achieve WT polarized growth characteristics (narrow cell shapes (MI), limited branching, cytoskeletal polarization).

Competition for polarity factors between Spk and septum is disrupted by changes in Rsr1 cycling. The morphological and nuclear analyses indicate that the degree of disruption to the cytoskeleton and polarized growth processes of the *bud5*Δ/Δ strain are less than that of *rsr1*Δ/Δ and *bud*2Δ/Δ strains. A possible reason for the less severe phenotypes is that *bud5*Δ/Δ hyphae are able to direct and/or retain components of polarized growth machinery to hyphal tips more effectively than either *rsr1*Δ/Δ or *bud2*Δ/Δ strains. Cycling of Rsr1 at hyphal tips, in conjunction with the predicted interactions of Rsr1 with Cdc24 and Cdc42, sets up a potential mechanism for polarity factors to be retained in regions of active growth. I previously observed that localization of the Mlc1-Spk signal, a downstream marker of Cdc42 activity, was lost in *rsr1*Δ/Δ hyphae specifically at times of septation (81). This indicated that the ability to retain polarity factors like Mlc1during the completion of the cell cycle, may be reduced in *rsr1*Δ/Δ hyphae. To gain more information about how Rsr1 cycling was affecting the

localization and retention of Mlc1 to hyphal tips during septum formation, I quantified and compared fluorescence intensity values of Spks and septa, as a percent of the whole cell fluorescence, from time-lapse movies of WT, *rsr1*Δ/Δ, *bud2*Δ/Δ, and *bud5*Δ/Δ hyphae. A minimum of 40 frames per hypha were quantified spanning the times shortly before, during, and after septum formation was complete, and only movies in which polarized growth continued in the primary hypha were used for quantification purposes. Consistent with my earlier qualitative observations in *rsr1*Δ/Δ hyphae, the Spk-associated signal showed the greatest reduction in intensity when the signal from the septum was at its peak (Fig.3.4). Quantitative fluorescence data from time-lapse movies of *bud2*Δ/Δ and *bud5*Δ/Δ hyphae expressing Mlc1-YFP showed a similar relationship between the Spk and septum-localized signals. Somewhat surprisingly though, when the Mlc1-Spk and septum localizations were analyzed in the WT strain, a similar anti-correlated pattern was observed. This consistent fluctuation between the Spk and septum-localized signals in all strains, including WT, suggests a potential competition between the sites for polarity factors during septation events. To determine if the competition between these two sites of polarized growth is affected by changes in Rsr1 cycling, I averaged the percent of whole cell Mlc1-fluoresence that was localized to either the Spk or septum, from multiple hyphae, and compared those values between strains (Fig.3.5). The percent of Mlc1-fluorescence that localized to the Spks differed between all strains. WT showed the highest percentage of Spk-associated fluorescence, followed by *bud5*Δ/Δ, *rsr1*Δ/Δ, and finally *bud2*Δ/Δ (Fig.3.5A). Thus, of all the mutant strains, *bud5*Δ/Δ strains appear to be the best able to retain Mlc1-YFP at the Spk. Given the results showing that reduced Spk fluorescence levels are at their lowest when fluorescence levels at the septum are at their peak, it is tempting to speculate that the Spk-signal reduction might be due to a direct re-allocation of polarity factors from the Spk to the septum. If this were the case, I would expect a proportional *increase* in septal fluorescence in the mutant strains. However, when the percent of Mlc1-YFP fluorescence localized to septa was analyzed between strains, the fluorescent signals were equal to, or lower than those, of WT (Fig.3.5B). These results argue that the reduced Mlc1 Spk signal in the null mutant

strains is not because Mlc1-YFP is being re-allocated to the septum, because the mean septum fluorescence did not show increases in intensity that were proportional to losses observed at the hyphal tip. Rather, these results suggest that the Mlc1-YFP fluorescence had become delocalized in the null mutant strains, and in particular, the effect is greatest for the *bud2*Δ/Δ strain. These results are consistent with idea that Bud2 (or Rsr1-GDP) acts as a barrier to prevent loss of polarity components from hyphal tips to a competing site of polarized growth. Although Bud5 also has a role in this, its function may be less than that of Bud2, since the amount of mislocalization, inferred by the respective loss of fluorescence signal in the Spk and septum, was minimal in *bud5*Δ/Δ hyphae. These results are consistent with the observation that *bud5*Δ/Δ hyphae have a more hyphal MI than *bud2* hyphae (Fig.3.1). I hypothesize that mislocalization of Mlc1 in the Rsr1-cycling-deficient strains is a result of an imbalance in the ratio of Rsr1-GTP to GDP. Overall, these data are consistent with the idea that the GTP- and GDP-bound forms of Rsr1 influence the ability of polarity factors to localize to, and be maintained at, hyphal tips. Importantly, the total cellular levels of Mlc1-YFP did not differ between any of the strains by quantitative western blot analysis (Fig.3.5C, Fig.2.3D). Thus, it is unlikely that the fluorescence intensity differences in the mutant strains were due to changes in Mlc1-YFP expression levels.

The apparent greater increase in mislocalization of Mlc1 observed in the *bud2*Δ/Δ strain raised the possibility that vesicle delivery is misdirected in this strain. To test this, I analyzed the R^2 values derived from FRAP experiments of FM4-64 stained vesicles in WT, *bud2*Δ/Δ, and *rsr1*Δ/Δ GTs and mature hyphae. The R^2 value, or correlation co-efficient, is determined from the FRAP recovery curve, and represents the dependency of fluorescence recovery with respect to time. In GTs, R^2 values did not differ between strains (Table 3.2). In contrast, R^2 values obtained from mature *bud2*Δ/Δ hyphae were significantly lower than those from *bud2*Δ/Δ GTs, and lower than those of mature WT hyphae, and this finding was specific to the region in which the Spk normally localizes (the hyphal tip). R^2 values of *rsr1*Δ/Δ strains did not differ between stages of growth or from the R^2 values obtained in mature WT hyphae. These results show that the regular,

step-wise, amount of fluorescence recovered per unit time (i.e. the "pattern" of vesicle delivery) as observed in WT hyphae is disrupted in mature *bud2*Δ/Δ hyphae, and indicate that vesicle delivery to hyphal tips is disorganized. In addition, these data support the results of the time-lapse measurements, where *bud2*Δ/Δ hyphae showed a higher level of Mlc1-YFP mislocalization than *rsr1*Δ/Δ hyphae.

WT Rsr1 cycling is required for WT HSG expression. Thus far, I've shown that *C. albicans bud5*Δ/Δ strains (presumed enriched for Rsr1-GDP) appear to be less severely affected, with respect to cell biological markers of morphology than *bud2*Δ/Δ strains (presumed enriched for GTP-Rsr1). As an additional measure of hyphal development, I monitored and compared the expression of hyphal specific genes using qPCR, as previously described (81). When expression of the individual genes was compared between strains in GTs at 30 min of induction and mature hyphae at 4 hrs of induction, both *bud2*Δ/Δ and *bud5*Δ/Δ strains showed a significant increase in expression for each representative HSG above that of the *rsr1*Δ/Δ strain, and in some cases did reach WT levels (Supplemental Fig.3.3). To better assess how the overall expression of HSGs was impacted as a group, results for each strain were pooled and compared at each stage of hyphal development (GT versus mature hypha). Analysis of the pooled expression levels supported the general observations made with individually expressed HSGs that both *bud2*Δ/Δ and *bud5*Δ/Δ strains showed higher HSG expression as compared to the *rsr1*Δ/Δ strain, but reduced levels as compared to the WT strain (Fig.3.6A). Further, no significant differences were observed between the developmental stages for any individual strain. The finding that *bud2*Δ/Δ and *bud5*Δ/Δ strains did not differ with respect to HSG expression suggests that intact cycling is required, rather than a specific guanine nucleotide-bound form, for Rsr1 to provide WT levels of feedback to the hyphal transcriptional program. Together with the data presented in Chapter 2 (81), these results support the idea that Rsr1 cycling activity is important for promoting the hyphal developmental program at the transcriptional level.

Bud2 function (Rsr1-GDP) supports polarized growth initiation whereas Bud5 function (Rsr1-GTP) supports maintenance of polarity in mature hyphae. The

data presented in the previous chapter supports the idea that achieving a specific level and distribution of Cdc42 activity in GTs is important for the continued maintenance of hyphal growth (Fig.2.5C). The data also suggested that Rsr1 activity impacts GTs differently than mature hyphae (Fig.2.5D). Specifically, in GTs, Rsr1 activity appears to define the window of polarized secretion by preventing too much active Cdc42 from localizing to hyphal tips. In mature hyphae, Rsr1 activity maintains the window of polarized secretion by promoting the retention of active Cdc42 and its effectors to hyphal tips. To evaluate the role of Rsr1 cycling on the level and distribution of Cdc42 activity, I compared the localization characteristics of Bem1-YFP, a proxy of Cdc42-GTP localization, in WT, *bud2*Δ/Δ, and *bud5*Δ/Δ GTs and mature hyphae.

The ability to localize Bem1-YFP to growth sites of *bud2*Δ/Δ and *bud5*Δ/Δ cells, incubated for a short time (30 min) in hyphal-induction media, did not differ from that of WT cells (Fig.3.7A). However, I noted a difference in the number of successful polarization (i.e. emergence) events between the strains. I categorized the cells with Bem1-YFP localization as either incipient GT (IGT) or emerged GT (EGT), and determined the average ratio of IGT to EGT per high-power field. Both *bud5*Δ/Δ and *bud2*Δ/Δ strains had a ~ 1:1 ratio of IGT to EGT, whereas WT strains showed a 4:1 ratio at the same time point. This shows that while the number of cells with Bem1-YFP localization for either strain did not differ from WT, both *bud2*Δ/Δ and *bud5*Δ/Δ GTs emerged more frequently. When the percent of cells with distinct Bem1-YFP localizations was compared between *bud2*Δ/Δ and *bud5*Δ/Δ strains, the percent of *bud5*Δ/Δ cells with a Bem1-YFP signal was significantly greater than that of *bud2*Δ/Δ cells ($P=0.002$). These data suggest that *bud5*Δ/Δ strains, predicted to be enriched for Rsr1-GDP over Rsr1-GTP, have a greater ability to polarize than *bud2*Δ/Δ cells, which are predicted to be enriched for Rsr1-GTP over Rsr1-GDP. In addition, I observed that a small but consistent percentage of *bud5*Δ/Δ IGTs had two or more distinct Bem1-YFP clusters simultaneously (Fig.3.7B). Further, many *bud5*Δ/Δ cells had multiple small outgrowths that no longer showed Bem1-YFP localization to those tips, which were likely aborted attempts at GT emergence. When images of WT, *rsr1*Δ/Δ, and *bud2*Δ/Δ

strains taken at the same induction time were carefully inspected for similar defects, no evidence of multiple clustering was observed for either WT or *rsr1*Δ/Δ, and only one instance was observed in *bud2*Δ/Δ strains. Similarly, no such aborted GT emergence sites were observed in WT, and only a few instances were observed in *bud2*Δ/Δ and *rsr1*Δ/Δ strains. Thus, these data support the idea that Rsr1-cycling influences the activity of Cdc42, and impacts polarity establishment and early GT growth.

In comparing the Rsr1 cycling mutant strains with respect to Bem1 localization characteristics at 30 min of hyphal induction, the Bem1 intensity index of *bud2*Δ/Δ strains was reduced compared to WT. In comparison, the intensity index of *bud5*Δ/Δ strains was intermediate to that of WT and *bud2*Δ/Δ strains (Fig.3.7C). Analysis of the individual index components revealed that despite fluorescence intensities that were higher than WT, the indices for both *bud2*Δ/Δ and *bud5*Δ/Δ cells were reduced due to a broader distribution of the fluorescence signal. Importantly, these increases in fluorescence intensity and distribution, while greater than WT, were far more modest than those previously observed in *rsr1*Δ/Δ cells. Previously, I showed a correlation between the reduced Bem1-YFP intensity indices of the *rsr1*Δ/Δ strain, and a reduced HSG expression profile. In comparing these results in *bud2*Δ/Δ and *bud5*Δ/Δ strains (Figs.3.6, 3.7), it is possible that the increased HSG expression level observed for *bud2*Δ/Δ and *bud5*Δ/Δ at 30 min of induction, as compared to *rsr1*Δ/Δ strains, is related to the more modest levels of change in the measured parameters of the Bem1 intensity index. These differences could reflect a change in the level of Cdc42 activation that is closer to that observed in WT, and might explain the increased HSG expression levels in *bud2*Δ/Δ and *bud5*Δ/Δ despite having a lower than WT Bem1-YFP intensity index. Still, these data support the idea that a balanced ratio of Rsr1-GTP to Rsr1-GDP is required to create a more focused Cdc42 cluster in GTs, which is needed to achieve WT HSG expression levels.

As compared to GTs after 30 min of induction, mature *bud2*Δ/Δ and *bud5*Δ/Δ hyphae after 4 hr of induction had different phenotypes with respect to Bem1 localization characteristics. Both *bud2*Δ/Δ and *bud5*Δ/Δ strains showed a significant decrease in the

ability to localize Bem1-YFP to hyphal tips as compared to the WT strain, with *bud5*Δ/Δ strains showing the most severe defect (Fig.3.7A). These results seemed somewhat surprising at first, because the morphological defects and the Mlc1-YFP mislocalization defect had been less severe in *bud5*Δ/Δ hyphae. However, the Mlc1-YFP time-lapse assay looks at how well the polarity component is retained at hyphal tips only during the period of time (generally < 90 min) during the transition from GT to mature hyphal growth (e.g. period of septum formation). Results from the Mlc1-YFP localization analysis in *bud2*Δ/Δ hyphae support the idea that polarized growth can be misdirected to a high degree (as a result of competition between the Spk and the septum); yet, *bud2*Δ/Δ hyphae are still able to direct growth back to hyphal tips after completion of the cell cycle (Mlc1-YFP leaves the septum). The ability of *bud2*Δ/Δ hyphae to redirect growth back to hyphal tips, despite mislocalization during septum formation, is consistent with data showing that a higher percentage of mature *bud2*Δ/Δ hyphae have a localized Bem1-YFP tip signal than *bud5*Δ/Δ hyphae. The ability to reorient growth to hyphal tips after septation, despite the high degree of mislocalization, is likely due to Bud5 activity still being present at the tips of *bud2*Δ/Δ hyphae. Following this logic, it makes sense that fewer mature *bud5*Δ/Δ hyphae show localized Bem1-YFP tip signal, since Bud5 is not present to help counteract the competition between Spk and septum, and maintain growth at the tips of mature hyphae.

The Bem1-YFP intensity indices were also assessed in mature hyphae of WT, *bud2*Δ/Δ and *bud5*Δ/Δ strains. Mature *bud5*Δ/Δ hyphae had Bem1-YFP intensity indices that were significantly increased as compared to both mature WT hyphae and *bud5*Δ/Δ GTs (Fig.3.6B). The Bem1 intensity indices of mature *bud2*Δ/Δ hyphae were intermediate as compared to mature WT and *bud5*Δ/Δ hyphae, and were significantly increased as compared to *bud2*Δ/Δ GTs. Analysis of the individual intensity index components in *bud2*Δ/Δ and *bud5*Δ/Δ hyphae showed that mature hyphae had reduced Bem1-YFP signal areas and widths as compared to GTs, while the overall fluorescence intensities remained unchanged. Therefore, the changes in signal area and width are primarily responsible for the changes in the intensity index between the two

developmental stages. These results are consistent with those reported in Chapter 2 (81) (Fig.2.5), where only a sub-population of mature hyphae that had intensity indices equal to or higher than WT, were able to maintain Bem1-YFP localization at their tips, and again support the idea that an optimum balance between the level of Cdc42 activity and its spatial distribution is required to maintain hyphal morphogenesis.

IV. Discussion

Through cycling, cellular GTPases are able to promote the activity of their substrates in one region while suppressing it in others to create discrete zones of activity within the cell. The data presented here are consistent with my previous conclusion from Chapter 2 (81) demonstrating that, in *C. albicans*, Rsr1 activity has a novel role in controlling the amount and distribution of Cdc42 activity at hyphal tips (Fig.2.5A, D, 3.7C). The localization of Bud5 and Bud2 (Fig.2.1 B, C), and the defects associated with their deletion, suggest that three zones of Rsr1 activity are created in the actively growing hyphal compartment, which impact Cdc42 activity (Fig.3.8). A zone of activation is generated at hyphal tips during GT emergence by the localization of Bud5, and a distinct zone of deactivation is created by the ring-like, subapical, localization of Bud2. These zones act together to focus Cdc42 activity during GT emergence and are maintained at hyphal tips throughout development. A third zone, a zone of inhibition, is created by the more diffuse localization of Bud2 in the actively elongating compartment. In mature hyphae, this zone prevents the spontaneous activation of Cdc42 in actively elongating, apical hyphal compartments. All three of these zones likely act in concert to create a sink-like draw for polarity components that drive continuous polarized growth at hyphal tips. After the cell cycle is complete and the septum has formed, the mother cell returns to a neutral state until growth is once again activated in later cell cycles (i.e. no gradient of Cdc42 activity) and the daughter cell continues to elongate.

The zones of activation and deactivation help to generate the narrow hyphal morphology. Data from the MI and Bem1 intensity index support the idea that the zones

of activation and deactivation act in concert to control morphogenesis. When in balance, Rsr1-GTP (zone of activation) and Rsr1-GDP (zone of deactivation) create a narrow window of Cdc42 activity that defines hyphal widths and influences hyphal cell lengths (Fig. 3.1, Supplemental Fig.3.1, Fig.3.7). The zone of activation directs growth to the region and, to some extent, contributes to the shape of the hypha. However, the zone of deactivation appears to have a greater influence on morphogenesis. The MI of the *bud2*Δ/Δ strain was not different from that of the *rsr1*Δ/Δ strain, whereas the *bud5*Δ/Δ strain had a more "hyphal" MI (Fig.3.1, Supplemental Fig.3.1). I interpret these results to mean that the zone of activation, by itself, is not able to create the narrow window of activity needed to generate the hyphal cell shape. On the other hand, the zone of deactivation does, to a large extent, control the size of the growth region, but by itself, cannot focus the window of active growth to the same extent as WT. The subapical enrichment of Bud2, which defines the zone of deactivation, as opposed to its more diffuse localization throughout the hypha (the zone of inhibition), seems more likely to act in delimiting the region of active growth. Results from the branch analysis and observations from Mlc1-YFP time-lapse analysis suggest that all three zones contribute to the occurrence of branch formation and placement during hyphal morphogenesis. The sink-like draw created by the zone of activation and deactivation may help to retain polarized growth components to hyphal tips, while the zone of inhibition limits the formation of competitive growth clusters. The branch analysis shows a high frequency of ectopic branch placement, including branching in the apical compartment, of *bud2*Δ/Δ and *rsr1*Δ/Δ hyphae (Fig.3.2, Supplemental Fig. 3.2). Observations from the time-lapse analyses of Mlc1-YFP localization in Chapter 2 (81) show that competitive growth sites in the apical compartment occur around the time of septum formation, when polarity components are lost from hyphal tips (Fig.2.3E, Fig.3.5). It follows then that the *bud2*Δ/Δ strain shows the highest occurrence of apical branching because *bud2*Δ/Δ hyphae are the least able to retain polarity components to hyphal tips during septation (Fig.3.5). Accordingly, the *bud5*Δ/Δ shows the least occurrence of apical branch formation because it had the greatest ability to retain polarity components to hyphal tips. These data support

the idea that the zones of activation and deactivation contribute to single site growth by limiting the activity of Cdc42 to hyphal tips leading to better retention of polarity components during septum formation.

The data suggest that the zone of inhibition is also important in preventing apical branching and maintaining tip-focused growth. In my model, the zone of inhibition covers the entire actively elongating cell up to the zone of deactivation. Time-lapse analyses of Mlc1-YFP localization show that apical branches most often occur in the central portion of the apical compartment, rather than "tip-splitting" or branching adjacent to septa (Movies S2.3 and S2.4). As a cell's length increases, the zone of inhibition's role in preventing spontaneous activation of Cdc42 may extend the length over which the zones of activation and deactivation are able to maintain the sink-like draw of polarity components to hyphal tips. This, in effect, would prevent branching in actively elongating compartments and contribute to maintenance of hyphal growth. In *S. pombe* "old end" growth and "new end" growth compete for polarity components, during N.E.T.O., a phenomenon dependent on cell length. As the length of the cell increases, the ability of a single site to effectively draw polarity components decreases and a secondary site is able to initiate and compete for polarity components. Data from *S. pombe* and *S. cerevisiae* suggest that, if sufficient amounts of polarity components are present in the cell, two sites can be maintained; if not, a single site will win (34, 50). By preventing spontaneous clusters of active Cdc42 from forming, growth components can be continuously directed to hyphal tips despite increasing cell lengths. Consequently, the ability of the zone of inhibition to limit spontaneous Cdc42 activity may also play a role in the timing of septum formation. Finley and colleagues showed that septum formation was more dependent on cell length than the length of time in the cell cycle (38). The distance over which the cell is able to maintain the diffuse localization of Bud2 extending back from the tip may be limited; at which point, that distance may be involved in determining the site of septum formation. This distance may be critical to the ability of the cell to maintain tip-growth during the transition between GT and mature hypha, in that too much competition might occur with shorter cell lengths. This could result in an

increase the period of competition, and might appear as the signal "bouncing" between the two growth sites.

Results from the analysis of Bem1 localization and intensity index support the idea that the zones of activation and inactivation impact both the frequency GT emergence and the maintenance of growth in the mature hypha (Fig.3.7A, C). In GTs, Bem1 localization data from *bud5*Δ/Δ and *bud2*Δ/Δ strains suggest that the region of inactivation supports clustering and polarization events in GTs, whereas the region of activation may be needed to limit the frequency of clustering (Fig.3.7A, B). A computational model of particle clustering uses the rate of Cdc42 activation (Kon) and the level of feedback (Kfb) to predict the frequency and efficiency of polarization (3). In addition, the model also factors in the rate of lateral diffusion across the membrane (*D*). Relatively small ratios of Kon/Kfb were found to promote clustering and polarization by decreasing the frequency of activation and enhancing feedback. Not surprisingly, when lateral diffusion rates were assessed as part of the model, their results suggested that high lateral diffusion rates reduced the frequency of polarization events because spontaneous localizations quickly became uniform. In applying these results to the polarization data presented here, it would mean that Rsr1-GTP via Bud5 (zone of activation) is acting to slow the K_{on} of Cdc42. This is the most likely explanation since Rsr1-GTP is known to interact with the Cdc42 GEF, Cdc24, in *S. cerevisiae*, and further, my data showing that *bud5*Δ/Δ hyphae form multiple clusters of Bem1-YFP is consistent with a higher K_{on}/K_{fb} ratio for Cdc42 (Fig.2.5D and 3.7C). The role of Rsr1-GDP, in the zone of deactivation, is most likely to limit lateral diffusion of the zone of activation. Indeed, the Bem1-YFP intensity index of the *bud2*Δ/Δ strain at 30 min of hyphal induction is the lowest of all the strains. Growth maintenance was also impacted when Rsr1 cycling was disrupted. Results from Bem1 localization analyses in mature hyphae show that a higher frequency of successful polarization events in GTs is associated with a reduced ability to maintain growth in mature hyphae. This suggests that in WT strains polarization and initiation of GT emergence may be minimized to increase the duration of polarized growth. Together, these data are in agreement with those from Chapter 2 showing that Rsr1cycling controls

the amount and distribution of Cdc42 at hyphal tips, and extends them to show the different roles of Rsr1 GTP/GDP in limiting the frequency of polarization events and promoting hyphal growth maintenance.

Overall, the tight regulation of these zones suggest the presence of a mechanism that promotes initial polarization events while conserving cytosolic pools of Cdc42 needed for continuous polarized growth. Unlike elongation in several other major taxonomic groups, including Ascomycetes, *C. albicans* elongation rates are linear and not pulsed (43, 45, 66, 87). In addition, *C. albicans*, unlike true fungal spores, require no *de novo* synthesis of proteins for GT emergence (43). This type of growth pattern suggests that a constant supply of polarized growth components is quickly made ready for a faster response to induction, and for growth to be made continuous. The results presented here, and elsewhere (3, 49, 50) support the idea that altering polarization efficiencies can impact growth maintenance, and further that Rsr1 cycling impacts both emergence and maintenance by controlling the level and spatial distribution of Cdc42 activity. In WT strains, Rsr1-GTP in the zone of activation may reduce the K_{on} rate of Cdc42, decreasing the occurrence of clustering and increasing the frequency of successful polarizations. The zone of inactivation limits the window of Cdc42 activity, helping to focus the Cdc42 signal, and minimize the amount of Cdc42 required to achieve polarization. In addition, the focusing effect of these zones may also act to increase positive feedback to the system through enhancing the recruitment of polarity components to the region, via optimization of a polarized actin cytoskeleton (32, 46). The zone of inhibition contributes to this conservative mechanism of growth by preventing the formation of competing clusters of Cdc42, helping to "save" available growth components for hyphal tips. In addition, the zone of inhibition may be involved in determining the site where the septum will form. In other words, the site of septum formation may be where Bud2's effect is no longer maintained. Thus, for *C. albicans*, these zones help establish a conservative mechanism of polarization. This is an attractive model for continuous hyphal growth in *C. albicans* because it allows for the immediate emergence of GTs using "on hand" supplies of

polarized growth components, while at the same time reserving pools of these components that can be used to support continuous polarization.

V. Chapter 3 Tables & Figures

Table 3.1. Strains Used in This Study

Strain	Relevant Genotype	Source
BWP17	*ura3 Δ:: λimm434/ura3Δ:: λimm434 his1::hisG/his1::hisG arg4::hisG/arg4::hisG*	(100)
CA1243	(BWP17) *rsr1::dpl200/rsr1::dpl200 MLC1/MLC1-YFP:HIS1 rsr1::dpl200::rsr1:URA3*	(81)
CA7426	(BWP17) *bud2::HIS1/bud2::ARG4*	(45)
CA7453	(BWP17) *bud2::HIS1/bud2::ARG4 hisG arg4::hisG/arg4::URA3-ARG4*	(45)
CA8880	(BWP17) *rsr1::ARG4/rsr1::HIS1 arg4::hisG/ARG4-URA3::arg4::hisG*	(45)
CA8832	(BWP17) *rsr1::ARG4/rsr1::HIS1*	(45)
CA8841	(BWP17) *bud5::ARG4/bud5::HIS1*	(This study)
CA8870	(BWP17) *bud2::HIS1/bud2::ARG4 arg4::hisG/arg4::hisG MLC1/MLC1::YFP-URA*	(This study)
CA9151	(BWP17) *rsr1::ARG4/rsr1::HIS1 MLC1/MLC1-YFP:URA3*	(81)
CA8855	(BWP17) *bud5::HIS1/bud5::ARG4 ARG4-URA3::arg4::hisG*	(This study)
CA11710	(BWP17) *bud5::ARG4/bud5:: HIS1 MLC1/ MLC1::YFP-URA3*	(This study)
CA12156	(BWP17) *bud2::HIS1/bud2::ARG4 BEM1/ BEM1::YFP-URA3*	(This study)
CA12159	(BWP17) *bud5::ARG4/bud5::HIS1BEM1/ BEM1::YFP-URA3*	(This study)
CA12168	(JB7783) *BEM1/BEM1-YFP:URA3*	(81)
CA12183	(BWP17) *rsr1::ARG4/rsr1::HIS1 BEM1/BEM1-YFP:URA3*	(81)
CA12363	(BWP17) *rsr1::dpl200/rsr1::dpl200*	(81)
CA12388	(BWP17) *rsr1::dpl200/rsr1::dpl200 MLC1/MLC1-YFP:HIS1*	(81)
CA12570	(BWP17) *rsr1::dpl200/rsr1::dpl200 pURA3-rsr1::rsr1::dpl200*	(81)
CA12598	(BWP17) *rsr1::dpl200/rsr1::dpl200 pURA3-rsr1::rsr1::dpl200 BEM1/BEM1-YFP:HIS1*	(81)
JB6284	(BWP17) *his1::hisG/hisG::his1::HIS1 arg4::hisG/ARG4-URA3::arg4::hisG*	(13)
JB7783	(BWP17) *his1::hisG/hisG::his1::HIS1 arg4::hisG/ARG4::arg4::hisG*	(12)
MG7139	(BWP17) *MLC1/MLC1-YFP:URA*	(33)

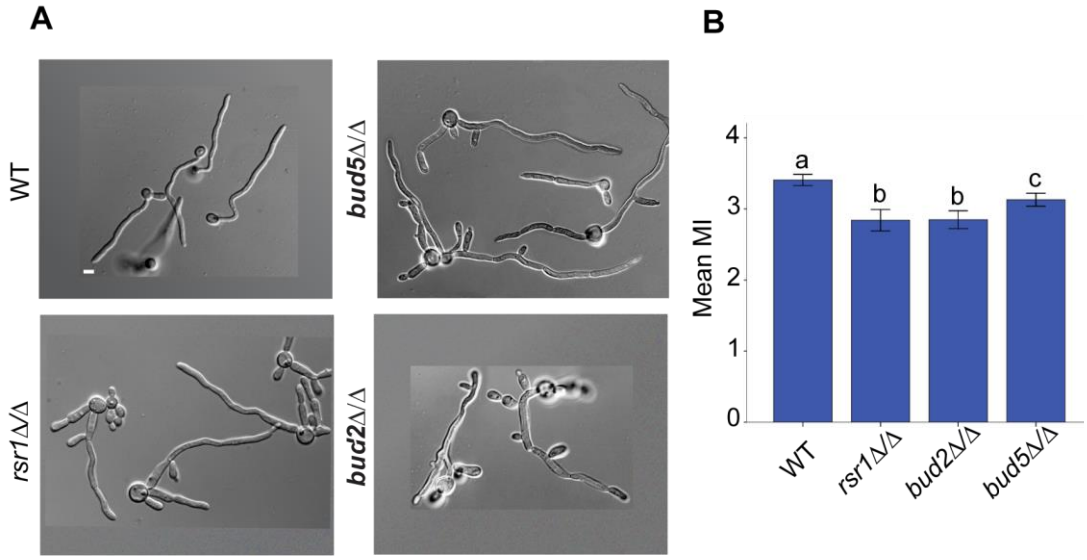

Fig.3.1. Mature Hyphae of *bud5*Δ/Δ Strains Are More Hyphal as Compared to *bud2*Δ/Δ and *rsr1*Δ/Δ Strains, and Are Less Hyphal as Compared to WT. A) Representative DIC images of WT (9955), *rsr1*Δ/Δ (8880), *bud2*Δ/Δ (7453), and *bud5*Δ/Δ (8855) strains. B) Bar graph showing MI results from the strains shown in A. Error bars show 95% CI. An average of ~75 cells per strain, were scored from 3 separate days of experiments. Data sharing the same letter designations are not significantly different from each other. Statistical significance defined as $P < 0.05$.

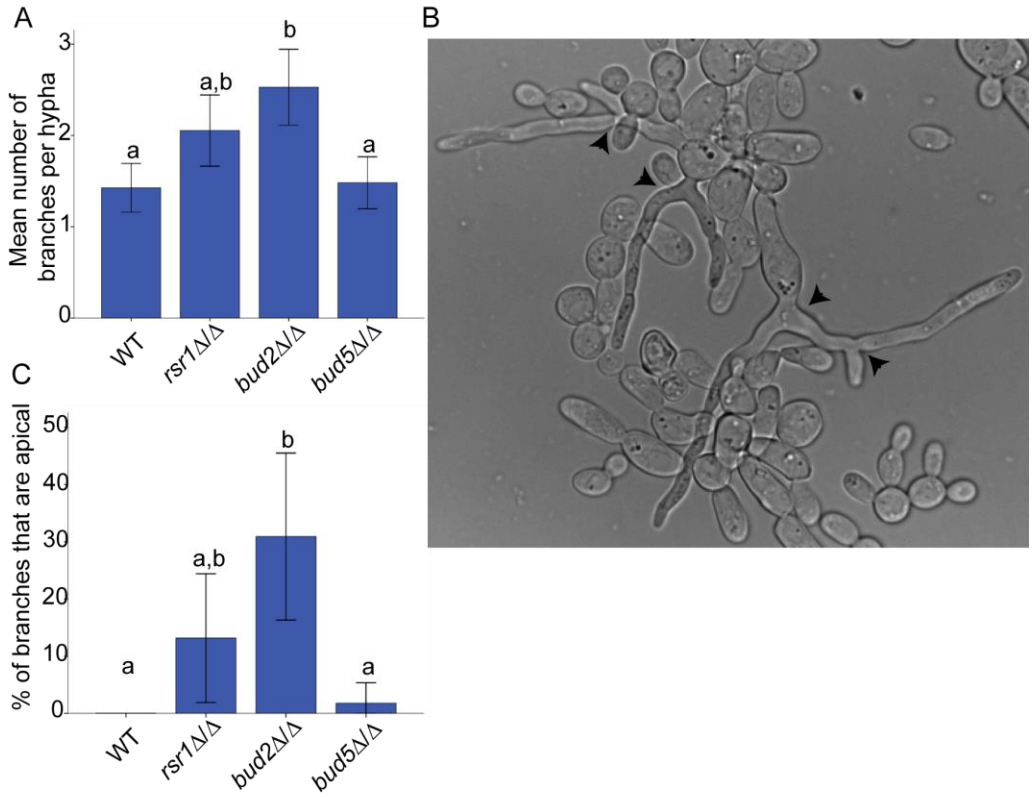

Fig.3.2. Mature Hyphae of *bud2*Δ/Δ Strains Branch More Frequently and in Ectopic Positions as Compared to *rsr1*Δ/Δ, *bud5*Δ/Δ, and WT Hyphae. A) Bar graph depicting the mean number of branches per hypha in WT (9955), *rsr1*Δ/Δ (8880), *bud2*Δ/Δ (7453), and *bud5*Δ/Δ (8855) strains. B) DIC image of *bud2*Δ/Δ hyphae exhibiting apical branches (arrowheads). Note that there is no visible septation in the vicinity of the branch, indicating that the branches are part of a continuous apical cell. C) Bar graph showing the percent of branches, scored in A, that were apically positioned. Error bars show 95% CI. An average of ~45 cells per strain were scored from 2 separate days of experiments. Data sharing the same letter designations are not significantly different from each other. Statistical significance defined as $P < 0.05$.

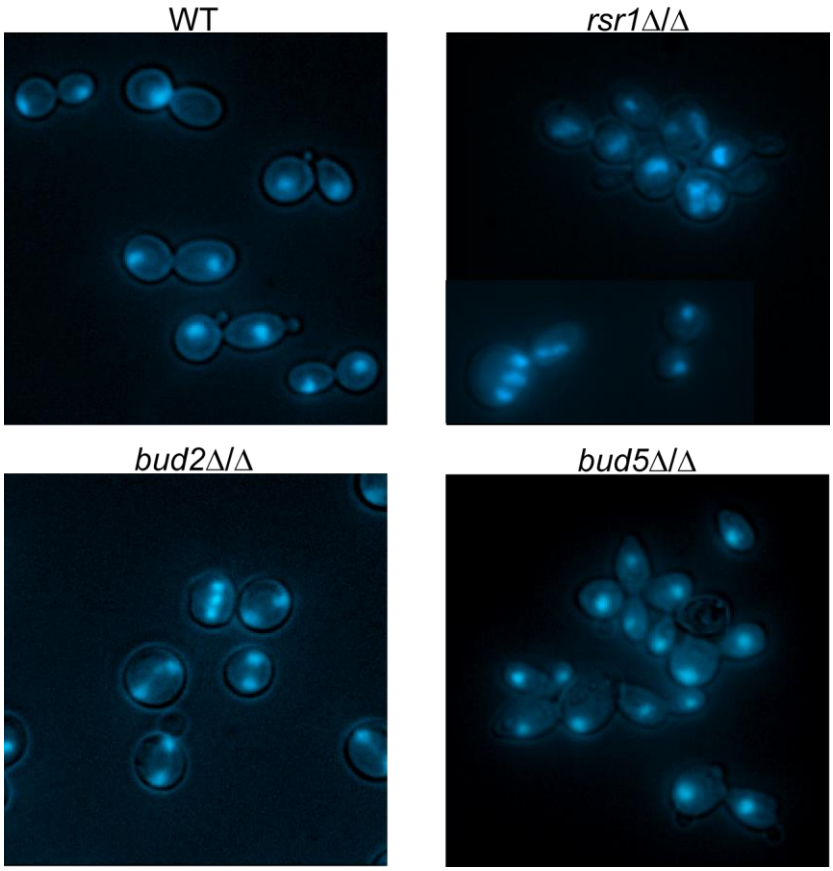

Fig.3.3. *rsr1*Δ/Δ and *bud2*Δ/Δ Strains Exhibit Multiple Nuclei Per Cell, but *bud5*Δ/Δ Strains Do Not. Representative images from DAPI stained yeast of WT (9955), *rsr1*Δ/Δ (8880), *bud2*Δ/Δ (7453), and *bud5*Δ/Δ (8855) strains.

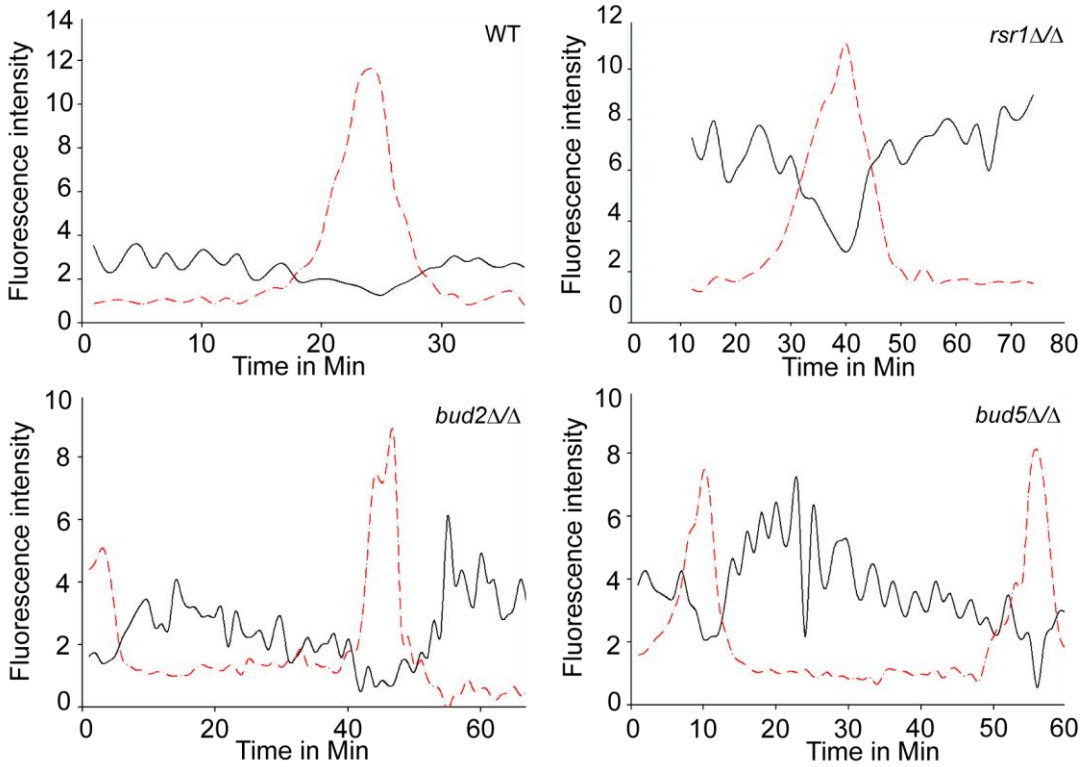

Fig.3.4. Spk and Septum Compete for the Polarity Factor Mlc1 During Hyphal Growth. Plots of the fluorescence intensities of Mlc1-YFP signals at the Spk (black solid line) and septum (red dashed). Data were collected from representative time-lapse movies during hyphal growth of WT (7139), *rsr1*Δ/Δ (9151), *bud2*Δ/Δ (8870), and *bud5*Δ/Δ (11710) strains. Intensity is expressed as a percent of whole cell fluorescence.

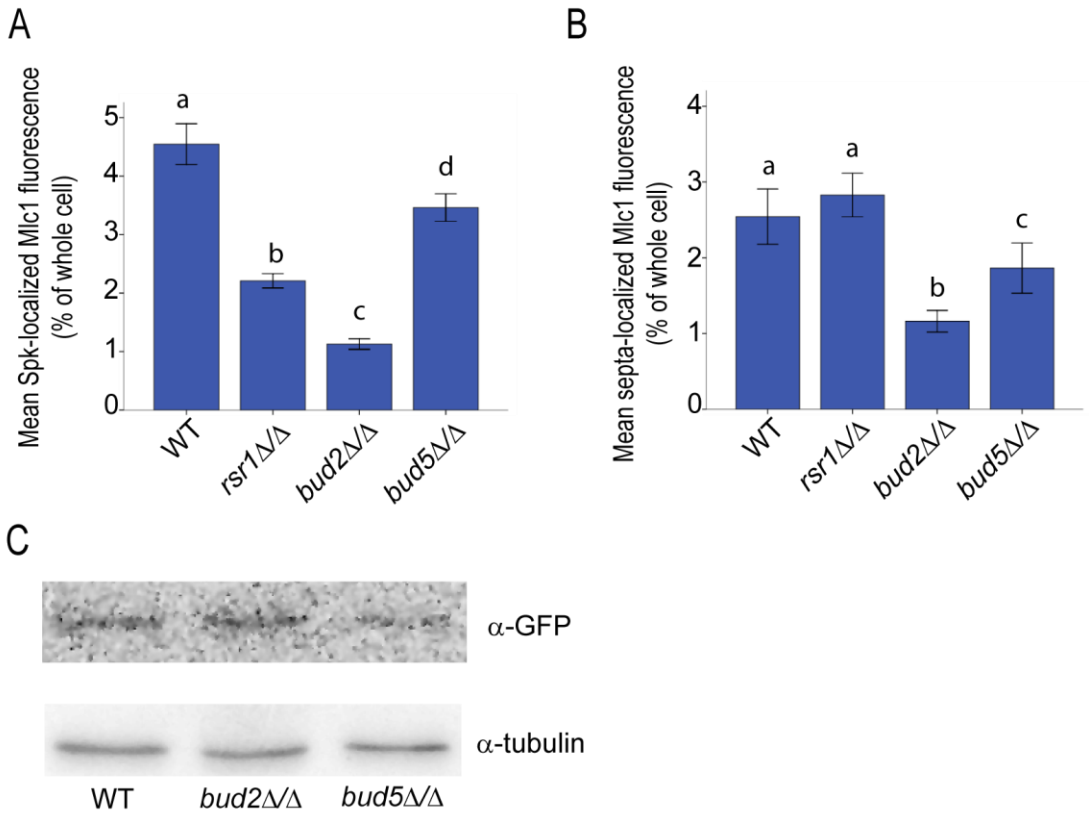

Fig.3.5. Competition Between Spk and Septum is Disrupted in *rsr1*Δ/Δ and Rsr1-cycling Deficient Strains. Bar graphs of mean fluorescence intensities of Mlc1-YFP at Spk (A) and septum (B) collected from time-lapse movies of WT (7139), *rsr1*Δ/Δ (9151), *bud2*Δ/Δ (8870), and *bud5*Δ/Δ (11710) strains growing as hyphae. Mlc1-YFP fluorescence intensities at each location are expressed as a percent of whole cell fluorescence. A minimum of 40 time points, spanning the time(s) of septation, were collected from 3-4 hyphae for each strain, and only hyphae able to complete septum formation were included in the analysis. Time-lapse images that were selected for quantitation were taken on a minimum of 3 separate days for each strain. Error bars show the 95% CI. Data sharing the same letter designations are not significantly different from each other. Statistical significance defined as $P < 0.05$. C) Representative western blot of protein lysates from strains listed in A after 4 hrs of growth in hyphal induction conditions. The background-subtracted ratio of Mlc1-YFP to tubulin was collected for each strain for each of 3 independent experiments; the means were calculated and compared using ANOVA. No significant differences were detected between strains (P=0.833).

Table.3.2. Vesicle Delivery to Hyphal Tips is Disrupted in *bud2*Δ/Δ Strains*

	Location/Stage of Growth	R^2	N
WT	*At hyphal tips*	p=0.684	
	GT	0.796	10
	Mature Hyphae	0.852	8
	10μm behind hyphal tips	p=0.064	
	GT	.847	10
	Mature Hyphae	.669	6
***rsr1*Δ/Δ**	*At hyphal tips*	p=0.665	
	GT	.710	4
	Mature Hyphae	.748	6
	10μm behind hyphal tips	p=0.032*	
	GT	.889	4
	Mature Hyphae	.528	7
***bud2*Δ/Δ**	*At hyphal tips*	p<0.001*	
	GT	.891	12
	Mature Hyphae	.594	11
	10μm behind hyphal tips	p=0.528	
	GT	.839	9
	Mature Hyphae	.775	9

*Table of R^2 values obtained during photobleaching experiments performed with *bud2*Δ/Δ (7453), *rsr1*Δ/Δ (8880) and WT (9955) strains. Independent photobleaching experiments were performed over multiple days at either the apex of the hyphal tip (Spk region) or 10μm behind the hyphal tip in GTs and mature hyphae. Significant statistical differences ($P<0.05$) are denoted by asterisks, and reflect the comparison of the mean R^2 values of GTs and mature hyphae for each strain, within a given region.

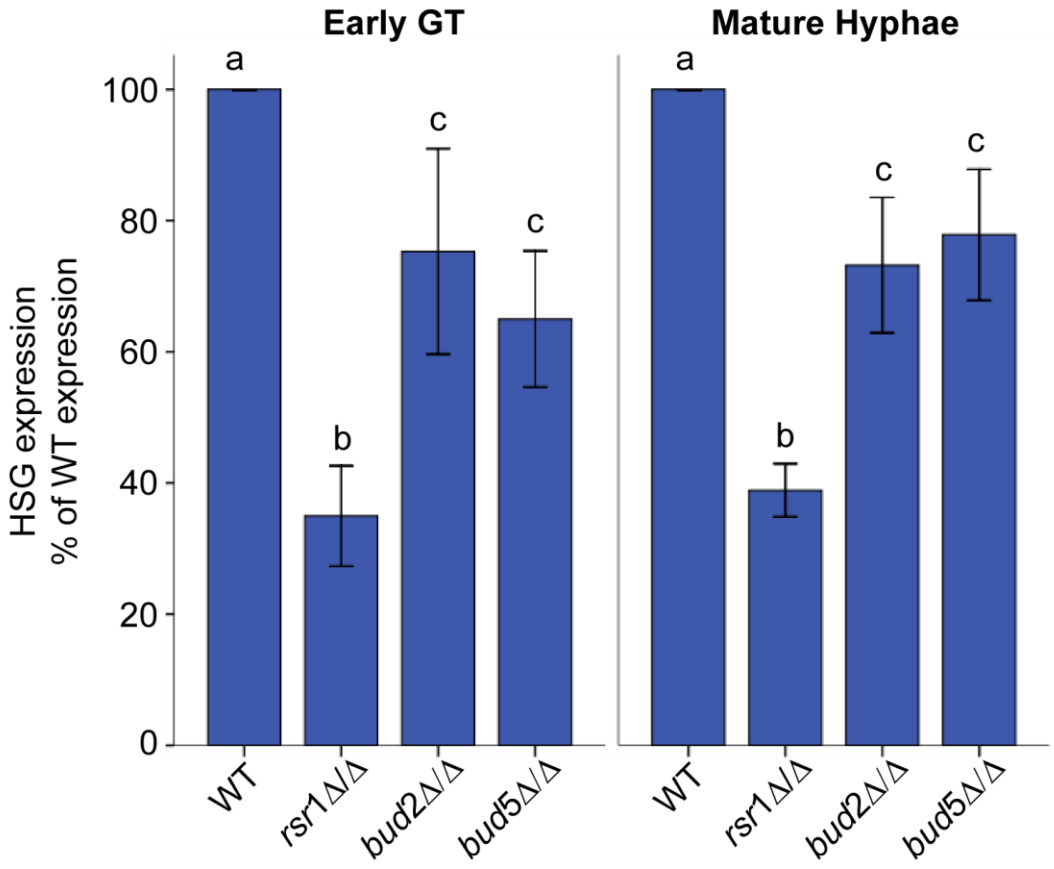

Fig.3.6. Comparison of HSG Expression Between WT and Rsr1-Cycling Deficient Strains, in GTs and Mature Hyphae. Bar graph showing the mean HSG expression levels for WT (9955), *rsr1*Δ/Δ (8880), *bud2*Δ/Δ (7453) and *bud5*Δ/Δ (8855) strains. Error bars show 95% CI. Data is represented as the mean pooled HSG expression level for three independent experiments. Data sharing the same letter designations are not significantly different from each other. Statistical significance defined as $P < 0.05$.

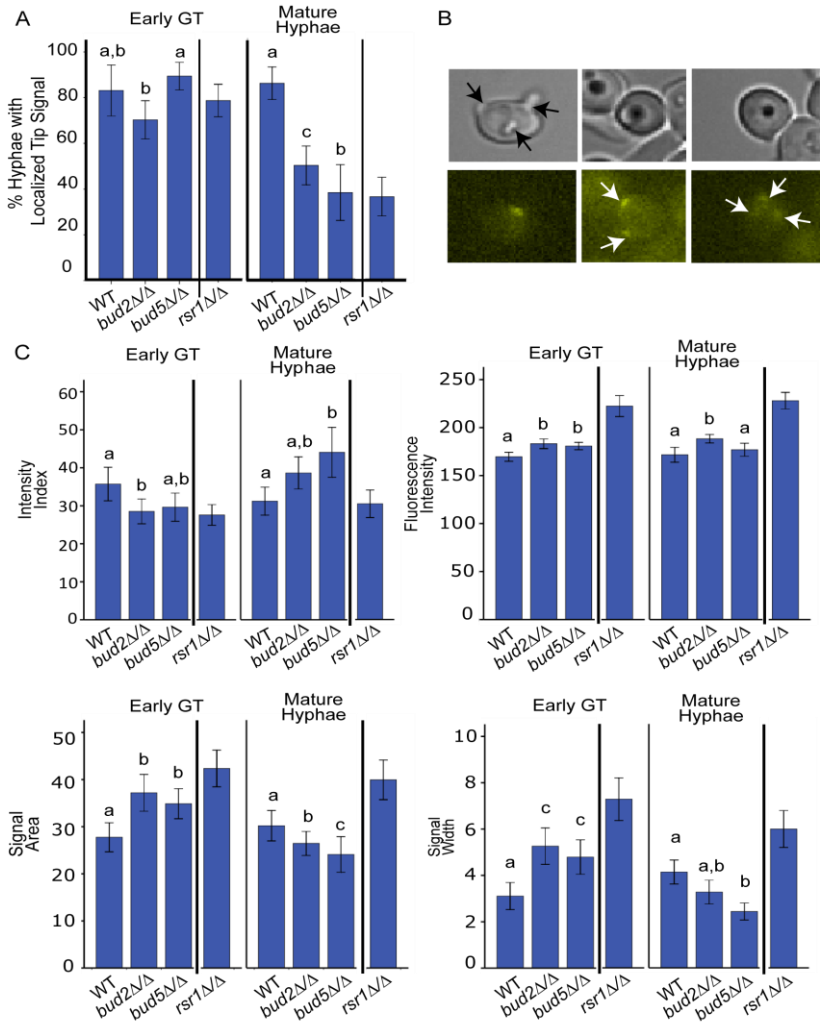

Fig.3.7. The Localization of Bem1-YFP to Hyphal Tips Differs Between *bud2Δ/Δ* and *bud5Δ/Δ* Strains. A) Bar graph showing the percent of GTs and mature hyphae with tip localization of Bem1-YFP in WT (12168), *bud2*Δ/Δ (12156) and *bud5*Δ/Δ (12159) strains. Data from *rsr1*Δ/Δ strains, shown in A and C, is reprinted from Chapter 2 for ease of comparison. B) Representative DIC and fluorescence images from *bud5*Δ/Δ strain expressing Bem1-YFP (12159). In the far left DIC panel, the black arrows indicate aborted attempts at polarized growth. In the middle and far right fluorescence panels, the white arrows indicate multiple, distinct Bem1-YFP clusters within the same cell. C) Bar graphs of the intensity index and index components for the strains listed in A. Error bars indicate 95%CI. Data sharing the same letter designations are not significantly different from each other. Statistical significance defined as $P < 0.05$.

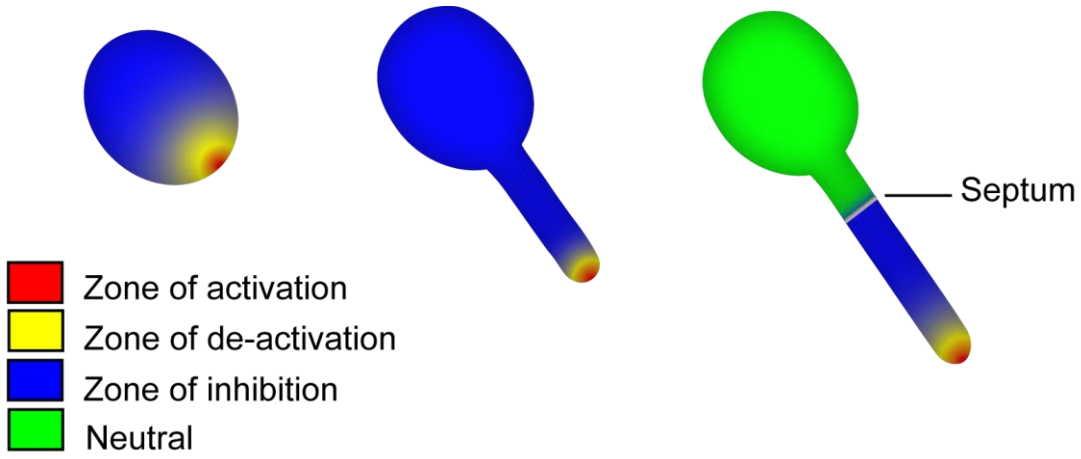

Fig.3.8. Model of how Rsr1 Cycling Creates Zones of Cdc42 Activity at Hyphal Tips. Localization of the Rsr1 activator, Bud5, provides positive feedback at the very apex of the hyphal tip. Bud2 activity provides negative spatial regulation, through its subapical localization, and also creates a zone of inhibition though its more diffuse localization within the apical compartment.

Chapter 3 Supplemental Tables & Figures

Supplemental Table.3.1. Oligonucleotide Primer Sequences Used in This Study

Primer Name	Primer Sequence (5'→3')	Source
1076 *MLC1-YFP* F	AAAGGGGTCAATGTAACTTCTGATGGAAATGTG	
	GATTATGTTGAATTTGTCAAATCAATTTTAGAC	(93)
	CAAGGTGGTGGTTCTAAAGGTGAAGAATTATT	
1077 *MLC1-YFP-HIS1* R	CCAATTCGAACAAGACTATACAATAACTATAAT	
	TTGTAAAACTTGTAGTATATATATTTCAATGGTT	(93)
	AATTGTCTAGAAGGACCACCTTTGATTG	
1265 *rsr1::dpl200* R	TCACATAATTGTGCAGCACTTGCTTCCTGAGCT	
	AGACTTTGGGTGATCATTAATTGATTGTTTCAAT	(This study)
	CTGTGTGGAATTGTGAGCGGATA	
1327 *MLC1-YFP-HIS1* R	CCAATTCGAACAAGACTATACAATAACTATAAT	
	TTGTAAAACTTGTAGTATATATATTTCAATGGTT	(93)
	AATTGGAATTCCGGAATATTTATGAGAAAC	
1460 *rsr1::dpl200* F	AGGTATGTACATTCAACAAAAGCCCGTTACACT	
	TGTATTTCAATAACCCTATATACTAACTTTTGTT	(This study)
	TTGGTTTTCCCAGTCACGACGTT	
2602 *BEM1-YFP-HIS1* R	TTTCCTCTCAACTTGAAAATATATATATATATAT	
	ATATAATACAAAAGTAAAACAATTCTTCTCGAA	(This study)
	TTCCGGAATATTTATGAGAAAC	
2601 *BEM1-YFP* F	TGAAGTTAATGATGATGAAAAATTTCAAAGTAT	
	TTTATTTGATAAATGTAAATTAATGGTTTTAGTA	(This study)
	TATGGTGGTGGTTCTAAAGGTGAAGAATTATT	
2739 *BEM1-YFP-URA3* R	TTTCCTCTCAACTTGAAAATATATATATATATAT	
	ATATAATACAAAAGTAAAACAATTCTTCTCTCT	(This study)
	AGAAGGACCACCTTTGATTG	
4429 RSR1F	GAGAGATTATAAAGTCGTAGTA	(This study)
4430 RSR1R	TCACATAATTGTGCAGCACTT	(This study)
4456 ACT1F	ATGTTCCCAGGTATTGCTGA	(55)
4457 ACT1R	ACATTTGTGGTGAACAATGG	(55)
4458 ECE1F	CCAGAAATTGTTGCTCGTGTTG	(55)
4459 ECE1R	CAGGACGCCATCAAAAACG	(55)

Supplemental Table.3.1 Continued

4460 HGC1F	AAAGCTGTGATTAAATCGGTTTTGA	(55)
4461 HGC1R	AATTGAGGACCTTTTGAATGGAAA	(55)
4462 HWP1F	CGGAATCTAGTGCTGTCGTCTCT	(55)
4463 HWP1R	TAGGAGCGACACTTGAGTAATTGG	(55)
4464 HYR1F	CTCAACCTCAGTGCTGCATTAGAA	(55)
4465 HYR1R	AGCCCAAGTAGCACCAGAATGA	(55)
5410 CDC42F	TCCCCAATCACCCAGGAA	(55)
5411 CDC42R	TGCAGCTACTATAGCCTCGTCAA	(55)

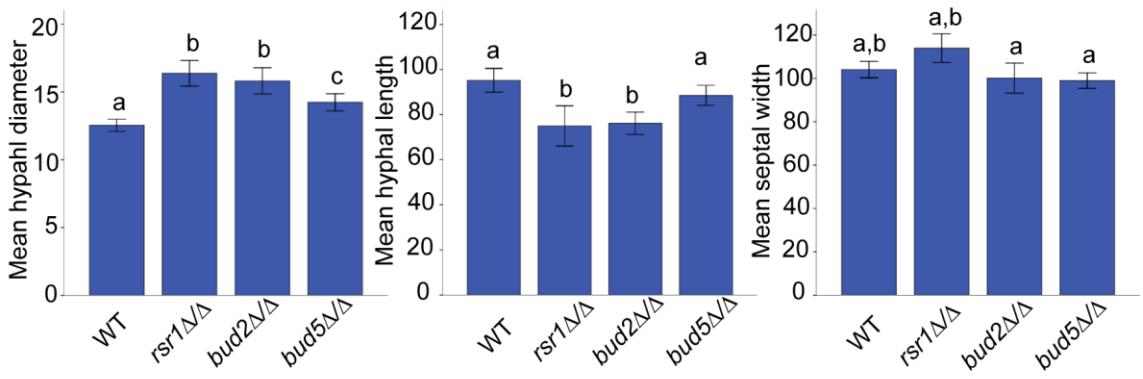

Supplemental Fig.3.1. *bud5*Δ/Δ Strains Show Full and Partial Recovery, Respectively, of Hyphal Length and Width as Compared to *rsr1*Δ/Δ Strains. Error bars show 95% CI. An average of ~75 cells per strain, were scored from 3 separate days of experiments. Data sharing the same letter designations are not significantly different from each other. Statistical significance defined as $P < 0.05$.

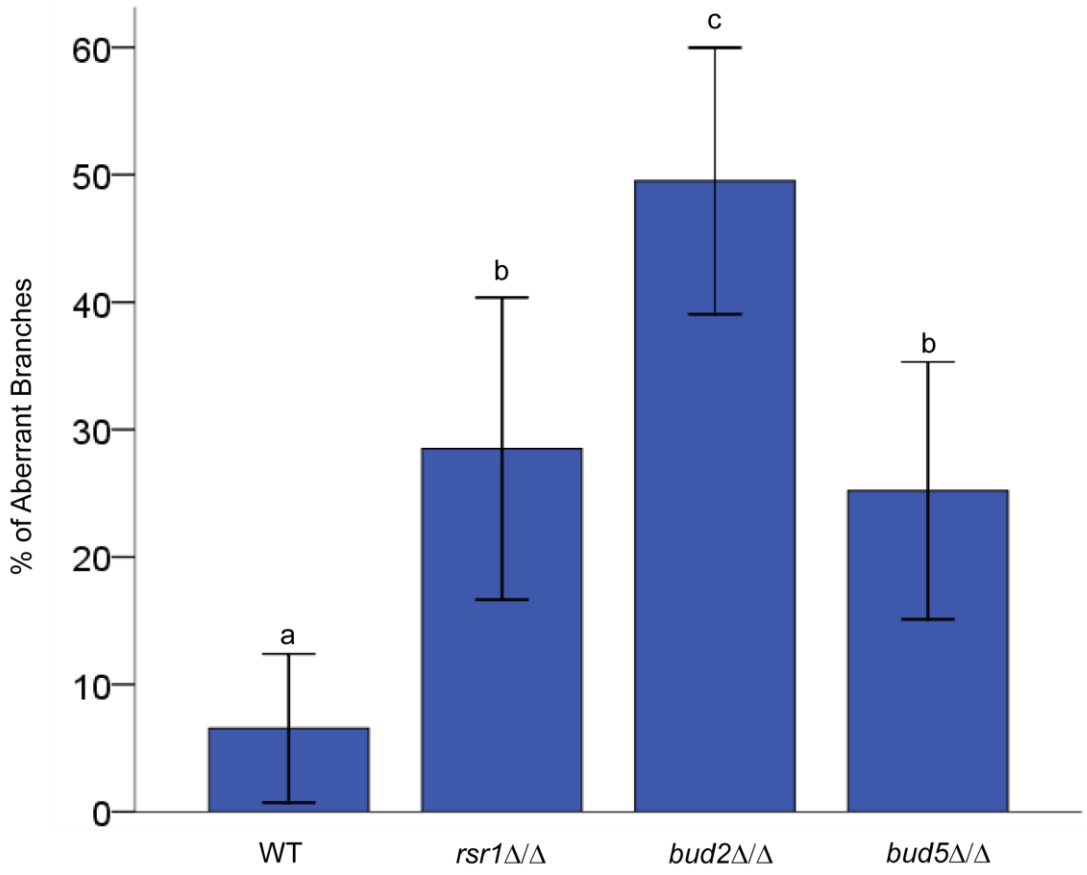

Supplemental Fig.3.2. Aberrant Branching Frequency of WT, *rsr1*Δ/Δ, and Rsr1-Cycling Mutant Strains. Frequency of branches that were >10 µm from septa and branches that formed in the apical compartment of the hypha in WT (9955), *rsr1*Δ/Δ (8880), *bus2*Δ/Δ (7453), and *bud5*Δ/Δ (8855) strains. Bars of the same letter designation are not statistically different from one another (P<0.05).

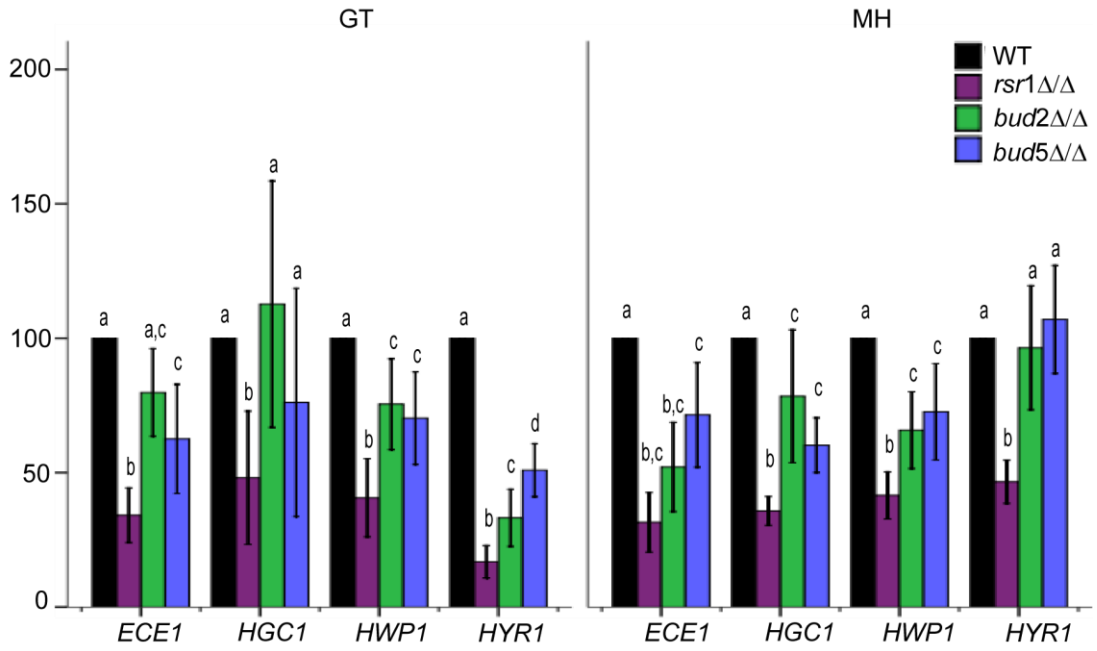

Supplemental Fig.3.3. Comparison of Expression Levels of HSGs in WT, *rsr1Δ/Δ* and Rsr1-cycling mutants. Bar graph showing the mean expression levels of *ECE1*, *HWP1*, *HGC1*, and *HYR1* in GTs and mature hyphae (MH) of the strains listed in Fig.3.6. Error bars show 95% CI. Data is represented as the mean of three independent experiments. Data sharing the same letter designations are not significantly different from each other. Statistical significance defined as $P < 0.05$.

Chapter 4

Conclusions and Perspectives

Initiation and maintenance of polarized growth are critical steps in processes such as cell division, cell migration, and the generation of cell shape across all of Eukarya. The opportunistic fungal pathogen *C. albicans* is an interesting model system in which to study the mechanisms of polarized growth because of its plasticity in cell shape, and the extreme nature of polarization during its hyphal development. Further, because there is such a strong link between the hyphal growth form and virulence, an understanding of hyphal development could provide insight into mechanisms *C. albicans* pathogenesis.

The foundation for my thesis work is based on previous findings from the Gale laboratory that deletion of *C. albicans* Rsr1 results in additional morphological defects, which could not be attributed to the proposed function of Rsr1 in *S. cerevisiae* BSS (45). The goals of my work were to address the following, within the context of *C. albicans* hyphal development: 1) identify and, when possible, quantify specific aspects of cellular dysfunction caused by loss of Rsr1, 2) assess the different roles of Rsr1-GDP and Rsr1-GTP, and 3) identify potential mechanisms by which Rsr1 activity is involved in polarized growth. As part of this work I have developed and employed a number of assays that utilize quantitative fluorescent microscopy (QFM). It should be noted that while there are currently many fluorescent tools available for use in *C. albicans* research, very few groups use quantitative approaches with fluorescent microscopy to address their research questions. My work contributes to the emerging use of QFM in answering cell biological questions, not with simple qualitative comparisons, but with relevant metrics with which to test hypotheses about cellular morphogenesis in both time and space. My work identifies a role for Rsr1 cycling in generating a focused cluster of Cdc42 at hyphal tips. In doing this, Rsr1 affects the efficiency with which polarization is established, the maintenance of constitutive polarized secretion at the hyphal tips, and the degree to which the hyphal transcriptional program is expressed. Results from my work and works of others support the notion that requirements for polarized growth in *C. albicans* differ from those of *S. cerevisiae*.

The fact that *C. albicans* hyphal growth can maintain cell-cycle independent linear growth rates over extreme distances, and requires no *de novo* protein synthesis

gives rise to the idea that there is potentially a higher demand for polarized growth components during hyphal development. The narrow width of the hyphal tube and maintenance of a single axis of growth in the apical cell both, theoretically, decrease the amount of Cdc42 and other polarized growth components needed to maintain growth, and therefore help meet the higher demands of the hyphal growth form. The inability of *rsr1*Δ/Δ and Rsr1 cycling mutants to generate a WT focus of Cdc42 activity and maintain polarized growth, suggests that focusing Cdc42 activity may be a critical aspect of its own conservation, and that focusing is required for the transition to, and maintenance of, polarized growth in mature hyphae. Based on these findings, I propose that Rsr1 contributes to a conservative mechanism of polarization that supports the unique growth parameters of *C. albicans* hyphal development. Finally, the results herein raise new questions about the function of Rsr1 and its cycling components during yeast growth vs. hyphal growth in *C. albicans*; for example, how Rsr1's interactions with other polarized growth components may be altering their function and impacting cell signaling, and the potential evolutionary differences between CaRsr1 and ScRsr1 that contribute to the extended role of CaRsr1 in polarized growth.

As part of this work, I developed a novel method to quantify and compare fluorescent signals at hyphal tips: the intensity index. The intensity index imparts two advantages for measuring fluorescence signals at hyphal tips. First, the intensity index, as used herein, accounts for both the shape of the fluorescent signal as well as the fluorescent intensity per unit volume[1]. The idea of tracking the shape, or distribution, of fluorescence signals along with the fluorescence intensity allows us to identify spatial differences in fluorescent localization not afforded by using integrated measurement of volume, which (usually) assumes a sphere. This was of particular value in measuring the fluorescent signal localization of FM4-64 and Mlc1-YFP, since the "shapes" of these fluorescent signals are known to change from a crescent localization (polarisome) in

[1] since all images compared were taken with equal numbers of z-stacks, then merged as part of processing, the units were reported as area, but reflect the fluorescence intensity acquired over a standard z-plane distance i.e. volume

yeast and pseudohyphae, to a spherical localization (Spk) during hyphal growth. This is important because it is theoretically possible for both a polarisome and a Spk to have identical volumes and intensities, but occupy different shapes, and because it is specifically a *difference in shape*, rather than volume, area, or intensity of these markers that has been used as a hallmark in distinguishing growth forms. The second advantage of the intensity index is that it is unimetric, and it allows the comparison of fluorescent signals of varying sizes by relating them to the individual cell. This permitted us to compare the fluorescent signals between cells of differing sizes and led us to identifying the importance of a focused activity at hyphal tips (i.e. Bem1) during hyphal development.

The results from assays utilizing the intensity index infer that pseudohyphae and yeasts have a reduced intensity index of tip-localized polarity proteins as compared to those of hyphae. However, it remains unresolved whether the intensity index observed for indicators like Bem1-YFP in WT hyphae are a theoretical optimum unique to hyphae, or simply an optimal focus for polarized growth. That is, does all polarized growth, irrespective of growth form, start with an optimal focus that dissipates with time in the non-hyphal morphologies (more like an "On/Off" system), or do the different morphologies possess unique thresholds for Cdc42 activity and its distribution? It would be interesting to compare the Bem1 intensity index taken from the earliest stages of budding yeast and compare them to the earliest stages of GT emergence to differentiate between these two possibilities. Utilizing the intensity index, I could determine the extent to which the focus of Cdc42 activity correlates with polarized growth, and to what extent reductions in focus correlate with a switch to isotropic growth. Determining the empirical value of this potential threshold (that correlates with polarized growth) may give insight into the intrinsic requirements for polarization in *C. albicans* as well as other eukaryotic organisms. Alternatively, differences in the intensity index for budding yeast, pseudohyphae, and emerging hyphae could indicate that there are unique parameters that determine the level and distribution of Cdc42 for each growth form, and that the cell has

mechanisms for generating different levels of Cdc42 focus in response to environmental stimuli.

The results and conclusions generated from my thesis research have also raised new questions about hyphal development and the role of Rsr1 in morphogenesis. My results, and previous results from the Gale lab (45), show that the patterns of localization for each component of the Rsr1 cycling module (Rsr1, Bud5, and Bud2) during hyphal development differ from those observed during yeast form growth. First, during hyphal development Rsr1 has a more uniform distributed across the cell membrane showing little to no enrichment of Rsr1 at hyphal tips. In comparison, during yeast form growth Rsr1 appears enriched at bud tips (45). Second, Bud5 and Bud2 show persistent localizations to regions of active growth at hyphal tips that are distinctly different from their cell cycle dependent localizations as inferred from yeast growth in *S. cerevisiae* (59, 69). This raises questions about what directs these changes in localization between hyphal form growth and yeast, how localization becomes uncoupled from the cell cycle, and how these changes impact polarized growth. One potential mechanism for the changing Rsr1 localization between hyphal form growth and yeast may be through dimerization of Rsr1. In *S. cerevisiae*, Rsr1 was shown to interact with itself and Cdc42 in both *in vivo* and *in vitro* assays (59). The Rsr1-Rsr1 interactions depended upon the guanine nucleotide bound state of Rsr1 (Rsr1-GDP favors dimerization), and temperature (25^0C favored the interaction over 30^0C). Using bimolecular fluorescence complementation, the same study showed that as a dimer, Rsr1 was more efficiently recruited by its GEF, Bud5, to the mother-bud neck at the completion of the cell cycle. These results suggest the possibility that shifts in temperature and/or the guanine nucleotide bound state of Rsr1 may alter its ability to interact with itself and could influence localization of Rsr1 at specific times during the cell cycle. It would be interesting to test, using bimolecular fluorescence complementation, the extent to which this interaction influences Rsr1 localization and function during both hyphal and yeast morphogenesis in *C. albicans* as it could give insight into how polarized growth is reprogrammed between the two morphological forms.

The signal/marker that dictates the localization of the Rsr1 GEF, Bud5, and GAP, Bud2, and how the differences in localization between the growth forms are achieved, also remains unknown in *C. albicans*. In *S. cerevisiae*, Bud5 localization is affected by ploidy. In diploid cells Bud5 localization is disrupted by the deletion of ScBud8 and to a lesser extent ScBud9, whereas in haploid cells Bud5 localization shows strong dependence on the presence of Axl2 and Bud3 (59, 69). *C. albicans* is not known to undergo a traditional sexual cycle, and little is known about how the DNA content of *C. albicans* changes, much less the impact of these changes on cellular function. Sequencing of the *C. albicans* genome has revealed that there are no orthologous sequences to either Bud8 or Bud9. Unpublished work from the Gale lab indicates that Axl2 is not likely involved in Bud5 localization, because while *bud*5Δ/Δ strains show reduced cytotoxicity in *in vitro* assays of cell damage, *axl2*Δ/Δ strains do not. A Bud3 ortholog has been identified (uncharacterized ORF in the *Candida* Genome Database(51)) and may prove to be an interesting avenue of investigation for control of Bud5 localization. What is known of Bud2 localization also comes from *S. cerevisiae*, where its localization to the mother-bud neck has shown dependency on the septin Cdc12. In *C. albicans* Cdc12 is essential, and the temperature sensitive mutant, *cdc12-6*, shows defects in maintenance of hyphal growth that are reminiscent of those of the *bud2*Δ/Δ strain(Li 2012). Growth in the primary hyphae is often abandoned and a secondary ectopic GTs will often form adjacent to the primary growth site. In *S. cerevisiae* Bud2 localization is also dependent on Rsr1 itself. In the absence of Rsr1, Bud2 localizes to the proper incipient bud site in G1 but then moves to a random position just prior to bud emergence (75). It is possible that both of these factors could be influencing the maintenance of Bud2 localization to polarized growth sites. Further potential changes in their associations could be important for the coupling/uncoupling of Bud2 localization to/from the cell cycle.

Another interesting hypothesis to be tested, based on my findings, is that the mechanism by which Rsr1-cycling focuses Cdc42 activity may be by altering the rate of Cdc42 GTP/GDP cycling at hyphal tips. Results from *3X* (*bem3*Δ/Δ *rga2*Δ/Δ *rsr1*Δ/Δ)

strains demonstrate that slowing the rate of Cdc42 exchange can compensate for many of the *rsr1*Δ/Δ phenotypes (Fig.2.4, 2.5). Further, the polarization patterns and frequencies observed in Bem1 localization studies of *bud2*Δ/Δ and *bud5*Δ/Δ GTs (Fig.3.7A, B) are consistent with the predicted polarization frequencies associated with lower and higher K_{on}/K_{fb} ratios for Cdc42, respectively (3). Given that Rsr1 likely interacts with both Cdc42 and Cdc24 (73), my results are consistent with the idea that Rsr1 affects K_{on} rather than K_{fb}, and that Rsr1 acts to slow the activation (K_{on}) of Cdc42. In support of this idea, data presented in Appendix A show that HSG expression is further reduced when Cdc24 is overexpressed in an *rsr1*Δ/Δ strain and that WT (i.e. Rsr1 present) HSG expression is unaffected by overexpression of Cdc24. In addition, it also remains open as to whether Cdc42 cycling rates are differentially affected by the yeast-to-hyphal transition. I suggest that Rsr1 acts to slow Cdc42 activation. I would test this hypothesis using FRAP to compare the exchange rate of Bem1-YFP at during both yeast and hyphal growth. Bem1 is an ideal candidate for this experiment as it is both a proxy for Cdc42-GTP and it is predicted to be highly dynamic (50). The faster recovery times associated with increased rates of exchange would ease the experimental challenge of the hyphal tip growing outside of the selected region of interest prior to recovery (personal observations and (56)). Based on my current results, I predict that *rsr1*Δ/Δ strains would show a faster Bem1 recovery than WT in either growth form, and that the Bem1-YFP signal would show an increased rate of exchange in yeast (during budding) over those in the WT hyphal growth form.

My results also support an important role for actin in hyphal development. The role of the actin cytoskeleton during polarized growth has been a subject of debate in *S. cerevisiae*, with some studies showing that polarization can proceed independently of organized actin cables (17), while others show that actin cables are essential for Cdc42 recycling during polarization events (90). In *C. albicans*, the initial clustering of Cdc42 at sites of polarization during yeast form growth does not require F-actin (46), whereas GT emergence and maintenance of hyphal growth have been shown to be F-actin dependent (2, 33, 46). In fact, mutant strains with defects in hyphal morphology almost

always show disruption to the organization of the actin cytoskeleton. The results from my work presented here indicate that actin cable orientation at hyphal tips is potentially involved in reinforcing the localization of active Cdc42 at hyphal tips (Fig.2.5) and the up regulation of the hyphal program (Fig.2.4B), because the recovery of the Bem1-tip signal in *3X* strains was likely the result of an actin dependant mechanism. In addition to the requirement for actin cables, previous work indicates that pools of free actin may act as sensors during hyphal growth in *C. albicans* (98, 107). A pool of free actin is needed as part of a tripartite signaling complex with Cry1 and Cap1, which increases production of the second messenger signaling molecule cAMP, to enable the up-regulation of the hyphal transcriptional program. Together these results are consistent with the idea that a balance between actin polymerization and depolymerization within a spatially restricted area is needed for polarized growth and for full induction of the hyphal program. Data from Chapter 2 suggest that actin cable orientation can be influenced by hydrolysis rates of Cdc42 (i.e. GAP deletion) and by changes in spatial regulation of Cdc42 (i.e. Rsr1 deletion). It would be interesting to further investigate how changes in hydrolysis rates of Cdc42, by the sequestration of Rga2, might affect actin dynamics between hyphal and yeast growth forms; and related to this, how the spatial regulation of Cdc42, by Rsr1, influences actin dynamics at hyphal tips, because, changes in hydrolysis rates of Cdc42 and its spatial regulation might influence the availability of free actin to increase cellular cAMP levels. These data could be used to create a computational model that could inform us about how Cdc42 activity and the actin cytoskeleton act together to couple cell biological features of hyphal morphogenesis with hyphal gene expression. Finally, work done in *N. crassa*, suggests that changes in actin cytoskeletal dynamics influence the ability of fungal hyphae to invade (94). An apical clear zone, associated with the depolymerization of actin, was observed in only the tips of invading *N. crassa* hyphae, suggesting a link between the regulation of actin dynamics at hyphal tips and the ability to invade. Further, it was suggested that the depolymerization of actin, during invasion events, might represent a mechanism to allow tip yielding during substrate penetration. It would be interesting to use the fluorescent reporter, Lifeact, to watch actin dynamics as

part of a model of *C. albicans* invasion in real-time (14, 15). I would expect that similar changes in actin dynamics would exist during *C. albicans* tissue invasion; however, the changes may only be temporary, since the force needed to penetrate host cell membranes is likely greater than that required for growth inside the cell. At which point, it might be interesting to look at how actin polarization is re-established after the event and what proteins are required for that process.

Finally, there is the question of how the CaRsr1 protein exhibits differences in function as compared to the ScRsr1 protein. A comparison of the CaRsr1 and ScRsr1 protein sequence domains by SMART (63) analysis reveals that CaRsr1 contains a low complexity region (LCR) in its C-terminus that is not found in the sequence from *S. cerevisiae* (Fig.4.1A). LCR's are similar to tandem repeat sequences and are thought to arise by similar mechanism (30). In general, as a domain, LCRs impart a greater number and/or flexibility in binding partners to the protein, and the position of the LCR enhances these effects (C-terminal localization > central localization) (30). To test if the potential role of LCR in CaRsr1function, I would assess the phenotypes of a CaRsr1$^{LCR\Delta/\Delta}$ strain. In addition, because LCR's are associated with an ability to interact with a greater number of proteins, I think it would also be important to more fully characterize the binding partners for CaRsr1. ScRsr1's interaction with Cdc42 and Cdc24 has been well established (11, 59, 61, 65, 73-75), and while the phenotypes of CaRsr1 most certainly support this predicted interaction, my results do not preclude the possibility that Rsr1 has other biologically significant interactions. ScRsr1 was also shown to act as a multi-copy suppressor of a temperature-sensitive mutation in Ras2, which stimulates the production of cAMP. Investigating new protein-protein interactions for CaRsr1, as well as the potential importance of the CaRsr1 LCR, may shed new light on the differences in function between these two organisms and the evolution of protein function.

THIS PAGE WAS INTENTIONALLY LEFT BLANK

Bibliography

1. **Adams, A. E., D. I. Johnson, R. M. Longnecker, B. F. Sloat, and J. R. Pringle**. 1990. *CDC42* and *CDC43*, Two Additional Genes Involved in Budding and the Establishment of Cell Polarity in the Yeast *Saccharomyces cerevisiae*. The Journal of Cell Biology **111**:131-142.
2. **Akashi, T., T. Kanbe, and K. Tanaka**. 1994. The Role of the Cytoskeleton in the Polarized Growth of the Germ Tube in *Candida albicans*. Microbiology **140**:271-280.
3. **Altschuler, S. J., S. B. Angenent, Y. Wang, and L. F. Wu**. 2008. On the Spontaneous Emergence of Cell Polarity. Nature **454**:886-889.
4. **Banerjee, M., D. S. Thompson, A. Lazzell, P. L. Carlisle, C. Pierce, C. Monteagudo, J. L. Lopez-Ribot, and D. Kadosh**. 2008. *UME6*, a Novel Filament-Specific Regulator of *Candida albicans* Hyphal Extension and Virulence. Molecular Biology of the Cell **19**:1354-1365.
5. **Bartnicki-Garcia, S., D. D. Bartnicki, G. Gierz, R. Lopez-Franco, and C. E. Bracker**. 1995. Evidence That Spitzenkörper Behavior Determines the Shape of a Fungal Hypha: A Test of the Hyphoid Model. Experimental Mycology **19**:153-159.
6. **Bartnicki-Garcia, S., F. Hergert, and G. Gierz**. 1989. Computer Simulation of Fungal Morphogenesis and the Mathematical Basis for Hyphal (Tip) Growth. Protoplasma **153**:46-57.
7. **Bassilana, M., and R. A. Arkowitz**. 2006. Rac1 and Cdc42 Have Different Roles in *Candida albicans* Development. Eukaryotic Cell **5**:321-329.
8. **Bassilana, M., J. Hopkins, and R. A. Arkowitz**. 2005. Regulation of the Cdc42/Cdc24 GTPase Module During *Candida albicans* Hyphal Growth. Eukaryotic Cell **4**:588-603.
9. **Bauer, Y., Knechtle, P., Wnedland, J., Helfer, H., Philippsen, P.** 2004. A Ras-like GTPase is Involved in Hyphal Growth Guidance in Filamentous Fungus *Ashbya gossypii*. Molecular Biology of the Cell **15**:4622-4632.
10. **Bender, A.** 1993. Genetic Evidence for the Roles of the Bud-Site-Selection Genes *BUD5* and *BUD2* in Control of the Rsr1p (Bud1p) GTPase in Yeast. Proceedings of the National Academy of Sciences **90**:9926-9929.
11. **Bender, A., and J. R. Pringle**. 1989. Multicopy Suppression of the *cdc24* Budding Defect in Yeast by *CDC42* and Three Newly Identified Genes Including the Ras-Related Gene *RSR1*. Proceedings of the National Academy of Sciences **86**:9976-9980.
12. **Bensen, E. S., A. Clemente-Blanco, K. R. Finley, J. Correa-Bordes, and J. Berman**. 2005. The Mitotic Cyclins Clb2p and Clb4p Affect Morphogenesis in *Candida albicans*. Molecular Biology of the Cell **16**:3387-3400.
13. **Bensen, E. S., S. G. Filler, and J. Berman**. 2002. A Forkhead Transcription Factor is Important for True Hyphal as Well as Yeast Morphogenesis in *Candida albicans*. Eukaryotic Cell **1**:787-798.

14. **Berepiki, A., A. Lichius, and N. D. Read**. 2011. Actin Organization and Dynamics in Filamentous Fungi. Nature Reviews Microbiology **9**:876-887.
15. **Berepiki, A., A. Lichius, J.-Y. Shoji, J. Tilsner, and N. D. Read**. 2010. F-Actin Dynamics in *Neurospora crassa*. Eukaryotic Cell **9**:547-557.
16. **Biswas, S., P. Van Dijck, and A. Datta**. 2007. Environmental Sensing and Signal Transduction Pathways Regulating Morphopathogenic Determinants of *Candida albicans*. Microbiology and Molecular Biology Reviews **71**:348-376.
17. **Bose, I., J. E. Irazoqui, J. J. Moskow, E. S. G. Bardes, T. R. Zyla, and D. J. Lew**. 2001. Assembly of Scaffold-Mediated Complexes Containing Cdc42p, the Exchange Factor Cdc24p, and the Effector Cla4p Required for Cell Cycle-Regulated Phosphorylation of Cdc24p. Journal of Biological Chemistry **276**:7176-7186.
18. **Bracker, C. E., R. D. J. Murphy, and Lopez-Franco**. 1997. Laser Microbeam Manipulation of Cell Morphogenesis in Growing Fungal Hyphae *In* D. L. Farkas, and B. J. Tromberg (eds.), Functional imaging of optical manipulation of living cells. Proceedings of SPIE, 2983. International Society for Optical Engineering., Bellingham, Wash.
19. **Brand, A.** 2012. Hyphal Growth in Human Fungal Pathogens and Its Role in Virulence. International Journal of Microbiology.
20. **Brand, A., A. Vacharaksa, C. Bendel, J. Norton, P. Haynes, M. Henry-Stanley, C. Wells, K. Ross, N. A. R. Gow, and C. A. Gale**. 2008. An Internal Polarity Landmark Is Important for Externally Induced Hyphal Behaviors in *Candida albicans*. Eukaryotic Cell **7**:712-720.
21. **Braun, B. R., and A. D. Johnson**. 1997. Control of Filament Formation in *Candida albicans* by the Transcriptional Repressor *TUP1*. Science **277**:105-109.
22. **Brunswik, H.** 1924. Untersuchungen über Geschlechts- und Kernverhältnisse bei der Hymenomycetengattung *CoprinusIn* K. Goebel (ed.), Botanische Abhandlungen, vol. 1-152. Gustav Fischer, Jena, Germany.
23. **Calderone, R. A., and C. J. Clancy**. 2012. Candida and Candidiasis. ASM press.
24. **Care, R. S., J. Trevethick, K. M. Binley, and P. E. Sudbery**. 1999. The MET3 promoter: a new tool for *Candida albicans* molecular genetics. Molecular Microbiology **34**:792-798.
25. **Carlisle, P. L., M. Banerjee, A. Lazzell, C. Monteagudo, J. L. Lopez-Ribot, and D. Kadosh**. 2009. Expression Levels of a Filament-Specific Transcriptional Regulator Are Sufficient to Determine *Candida albicans* Morphology and Virulence. Proceedings of the National Academy of Sciences **106**:599-604.
26. **Casamayor, A., and M. Snyder**. 2002. Bud-Site Selection and Cell Polarity in Budding Yeast. Current Opinion in Microbiology **5**:179-186.
27. **Chaffin, W. L.** 1984. The Relationship Between Yeast Cell Size and Cell Division in *Candida albicans*. Canadian Journal of Microbiology **30**:192-203.
28. **Chant, J., and I. Herskowitz**. 1991. Genetic Control of Bud-Site Selection in Yeast by a Set of Gene Products That Constitute a Morphogenetic Pathway. Cell **65**:1203-1212.

29. **Clarke, P. R., and C. Zhang**. 2008. Spatial and Temporal Coordination of Mitosis by Ran GTPase. Nat Rev Mol Cell Biol **9**:464-477.
30. **Coletta, A., J. Pinney, D. Solis, J. Marsh, S. Pettifer, and T. Attwood**. 2010. Low-Complexity Regions Within Protein Sequences Have Position-Dependent Roles. BMC Systems Biology **4**:43.
31. **Corvest, V., S. Bogliolo, P. Follette, R. A. Arkowitz, and M. Bassilana**. 2013. Spatiotemporal Regulation of Rho1 and Cdc42 Activity During *Candida albicans* Filamentous Growth. Molecular Microbiology **89**:626-648.
32. **Court, H., and P. Sudbery**. 2007. Regulation of Cdc42 GTPase Activity in the Formation of Hyphae in *Candida albicans*. Molecular Biology of the Cell **18**:265-281.
33. **Crampin, H., K. Finley, M. Gerami-Nejad, H. Court, C. Gale, J. Berman, and P. Sudbery**. 2005. *Candida albicans* Hyphae Have a Spitzenkörper That is Distinct From the Polarisome Found in Yeast and Pseudohyphae. Journal of Cell Science **118**:2935-2947.
34. **Das, M., T. Drake, D. J. Wiley, P. Buchwald, D. Vavylonis, and F. Verde**. 2012. Oscillatory Dynamics of Cdc42 GTPase in the Control of Polarized Growth. Science **337**:239-243.
35. **Ernst, J. F.** 2000. Transcription Factors in *Candida albicans*- Environmental Control of Morphogenesis. Microbiology **146**:1763-1774.
36. **Evangelista, M., K. Blundell, M. S. Longtine, C. J. Chow, N. Adames, J. R. Pringle, M. Peter, and C. Boone**. 1997. Bni1p, a Yeast Formin Linking Cdc42p and the Actin Cytoskeleton During Polarized Morphogenesis. Science **276**:118-122.
37. **Falgier, C., S. Kegley, H. Podgorski, T. Heisel, K. Storey, C. M. Bendel, and C. A. Gale**. 2011. *Candida Species* Differ in Their Interactions With Immature Human Gastrointestinal Epithelial Cells. Pediatr Res **69**:384-389.
38. **Finley, K. R., and J. Berman**. 2005. Microtubules in *Candida albicans* Hyphae Drive Nuclear Dynamics and Connect Cell Cycle Progression to Morphogenesis. Eukaryotic Cell **4**:1697-1711.
39. **Fischer-Parton, S., R. M. Parton, P. C. Hickey, J. Dijksterhuis, H. A. Atkinson, and N. D. Read**. 2000. Confocal Microscopy of FM4-64 as a Tool For Analysing Endocytosis and Vesicle Trafficking in Living Fungal Hyphae. Journal of Microscopy **198**:246-259.
40. **Gerami-Nejad, M., J. Berman, and C. A. Gale**. 2001. Cassettes for PCR-Mediated Construction of Green, Yellow, and Cyan Fluorescent Protein Fusions in *Candida albicans*. Yeast **18**:859-864.
41. **Gerami-Nejad, M., D. Hausauer, M. McClellan, J. Berman, and C. Gale**. 2004. Cassettes for the PCR-mediated construction of regulatable alleles in *Candida albicans*. Yeast **21**:429-436.
42. **Girbardt, M.** 1957. Uber die Substruktur von *Polystictus versicolor* L. Archiv fur Mikrobiologie **28**:255-269.
43. **Gow, N.** 1997. Germ Tube Growth of *Candida albicans*. Curr Top Med Mycol **8**:43–55.

44. **Harris, S. D., N. D. Read, R. W. Roberson, B. Shaw, S. Seiler, M. Plamann, and M. Momany**. 2005. Polarisome Meets Spitzenkörper: Microscopy, Genetics, and Genomics Converge. Eukaryotic Cell **4**:225-229.
45. **Hausauer, D. L., M. Gerami-Nejad, C. Kistler-Anderson, and C. A. Gale**. 2005. Hyphal Guidance and Invasive Growth in *Candida albicans* Require the Ras-Like GTPase Rsr1p and Its GTPase-Activating Protein Bud2p. Eukaryotic Cell **4**:1273-1286.
46. **Hazan, I., and H. Liu**. 2002. Hyphal Tip-Associated Localization of Cdc42 Is F-Actin Dependent in *Candida albicans*. Eukaryotic Cell **1**:856-864.
47. **Herrero, A. B., M. C. Lopez, L. Fernandez-Lago, and A. Dominguez**. 1999. *Candida albicans* and *Yarrowia lipolytica* as Alternative Models For Analysing Budding Patterns and Germ Tube Formation in Dimorphic Fungi. Microbiology **145**:2727-2737.
48. **Howard, R. J.** 1981. Ultrastructural Analysis of Hyphal Tip Cell Growth in Fungi: Spitzenkörper, Cytoskeleton and Endomembranes After Freeze-Substitution. Journal of Cell Science **48**:89-103.
49. **Howell, Audrey S., M. Jin, C.-F. Wu, Trevin R. Zyla, Timothy C. Elston, and Daniel J. Lew**. 2012. Negative Feedback Enhances Robustness in the Yeast Polarity Establishment Circuit. Cell **149**:322-333.
50. **Howell, A. S., N. S. Savage, S. A. Johnson, I. Bose, A. W. Wagner, T. R. Zyla, H. F. Nijhout, M. C. Reed, A. B. Goryachev, and D. J. Lew**. 2009. Singularity in Polarization: Rewiring Yeast Cells to Make Two Buds. Cell **139**:731-743.
51. **Inglis, D. O., M. B. Arnaud, J. Binkley, P. Shah, M. S. Skrzypek, F. Wymore, G. Binkley, S. R. Miyasato, M. Simison, and G. Sherlock**. 2012. The *Candida* Genome Database Incorporates Multiple *Candida species*: Multispecies Search and Analysis Tools With Curated Gene and Protein Information for *Candida albicans* and *Candida glabrata*. Nucleic Acids Research **40**:D667-D674.
52. **Irazoqui, J. E., A. S. Gladfelter, and D. J. Lew**. 2003. Scaffold-Mediated Symmetry Breaking by Cdc42p. Nat Cell Biol **5**:1062-1070.
53. **Irazoqui, J. E., A. S. Gladfelter, and D. J. Lew**. 2004. Cdc42p, GTP Hydrolysis and the Cell's Sense of Direction. Cell Cycle **3**:859-862.
54. **Irazoqui, J. E., A. S. Howell, C. L. Theesfeld, and D. J. Lew**. 2005. Opposing Roles for Actin in Cdc42p Polarization. Molecular Biology of the Cell **16**:1296-1304.
55. **Johnson, D. I.** 1999. Cdc42: An Essential Rho-Type GTPase Controlling Eukaryotic Cell Polarity. Microbiology and Molecular Biology Reviews **63**:54-105.
56. **Jones, L. A., and P. E. Sudbery**. 2010. Spitzenkörper, Exocyst, and Polarisome Components in *Candida albicans* Hyphae Show Different Patterns of Localization and Have Distinct Dynamic Properties. Eukaryotic Cell **9**:1455-1465.
57. **Kadosh, D., and A. D. Johnson**. 2001. Rfg1, a Protein Related to the *Saccharomyces cerevisiae* Hypoxic Regulator Rox1, Controls Filamentous

Growth and Virulence in *Candida albicans*. Molecular and Cellular Biology **21**:2496-2505.

58. **Kadosh, D., and A. D. Johnson**. 2005. Induction of the *Candida albicans* Filamentous Growth Program by Relief of Transcriptional Repression: A Genome-wide Analysis. Molecular Biology of the Cell **16**:2903-2912.
59. **Kang, P. J., A. Sanson, B. Lee, and H.-O. Park**. 2001. A GDP/GTP Exchange Factor Involved in Linking a Spatial Landmark to Cell Polarity. Science **292**:1376-1378.
60. **Köhli, M., V. Galati, K. Boudier, R. W. Roberson, and P. Philippsen**. 2008. Growth-Speed-Correlated Localization of Exocyst and Polarisome Components in Growth Zones of *Ashbya gossypii* Hyphal Tips. Journal of Cell Science **121**:3878-3889.
61. **Kozminski, K. G., L. Beven, E. Angerman, A. H. Y. Tong, C. Boone, and H.-O. Park**. 2003. Interaction Between a Ras and a Rho GTPase Couples Selection of a Growth Site to the Development of Cell Polarity in Yeast. Molecular Biology of the Cell **14**:4958-4970.
62. **Kozubowski, L., K. Saito, J. M. Johnson, A. S. Howell, T. R. Zyla, and D. J. Lew**. 2008. Symmetry-Breaking Polarization Driven by a Cdc42p GEF-PAK Complex. Current Biology : CB **18**:1719-1726.
63. **Letunic, I., T. Doerks, and P. Bork**. 2012. SMART 7: Recent Updates to the Protein Domain Annotation Resource. Nucleic Acids Research **40**:D302-D305.
64. **Lo, H.-J., J. R. Köhler, B. DiDomenico, D. Loebenberg, A. Cacciapuoti, and G. R. Fink**. 1997. Nonfilamentous *C. albicans* Mutants Are Avirulent. Cell **90**:939-949.
65. **Lo, W.-C., M. E. Lee, M. Narayan, C.-S. Chou, and H.-O. Park**. 2013. Polarization of Diploid Daughter Cells Directed by Spatial Cues and GTP Hydrolysis of Cdc42 in Budding Yeast. PLoS ONE **8**:e56665.
66. **Lopez-Franco, R., and C. Bracker**. 1996. Diversity and Dynamics of the Spitzenkörper in Growing Hyphal Tips of Higher Fungi. Protoplasma **195**:90-111.
67. **Lu, Y., C. Su, A. Wang, and H. Liu**. 2011. Hyphal Development in *Candida albicans* Requires Two Temporally Linked Changes in Promoter Chromatin for Initiation and Maintenance. PLoS Biol **9**:e1001105.
68. **Marco, E., R. Wedlich-Soldner, R. Li, S. J. Altschuler, and L. F. Wu**. 2007. Endocytosis Optimizes the Dynamic Localization of Membrane Proteins that Regulate Cortical Polarity. Cell **129**:411-422.
69. **Marston, A. L., T. Chen, M. C. Yang, P. Belhumeur, and J. Chant**. 2001. A Localized GTPase Exchange Factor, Bud5, Determines the Orientation of Division Axes in Yeast. Current Biology **11**:803-807.
70. **Merson-Davies, L. A., and F. C. Odds**. 1989. A Morphology Index for Characterization of Cell Shape in *Candida albicans*. Journal of General Microbiology **135**:3143-3152.
71. **Mitchison, J. M., and P. Nurse**. 1985. Growth in cell length in the fission yeast *Schizosaccharomyces pombe*. Journal of Cell Science **75**:357-376.

72. **Onsum, M. D., and C. V. Rao**. 2009. Calling Heads From Tails: The Role of Mathematical Modeling in Understanding Cell Polarization. Current Opinion in Cell Biology **21**:74-81.
73. **Park, H.-O., E. Bi, J. R. Pringle, and I. Herskowitz**. 1997. Two Active States of the Ras-Related Bud1/Rsr1 Protein Bind to Different Effectors to Determine Yeast Cell Polarity. Proceedings of the National Academy of Sciences **94**:4463-4468.
74. **Park, H.-O., P. J. Kang, and A. W. Rachfal**. 2002. Localization of the Rsr1/Bud1 GTPase Involved in Selection of a Proper Growth Site in Yeast. Journal of Biological Chemistry **277**:26721-26724.
75. **Park, H.-O., A. Sanson, and I. Herskowitz**. 1999. Localization of Bud2p, a GTPase-Activating Protein Necessary for Programming Cell Polarity in Yeast to the Presumptive Bud Site. Genes & Development **13**:1912-1917.
76. **Pfaller, M. A., and D. J. Diekema**. 2007. Epidemiology of Invasive Candidiasis: a Persistent Public Health Problem. Clinical Microbiology Reviews **20**:133-163.
77. **Pfaller, M. A., P. G. Pappas, and J. R. Wingard**. 2006. Invasive Fungal Pathogens: Current Epidemiological Trends. Clinical Infectious Diseases **43**:S3-S14.
78. **Phair, R. D., Gorski, S. A. and Misteli, T.** . 2004. Measurement of Dynamic Protein Binding to Chromatin *In Vivo*, Using Photobleaching Microscopy. Methods in Enzymology **375**:393-414.
79. **Phan, Q. T., P. H. Belanger, and S. G. Filler**. 2000. Role of Hyphal Formation in Interactions of *Candida albicans* with Endothelial Cells. Infection and Immunity **68**:3485-3490.
80. **Powers, S., T. Kataoka, O. Fasano, M. Goldfarb, J. Strathem, J. Broach, and M. Wigler**. 1984. Genes in *S. cerevisiae* Encoding Proteins With Domains Homologous to the Mammalian Ras Proteins. Cell **36**:607-612.
81. **Pulver, R., T. Heisel, S. Gonia, R. Robins, J. Norton, P. Haynes, and C. A. Gale**. 2013. Rsr1 Focuses Cdc42 Activity at Hyphal Tips and Promotes Maintenance of Hyphal Development in *Candida albicans*. Eukaryotic Cell:482-495.
82. **Rasband, W. S.** 1997-2004. Image J. U. S. National Institutes of Health, Bethesda, MD USA [http://rsb.info.nih.gov/ij].
83. **Reynaga-Pena, C. G., G. Gierz, and S. Bartnicki-Garcia**. 1997. Analysis of the role of the Spitzenkörper in fungal morphogenesis by computer simulation of apical branching in *Aspergillus niger*. Proceedings of the National Academy of Sciences **94**:9096-9101.
84. **Reynaga-Pena, C. G., G. Gierz, and S. Bartnicki-Garcia**. 1997. Analysis of the Role of the Spitzenkörper in Fungal Morphogenesis by Computer Simulation of Apical Branching in *Aspergillus niger*. Proceedings of the National Academy of Sciences **94**:9096-9101.
85. **Roberson, R. W. F., M. S.** . 1988. Ultrastructural Aspects of the Hyphal Tip of *Sclerotium rolfsii* Preserved by Freeze Substitution. Protoplasma **146**:143-149.

86. **Saville, S. P., A. L. Lazzell, C. Monteagudo, and J. L. Lopez-Ribot**. 2003. Engineered Control of Cell Morphology *In Vivo* Reveals Distinct Roles for Yeast and Filamentous Forms of *Candida albicans* During Infection. Eukaryotic Cell **2**:1053-1060.
87. **Sevilla, M.-J., and F. C. Odds**. 1986. Development of *Candida albicans* Hyphae in Different Growth Media-Variations in Growth Rates, Cell Dimensions and Timing of Morphogenetic Events. Journal of General Microbiology **132**:3083-3088.
88. **Sharpless, K. E., and S. D. Harris**. 2002. Functional Characterization and Localization of the *Aspergillus nidulans* Formin SEPA. Molecular Biology of the Cell **13**:469-479.
89. **Sherman, F.** 1991. Getting Started with Yeast, p. 3-20. *In* G. R. Fink, and C. Guthrie (eds.), Methods Enzymol.; guide to yeast genetics and molecular biology, vol. 194. Academic Press, Inc., San Diego, CA.
90. **Slaughter, B. D., A. Das, J. W. Schwartz, B. Rubinstein, and R. Li**. 2009. Dual Modes of Cdc42 Recycling Fine-Tune Polarized Morphogenesis. Developmental Cell **17**:823-835.
91. **Steinberg, G.** 2007. Hyphal Growth: a Tale of Motors, Lipids, and the Spitzenkörper. Eukaryotic Cell **6**:351-360.
92. **Stokes, C., G. P. Moran, M. J. Spiering, G. T. Cole, D. C. Coleman, and D. J. Sullivan**. 2007. Lower Filamentation Rates of *Candida dubliniensis* Contribute to Its Lower Virulence in Comparison With *Candida albicans*. Fungal Genetics and Biology **44**:920-931.
93. **Sudbery, P., N. Gow, and J. Berman**. 2004. The Distinct Morphogenic States of *Candida albicans*. Trends in Microbiology **12**:317-324.
94. **Suei, S., and A. Garrill**. 2008. An F-Actin-Depleted Zone is Present at the Hyphal Tip of Invasive Hyphae of *Neurospora crassa*. Protoplasma **232**:165-172.
95. **Tucker, S. L., and N. J. Talbot**. 2001. Surface Attachment and Pre-Penetration Stage Development by Plant Pathogenic Fungi. Annual Review of Phytopathology **39**:385-417.
96. **Ushinsky, S. C., D. Harcus, J. Ash, D. Dignard, A. Marcil, J. Morchhauser, D. Y. Thomas, M. Whiteway, and E. Leberer**. 2002. *CDC42* Is Required for Polarized Growth in Human Pathogen *Candida albicans*. Eukaryotic Cell **1**:95-104.
97. **VandenBerg, A. L., A. S. Ibrahim, J. E. Edwards, K. A. Toenjes, and D. I. Johnson**. 2004. Cdc42p GTPase Regulates the Budded-to-Hyphal-Form Transition and Expression of Hypha-Specific Transcripts in *Candida albicans*. Eukaryotic Cell **3**:724-734.
98. **Wang, Y., H. Zou, H.-M. Fang, and Y. Zhu**. 2010. Linking Cellular Actin Status with cAMP Signaling in *Candida albicans*. Virulence **1**:202-205.
99. **Wedlich-Soldner, R., and R. Li**. 2004. Closing the Loops: New Insights Into the Role and Regulation of Actin During Cell Polarization. Experimental Cell Research **301**:8-15.

100. **Wilson, B. R., D. Davis, B. M. Enloe, and A. P. Mitchell**. 2000. A Recyclable *Candida albicans URA3* Cassette for PCR Product-Directed Gene Disruptions. Yeast **16**:65-70.
101. **Wolf, J. M., D. J. Johnson, D. Chmielewski, and D. A. Davis**. 2010. The *Candida albicans* ESCRT Pathway Makes Rim101-Dependent and -Independent Contributions to Pathogenesis. Eukaryotic Cell **9**:1203-1215.
102. **Wolyniak, M. J., and P. Sundstrom**. 2007. Role of Actin Cytoskeletal Dynamics in Activation of the Cyclic AMP Pathway and *HWP1* Gene Expression in *Candida albicans*. Eukaryotic Cell **6**:1824-1840.
103. **Yu, X., and M. Cai**. 2004. The Yeast Dynamin-Related GTPase Vps1p Functions in the Organization of the Actin CytoskeletonVia Interaction with Sla1p. J Cell Sci **117**:3839-3853.
104. **Zhang, B., Y. Zhang, E. Shacter, and Y. Zheng**. 2005. Mechanism of the Guanine Nucleotide Exchange Reaction of Ras GTPase--Evidence for a GTP/GDP Displacement Model. Biochemistry **44**:2566-2576.
105. **Zheng, X.-D., R. T. H. Lee, Y.-M. Wang, Q.-S. Lin, and Y. Wang**. 2007. Phosphorylation of Rga2, a Cdc42 GAP, by CDK/Hgc1 is Crucial for *Candida albicans* Hyphal Growth. EMBO J **26**:3760-3769.
106. **Zheng, X., Y. Wang, and Y. Wang**. 2004. Hgc1, a Novel Hypha-Specific G1 Cyclin-Related Protein Regulates *Candida albicans* Hyphal Morphogenesis. EMBO J **23**:1845-1856.
107. **Zou, H., H.-M. Fang, Y. Zhu, and Y. Wang**. 2010. *Candida albicans* Cyr1, Cap1 and G-Actin Form a Sensor/Effector Apparatus for Activating cAMP Synthesis in Hyphal Growth. Molecular Microbiology **75**:579-591.

Appendix A

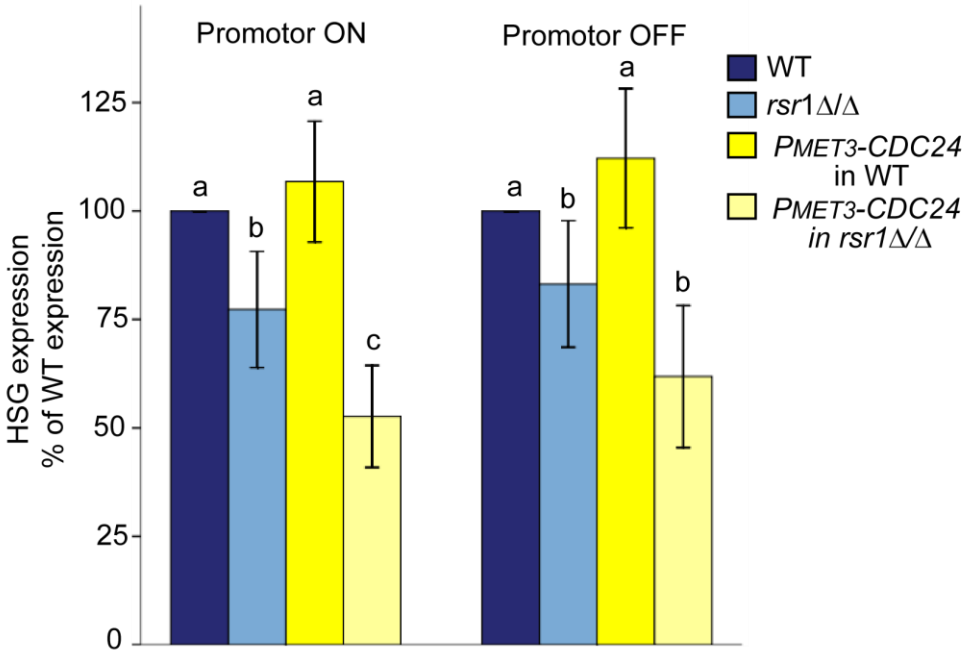

Appendix A. Overexpression of *CDC24* Does Not Rescue HSG Expression in *rsr1Δ/Δ* Strains. Bar graphs showing the mean pooled HSG expression levels in *C. albicans* strains with or without expression of *CDC24* via the *MET3* promoter. WT (12366) and *rsr1*Δ/Δ (12367) strains containing inducible *CDC24* alleles were grown in either the presence (repressing) or absence (inducing) of methionine or cysteine overnight at 30°C. Harvested cells were inoculated into fresh media under either repressing or inducing conditions. GTs and mature hyphae were harvested for mRNA extraction after 30 min and 4hr, respectively, of induction as previously described (81).

Strains used in these experiments

Strain	Relevant Genotype	Source
CA12366	(BWP17) *URA3*-P_{MET3}*::CDC24/CDC24*	(This study)
CA12367	(BWP17) *rsr1::ARG1/rsr1HIS1 URA3*-P_{MET3}*::CDC24/CDC24*	(This study)